



NKS-380  
ISBN 978-87-7893-466-6

---

**MEteorological uncertainty of ShOrt-range dispersion  
(MESO)**

Jens Havskov Sørensen<sup>1</sup>, Bjarne Amstrup<sup>1</sup>, Thomas Bøvith<sup>1</sup>  
Henrik Feddersen<sup>1</sup>, Rashpal Gill<sup>1</sup>, Martin Sørensen<sup>1</sup>  
Flemming Vejen<sup>1</sup>

Poul Astrup<sup>2</sup>, Neil Davis<sup>2</sup>

Bent Lauritzen<sup>3</sup>

Steen Cordt Hoe<sup>4</sup>

Jan Erik Dyve<sup>5</sup>

Patric Lindahl<sup>6</sup>

<sup>1</sup>Research and Development Dep., Danish Meteorological Institute

<sup>2</sup>Department of Wind Energy, Technical University of Denmark

<sup>3</sup>Center for Nuclear Technologies, Technical University of Denmark

<sup>4</sup>Nuclear Division, Danish Emergency Management Agency

<sup>5</sup>Norwegian Radiation Protection Authority

<sup>6</sup>Swedish Radiation Safety Authority

---

## Abstract

As shown by the MUD and FAUNA projects, the influence of meteorological uncertainties on long-range atmospheric dispersion calculations can be large depending on the weather situation, with significant implications for nuclear emergency preparedness and decision making. The question that the MESO project has answered is to what extent this also applies to short-range dispersion models employed up to, say, a hundred kilometres from the source.

The assessment of such uncertainties is facilitated by recent developments in numerical weather prediction modelling through the use of ensemble methodology. Currently, the computer resource demanding procedures are being implemented at a number of national weather services, thereby enabling future operational quantitative calculation of uncertainties of concentration and deposition patterns from accidental releases of radionuclides. Thereby, a more comprehensive basis for the decision making is provided.

Short-range atmospheric dispersion models differ from long-range models not only by the use of finer resolution terrain and land-use data, but also by the fact that short-range models may utilize weather radar data for simulation of wet deposition of radionuclides. Obviously, observational data, e.g. from radars, can be used only for hindcasting, but these data, which are expected to represent the precipitation intensity more accurately than model data, are useful for nuclear emergency preparedness in the period of time until radiological monitoring data have become available. However, there are a number of uncertainties and potential errors associated with such use of weather radar data.

Thus, the MESO project had two work packages: one devoted to the study of uncertainties of short-range atmospheric dispersion forecasting involving the use of meteorological model data only, the other focusing on hindcasting including the combined use of model data and weather radar data.

## Key words

nuclear emergency preparedness, short range atmospheric dispersion model, meteorology, uncertainty, ensemble prediction, weather radar estimated precipitation rate

NKS-380  
ISBN 978-87-7893-466-6

Electronic report, January 2017  
NKS Secretariat  
P.O. Box 49  
DK - 4000 Roskilde, Denmark  
Phone +45 4677 4041  
[www.nks.org](http://www.nks.org)  
e-mail [nks@nks.org](mailto:nks@nks.org)

# **MEteorological uncertainty of ShOrt-range dispersion (MESO)**

**Final Report of the NKS-B MESO activity  
(Contract: AFT/B(16)4)**

Jens Havskov Sørensen<sup>1</sup> (co-ordinator), Bjarne Amstrup<sup>1</sup>, Thomas Bøvith<sup>1</sup>,  
Henrik Feddersen<sup>1</sup>, Rashpal Gill<sup>1</sup>, Martin Sørensen<sup>1</sup>, Flemming Vejen<sup>1</sup>

Poul Astrup<sup>2</sup>, Neil Davis<sup>2</sup>

Bent Lauritzen<sup>3</sup>

Steen Cordt Hoe<sup>4</sup>

Jan Erik Dyve<sup>5</sup>

Patric Lindahl<sup>6</sup>

<sup>1</sup>Research and Development Department, Danish Meteorological Institute

<sup>2</sup>Department of Wind Energy, Technical University of Denmark

<sup>3</sup>Center for Nuclear Technologies, Technical University of Denmark

<sup>4</sup>Nuclear Division, Danish Emergency Management Agency

<sup>5</sup>Norwegian Radiation Protection Authority

<sup>6</sup>Swedish Radiation Safety Authority



## Table of contents

Introduction .....	5
Weather radar .....	7
Functionality.....	7
The DMI weather radar network .....	10
Sources of uncertainty and errors in weather radar observations.....	11
Precipitation rate estimation.....	12
Future: Calibration with rain gauge monitoring network.....	13
Meteorological ensemble prediction .....	14
Meteorological case studies.....	16
1 March 2016 .....	16
28 March 2016 .....	18
27 April 2016 .....	20
29 April 2016 .....	22
Source term .....	24
Atmospheric dispersion modelling.....	25
Ensemble statistics for atmospheric dispersion modelling.....	25
Short-range model RIMPUFF.....	26
Long-range model DERMA.....	26
Case studies .....	27
Discussion and conclusions.....	31
References .....	33
Appendix A .....	37
Short-range dispersion results .....	37
Release from Brokdorf NPP starting at 12 UTC on 2016-03-01 .....	37
Release from Brokdorf NPP starting at 00 UTC on 2016-03-28 .....	40
Release from Ringhals NPP starting at 12 UTC on 2016-04-27.....	43
Release from Brokdorf NPP starting at 06 UTC on 2016-04-29 .....	46
Appendix B .....	49
Long-range dispersion results .....	49
Release from Brokdorf NPP starting at 12 UTC on 2016-03-01 .....	49
Release from Brokdorf NPP starting at 00 UTC on 2016-03-28 .....	51
Release from Ringhals NPP starting at 12 UTC on 2016-04-27.....	53
Release from Brokdorf NPP starting at 06 UTC on 2016-04-29 .....	55

Appendix C .....	57
Radar estimated instantaneous precipitation rates.....	57

## Introduction

For nuclear emergency preparedness and management, the responsible authority had previously typically only one atmospheric dispersion prediction available in real time. And when asked: “How accurate is it?” the meteorologist at hand could at best give a rough estimate based on hand-waving arguments. However, rhetorically speaking, if you don't know how much confidence you can have in a prediction – is it then of any value? The situation has now changed. Due to the development of a new computer-resource demanding methodology, one can now provide quantitative estimates of the inherent meteorological uncertainty. Obviously, there are other sources of uncertainty, e.g. on the source term describing the temporal evolution of the release of the various different radionuclides from a nuclear accident, but these uncertainties are outside the scope of MESO.

Evidently, one should strive at reducing uncertainties. However, since uncertainties are inherent both in observational data and in the modelling process, uncertainties are unavoidable. Nevertheless, at least one should attempt at quantifying the uncertainties – any prediction is of little value without being accompanied by an estimate of the associated uncertainty.

As shown by the recently completed NKS-B projects MUD (Meteorological Uncertainty of atmospheric Dispersion model results) and FAUNA (Fukushima Accident: UNcertainty of Atmospheric dispersion modelling), cf. Sørensen *et al.* (2014) and (2016), respectively, the influence of meteorological uncertainties on long-range atmospheric dispersion calculations can be large, up to, say, an order of magnitude or two depending on the weather situation, with significant implications for nuclear emergency preparedness and decision making. The question that the MESO project is going to answer is to what extent this also applies to short-range dispersion models employed for nuclear emergency preparedness up to about a hundred kilometres from the source.

The project name, MESO, is an acronym for MEteorological uncertainty of ShOrt-range dispersion. However, the name also indicates the meteorological scale of the phenomena involved. Mesoscale meteorology is divided into three subclasses:

- Meso-alpha: 200–2000 km scale phenomena, e.g. fronts, squall lines, and cyclones.
- Meso-beta: 20–200 km scale phenomena, e.g. sea breezes, lake effects, and snow storms.
- Meso-gamma: 2–20 km scale phenomena, e.g. thunderstorm convection, and complex terrain flows.

Thus, the MUD and FAUNA projects considered the meso-alpha and beta scales (long range), whereas MESO considers meso-beta and gamma scales (short range).

The assessment of meteorological uncertainties is facilitated by recent developments in numerical weather prediction (NWP) modelling through the use of ensemble methodology. Currently, the computer-resource demanding procedures are being, or are planned to be, implemented at a number of national weather services. This development enables future operational quantitative calculation of uncertainties, as well as the most like predictions, of the concentration and deposition patterns from accidental releases of radionuclides to be used by nuclear decision-support systems (DSSs). Thereby, a more comprehensive basis for the decision making is provided than beforehand where only a single, deterministic prediction was available.

Short-range atmospheric dispersion models differ from long-range models not only by the use of finer resolution terrain and land-use data, but also by the fact that short-range models may utilize weather radar data for the simulation of wet deposition of radionuclides. Obviously, observational data, e.g. from radars, can be used only for hindcasting, but these data, which are expected to represent the precipitation intensity more accurately than NWP model data, are useful for nuclear emergency preparedness in the period of time until radiological monitoring data have become available. However, there are a number of uncertainties and potential errors associated with such use of weather radar data. These include the use of a parameterization of the precipitation rate depending on the attenuation of the reflected radar signal, filtering of false radar echoes arising from e.g. clutter or flocks of birds, precipitation from low clouds not being registered by the radar beam, and precipitation evaporating before reaching ground. A new possibility is facilitated by the next-generation dual-pole Doppler radars, namely observed distinction between rain and snow which can have important consequences for short-range modelling since deposition of radionuclides differs substantially between rain and snow.

Thus, the MESO project included two work packages: one devoted to the study of uncertainties of short-range atmospheric dispersion forecasting involving the use of NWP model data only, the other focusing on hindcasting including the combined use of NWP model data and weather radar data.

## Weather radar

Measurements of precipitation have traditionally been carried out using rain gauges on the ground. However, since the invention of radars and satellites, remote sensing techniques have provided improved mapping capabilities for precipitation. Especially, ground-based weather radars have become an indispensable tool for meteorology and hydrology today providing high resolution measurement of precipitation in the atmosphere.

## Functionality

Weather radars are radar systems made for observation of precipitation in the atmosphere (Meischner, 2004; Bech and Chau, 2012). Using the radar principle, they measure the location and properties of precipitation at a distance from the radar. As an active sensor it works by transmitting electromagnetic energy into its surroundings and by receiving the energy reflected by objects in its path. Through calibration of the weather radar, the received power can be translated into a measure of reflectivity of the precipitation. This reflectivity (measured in units of dBZ) varies for different precipitation intensities (low reflectivity for light precipitation and high reflectivity for heavy precipitation) and for different precipitation types (rain, hail, and snow). This is due to the difference in drop sizes and drop shapes of the hydrometeors.

Weather radars are typically ground-based, and sensing of the atmosphere is carried out by rotating an antenna around its vertical axis and by changing the pointing angle of the antenna (typically once for each revolution of the antenna), see Figure 1. The angle in the horizontal plane from geographical north in positive clockwise direction is called the azimuth angle and the tilt angle measured from horizontal and positive upwards is called the elevation angle. The range to a target is computed from the round-trip time of a pulse to the target and the speed of the electromagnetic energy (i.e., the speed of light).

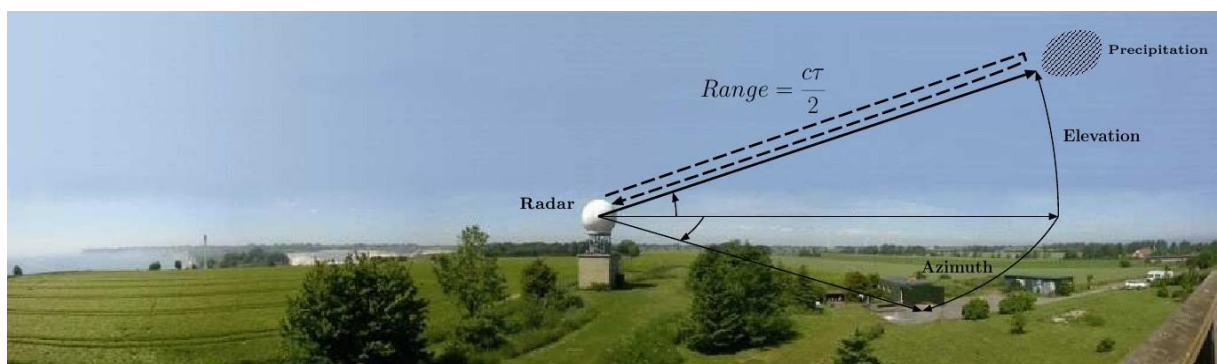


Figure 1 The working principle of a weather radar. Here the DMI weather radar at Stevns.

A complete radar system is a complex system comprised of many components (Skolnik, 2001): From the hardware in the transmitter, antenna, and receiver, to signal processors and data analysis and visualization software, all of which play together in the generation of weather radar data.

The signal processor of the weather radar typically receives data from a number of pulses which are integrated and sampled to a polar coordinate system, one scan for each revolution and elevation angle. For a typical weather radar, a 1 degree azimuth resolution is used and in the range direction, a resolution of 500 m or more is used (see Figure 2, left). The 1 degree beam width means that the resolution in the azimuth direction varies from metres close to the radar to kilometres at the maximum range of e.g. 240 km, while the range resolution is

constant throughout the data. When converted to Cartesian coordinates the data thus have a varying resolution even if the image has a specified pixel size.

Displaying a scan in Cartesian coordinates is called a PPI image (Plane Position Indicator) as seen in Figure 2, right. Since the radar rays normally rise with distance to the radar, the observed precipitation of course is close to the ground near the radar in the centre of the image and higher up in the atmosphere at far range from the radar. By using the data from several PPIs, a CAPPPI (Constant-Altitude PPI) can be constructed which shows the precipitation at a given height. Typically, a stack of CAPPPIs are produced at intervals of 1 km.

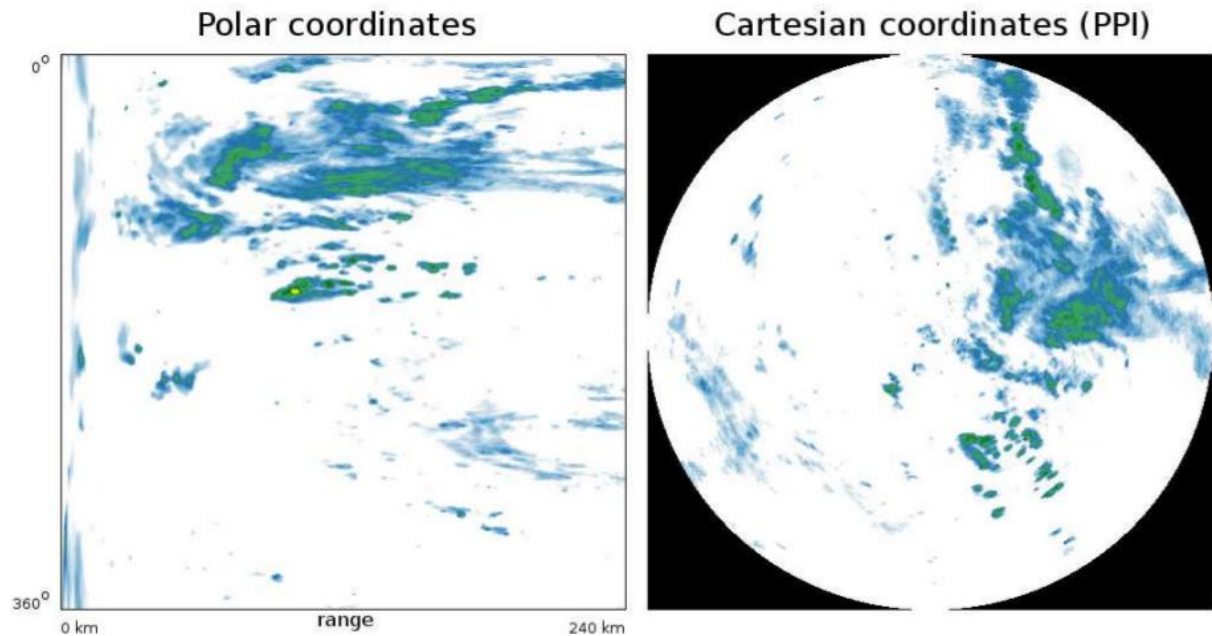


**Figure 2** A radar scan in polar and Cartesian coordinates.

Finally, the 2D image products, PPIs or CAPPPIs, are often composited into one image as seen in Figure 3.

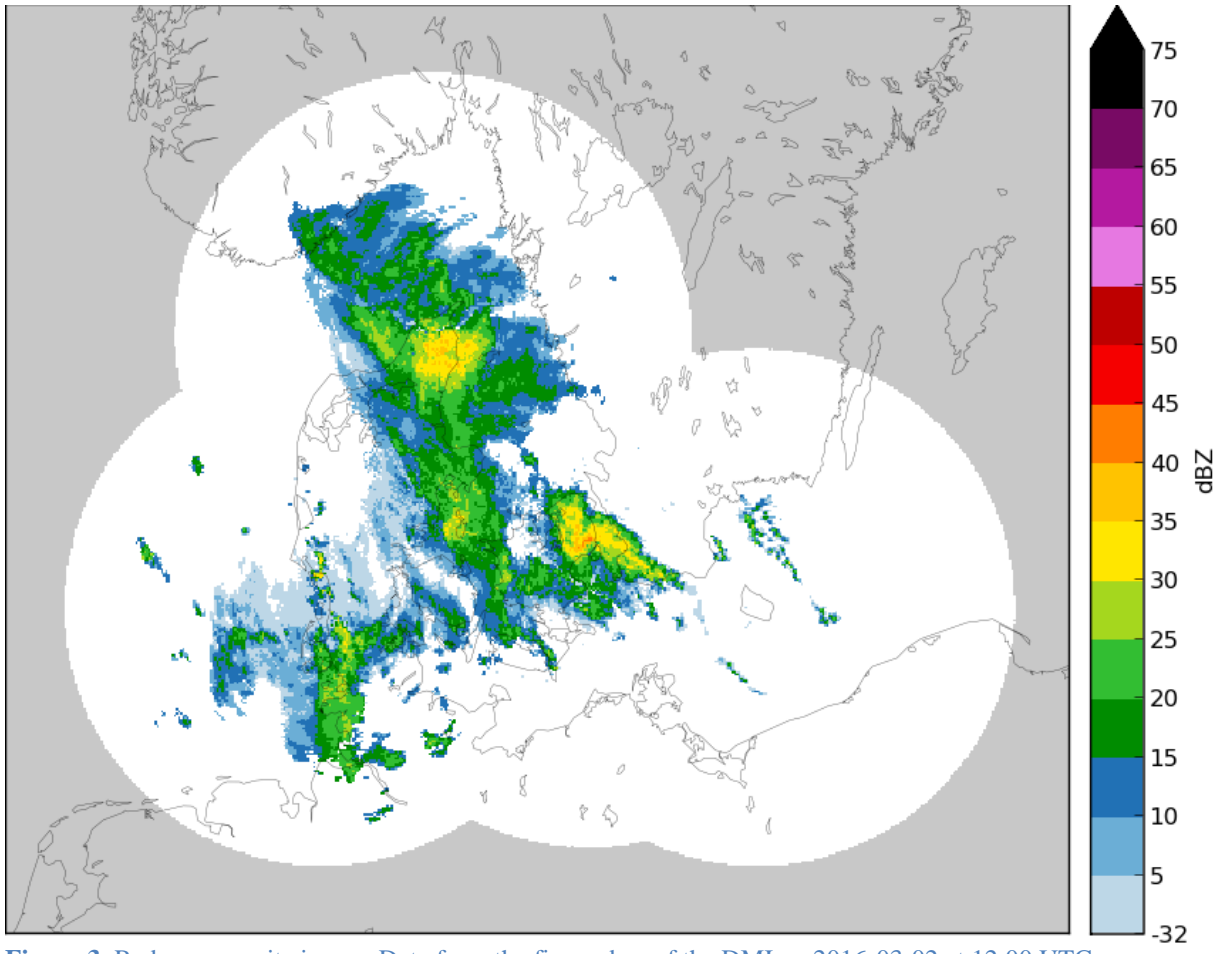


**Figure 3** Radar composite image. Data from the five radars of the DMI on 2016-03-02 at 12:00 UTC.

Most modern weather radars are Doppler radars which mean that they are able to measure the phases of the transmitted and received signals. The shift in phase is used to derive the radial velocity of the precipitation particles. In meteorology this is used to map the wind speed but it is also used in clutter detection because echoes from non-moving targets are unlikely to be precipitation.

A new technology in the field of weather radar is dual-polarization radars. These are radars with the capability to transmit and receive electromagnetic energy in two polarizations. Normally, weather radars are operated in horizontal polarization only (because falling rain drops are flattened as they fall and the backscatter is greater in the horizontal than the vertical). Dual-polarimetric radars (Bringi and Chandrasekar, 2001) provide a range of additional information besides radar reflectivity and the Doppler velocity. The differential reflectivity (the ratio between the horizontal (H) and vertical (V) power returns), the correlation coefficient (correlation between H and V power returns), and the differential phase (phase difference between H and V returns) enable improved hydrometeor classification (classification of precipitation type, e.g. rain, hail, or snow) as well as better clutter/precipitation discrimination (Gill *et al.*, 2012).

## The DMI weather radar network

For this project, data from the weather radars of the Danish Meteorological Institute (DMI) were used. The radar network is comprised of five C-band radars located in Rømø, Sindal, Virring, Stevns, and Bornholm (see Figure 4 for a map of the weather radar network). The first three are Doppler radars and the latter two are dual-polarization radars.

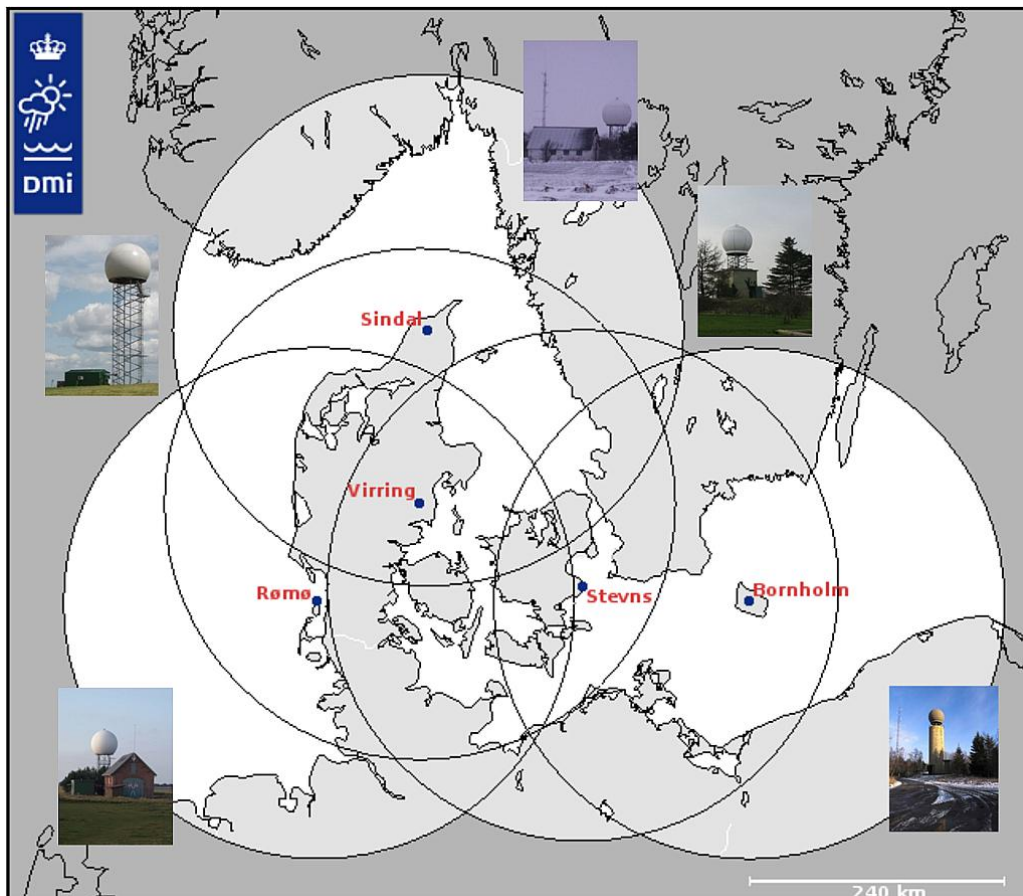
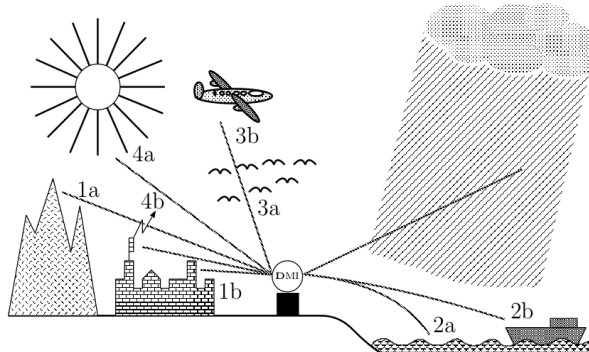


**Figure 4** The locations of the five radars of the DMI weather radar network. Range rings show the maximum range of 240 km from each radar site.

For this project, radar composites made of CAPPIs from all five radars were used. The data had been processed by DMI in-house software (Gill, 2010) to improve the data quality by inter-radar adjustment of the radar reflectivity and removal of non-precipitation echoes. The pixel size of the data was 500 m and the temporal resolution 10 minutes.

## Sources of uncertainty and errors in weather radar observations

Like any other sensor observation, weather radar observations are subject to errors and uncertainties. A significant source of errors is the occurrence of radar clutter (Bøvith, 2008), which for hydrometeorological applications is defined as radar echoes from non-precipitation targets. The types and sources of weather radar clutter are many as can be seen in Figure 5. Land clutter originates from man-made objects (e.g., houses, towers, or bridges) or the natural environment (e.g., mountains, hills, or fields), whereas sea clutter is caused by backscatter from the surface of oceans or lakes. Ships also show up as sea clutter. Airborne clutter is caused by reflections from airplanes or other man-made objects in the air, or biological targets like birds and insects. Finally, also interference from the sun or other transmitting antennas result in radar clutter.



- 1 Land clutter** from (a) mountains/earth surface or (b) buildings/windmills, etc.
- 2 Sea clutter** from (a) sea surface or (b) ships
- 3 Airborne clutter** from (a) biological targets (birds/insects) or (b) airplanes
- 4 Interference clutter** from (a) the sun or (b) transmitting antennas

Figure 5 Types of clutter illustrated. After Bøvith (2008).

In Figure 6 three examples of clutter in weather radar images are shown. The image on the left shows land clutter on the mountains of Norway and Sweden. Furthermore, land clutter close to the radar is seen. In the middle image, an example of interference clutter caused by solar radiation is seen (the pencil beam pattern), and on the right image strong sea clutter caused by anomalous propagation of the radar signal toward the sea surface is seen.

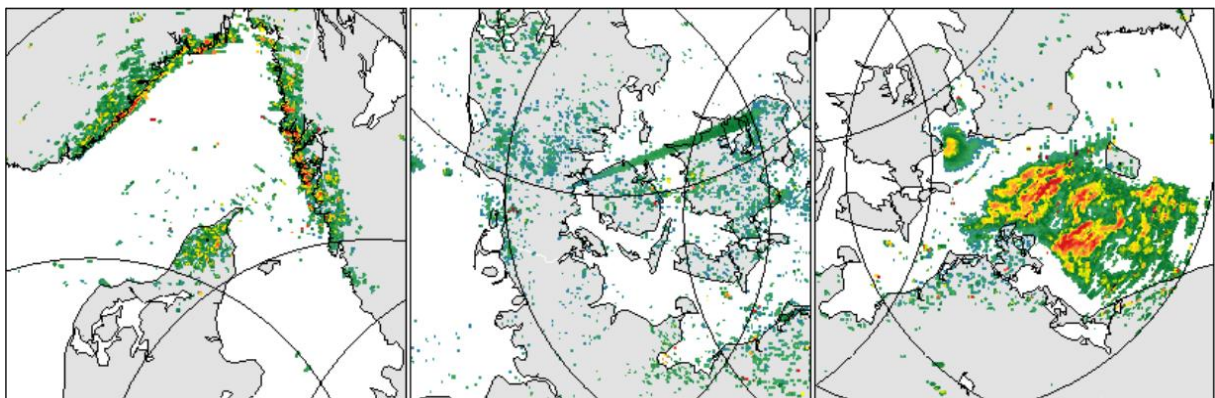


Figure 6 Land clutter (left), interference clutter (centre), and sea clutter (right).

Other sources of uncertainties are the effects of bright band (very strong radar reflections from melting hydrometeors in the melting layer of the atmosphere) and complete or partial blocking of the radar beams due to e.g. buildings or trees.

## Precipitation rate estimation

For many applications of weather radar, the radar reflectivity needs to be converted into precipitation rate (mm/h) (Figure 7) and several empirical methods exist for this. This derivation of precipitation rate on the ground on the basis of observation of radar backscatter in the atmosphere (often several kilometres up) has traditionally been carried out using simple power law relationships and has inherently a considerable uncertainty associated with it. The power law Z-R relationship is defined as  $Z = AR^b$ , where  $A$  and  $b$  are constants depending on the precipitation type and essentially the drop size distribution,  $Z$  is the radar reflectivity factor and  $R$  is the precipitation rate. The reflectivity factor  $Z$  is computed from the reflectivity dBZ as follows:  $Z = 10^{\text{dBZ}/10}$ . The precipitation type and the drop size distribution are unknown to the weather radar, and the assumptions about these, which must be made, contributes significantly to the uncertainty of the precipitation rate estimates.

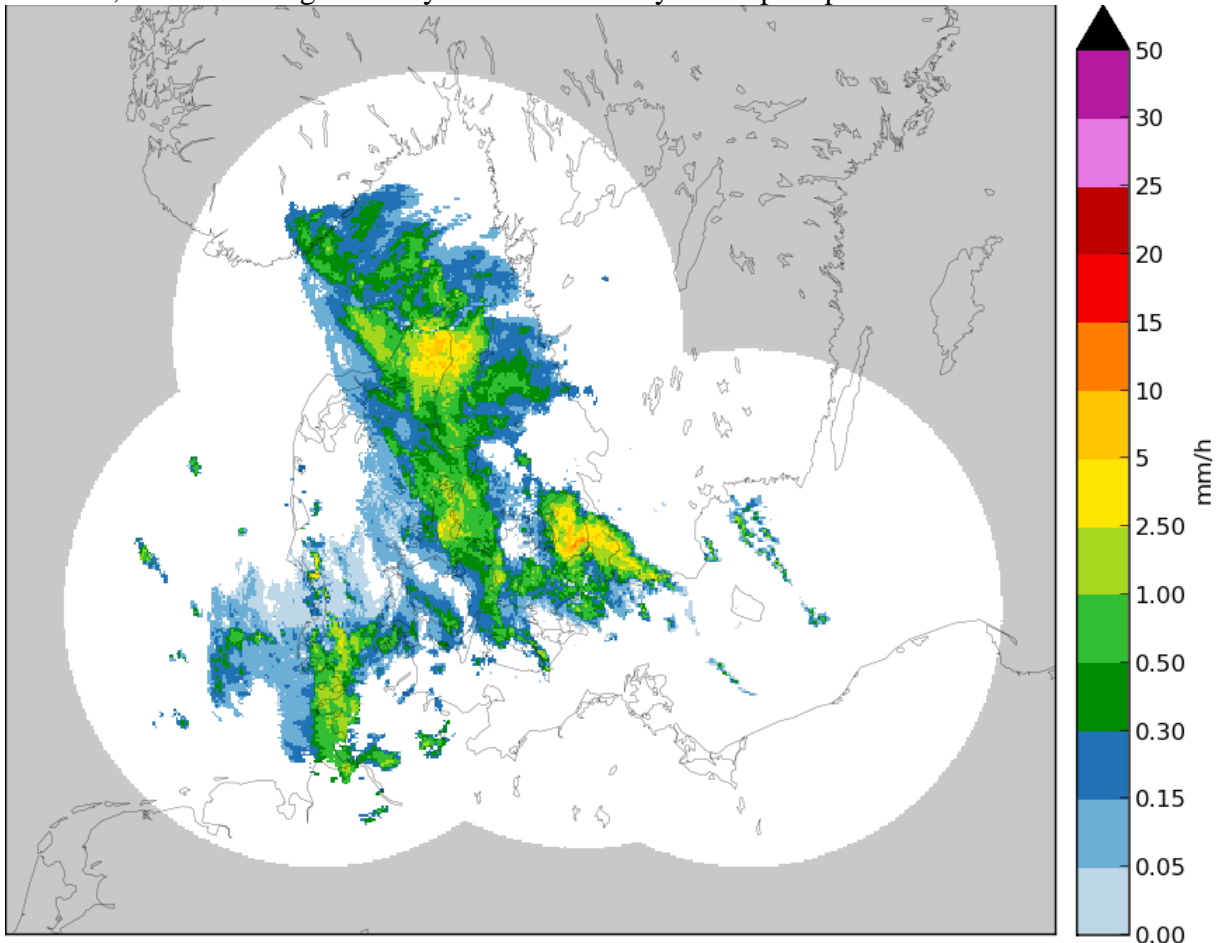
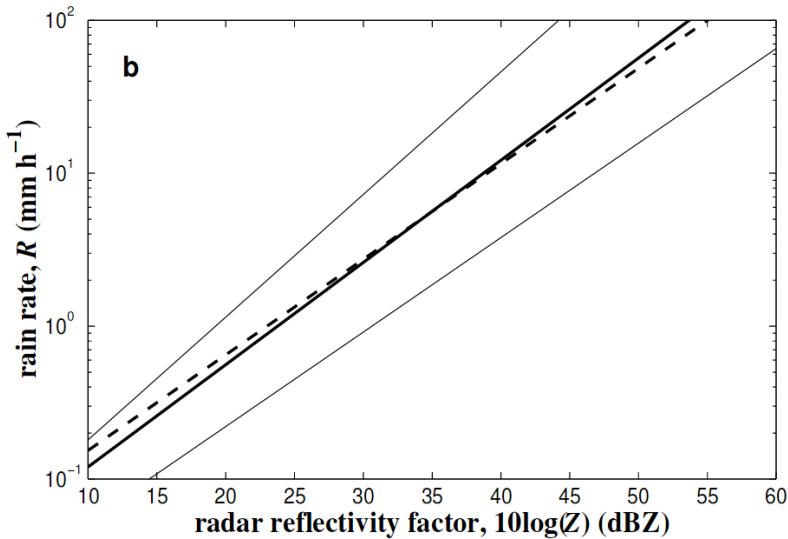


Figure 7 Precipitation rate derived from the reflectivity shown in Figure 3.

The first and most well-known power law relationship is the one proposed by Marshall and Palmer (1948) where  $Z = 200R^{1.6}$ . Many other empirical Z-R relationships have been proposed to accommodate to the predominant climatic characteristics of precipitation around the world. Figure 8 shows the large span of Z-R-values that the choice of Z-R relationship gives rise to. Uijlenhoet (2001) here illustrates the mean and envelope of 69 empirical Z-R relationships documented by Battan (1973). Notice the logarithmic scale of rain rate and hence the large uncertainties in deriving rain rate using Z-R relationships.



**Figure 8** The average of 69 empirical Z-R relationships (bold line) and their envelope (thin lines). The Marshall-Palmer relation is shown in bold dashed line for reference. After Uijlenhoet (2001).

In this project, the precipitation rates were computed using the standard Marshall-Palmer relation. It should be noted that the uncertainty imposed by the choice of Z-R relationship affects the precipitation *rates*. However, the spatial distribution pattern of precipitation, as well as the temporal evolution, is not affected by the choice of Z-R relationship. The geographical and temporal localization of precipitation is very well captured by the weather radar system, and thus also the deposition pattern based on the use of radar data by an atmospheric dispersion model.

### Future: Calibration with rain gauge monitoring network

An improved method for deriving precipitation rate from radar reflectivity is to combine the radar data with observations of precipitation rate by ground-based rain gauges. This potentially lowers the uncertainties of weather-radar derived quantitative precipitation estimates and removes the assumption of a certain Z-R relationship (drop size distribution). A dense network of rain gauges is preferred and the method is commonly used for deriving accumulated precipitation over longer time periods, typically 24 hours.

## Meteorological ensemble prediction

The DMI meteorological Ensemble Prediction System (DMI-EPS), which is currently based on the HIRLAM numerical weather prediction (NWP) model, involves 25 ensemble members. The horizontal resolution is  $0.05^\circ$ , corresponding to approximately 5.5 km, and vertically the model has 40 layers from the surface up to 10 hPa (approximately 30 km above the sea surface). The ensemble HIRLAM model is nested into ECMWF's global model. For the geographical coverage, see Figure 9.

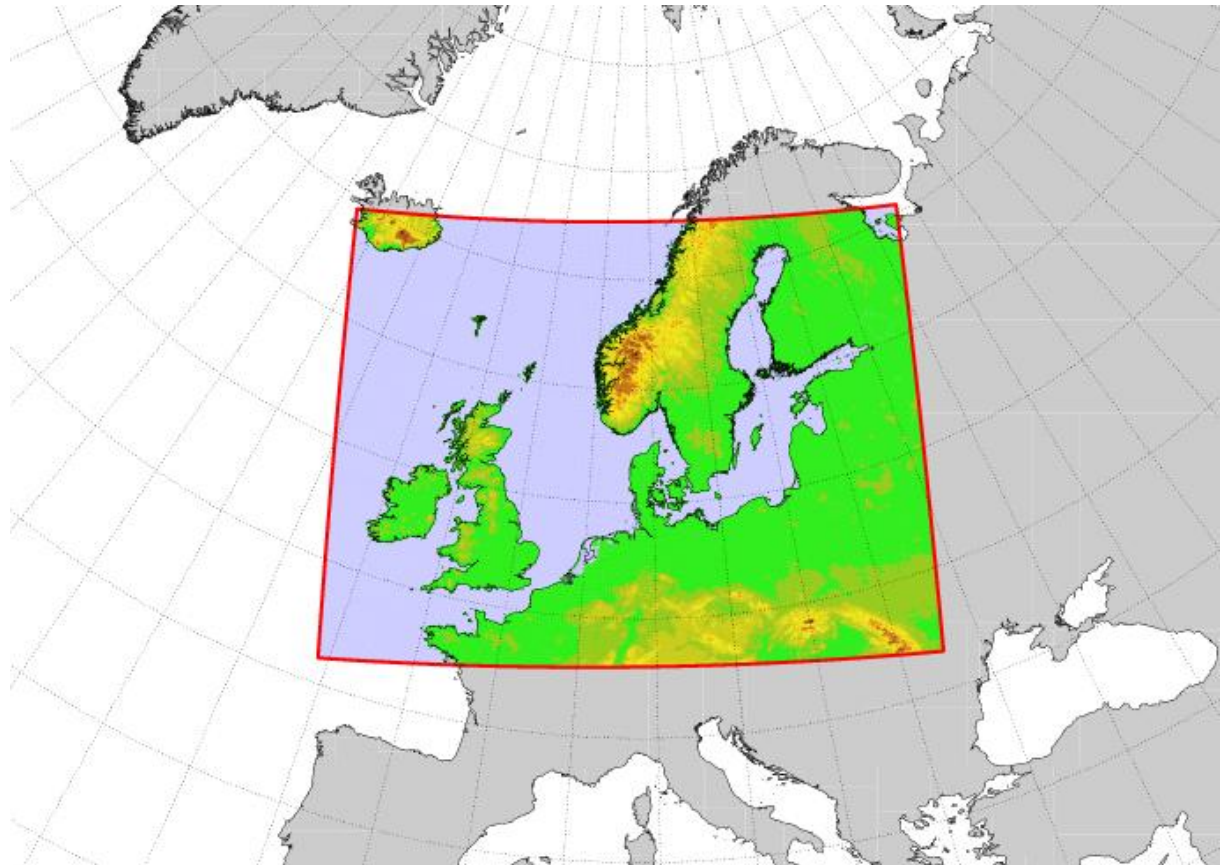


Figure 9 Geographic domain covered by DMI-EPS.

Meteorological forecast uncertainties arise from uncertainties in the initial and lateral boundary conditions and from model short-comings, particularly short-comings associated with parameterization of physical processes that take place on spatial scales that cannot be represented explicitly in the model. The initial condition uncertainty is assumed to be comparable to the forecast error for short (6–18h) forecasts, and so perturbations proportional to the forecast error are added to or subtracted from the initial conditions (Hou *et al.*, 2001). This approach is easily implemented, it can be generalized to also account for uncertainties in the lateral boundary conditions, it does not require input from a global ensemble prediction system, and the results are satisfactory compared to other, more advanced methods (Garcia-Moya *et al.*, 2011). The main drawback is that the number of perturbations is limited. Therefore, the initial condition perturbations are combined with model perturbations: 13 ensemble members use the STRACO cloud scheme (Sass, 2002), while the remaining 12 members use the Kain-Fritsch/Rasch-Kristjansson scheme (Kain, 2004; Rasch and Kristjansson, 1998), and in 13 members the total contribution from all physical parameterizations is perturbed stochastically (Feddersen, 2009) in order to represent the

otherwise unaccounted for uncertainty in the parameterizations, similarly to what has been done for ECMWF's ensemble prediction system for many years (Buizza *et al.*, 1999).

DMI's ensemble prediction system has been running operationally since April 2011. For short-range forecasts, i.e. up to two days in advance, the main uncertainties are those associated with clouds and convection, and so the main application of DMI-EPS has been to provide forecasters at DMI with a tool to predict the risk of severe precipitation events (rain or snow) 12 to 36 hours in advance. After an upgrade in 2016, the perturbations were modified in order to increase the spread in wind speed which should reflect uncertainty in wind predictions better.

## Meteorological case studies

Four meteorological scenarios have been selected with either stratiform (frontal) or convective precipitation well covered by the DMI weather radar system consisting of five radars. The DMI ensemble prediction system has been applied to these cases, both with an initial 54 hour forecast series, and covered by six-hourly analyses with hourly forecasts in between. In addition, the corresponding instantaneous precipitation intensity fields are derived from the measured radar reflectivity, see appendix C.

Both the numerical weather prediction ensemble data and the radar-estimated precipitation intensities are made available to the RIMPUFF short-range atmospheric dispersion model.

### 1 March 2016

At the beginning of the release from Brokdorf (at 12 UTC) the wind is southerly and a band of precipitation is moving eastwards from the North Sea as illustrated in Figure 10. The meteogram shown in Figure 11 shows the time evolution for Karup in Central Jutland, including the forecast uncertainty as represented by the 25 ensemble members. We note that the precipitation starts as snow, and that the strong southerly wind weakens and for a while turns westerly before returning to a south-southeasterly direction again.

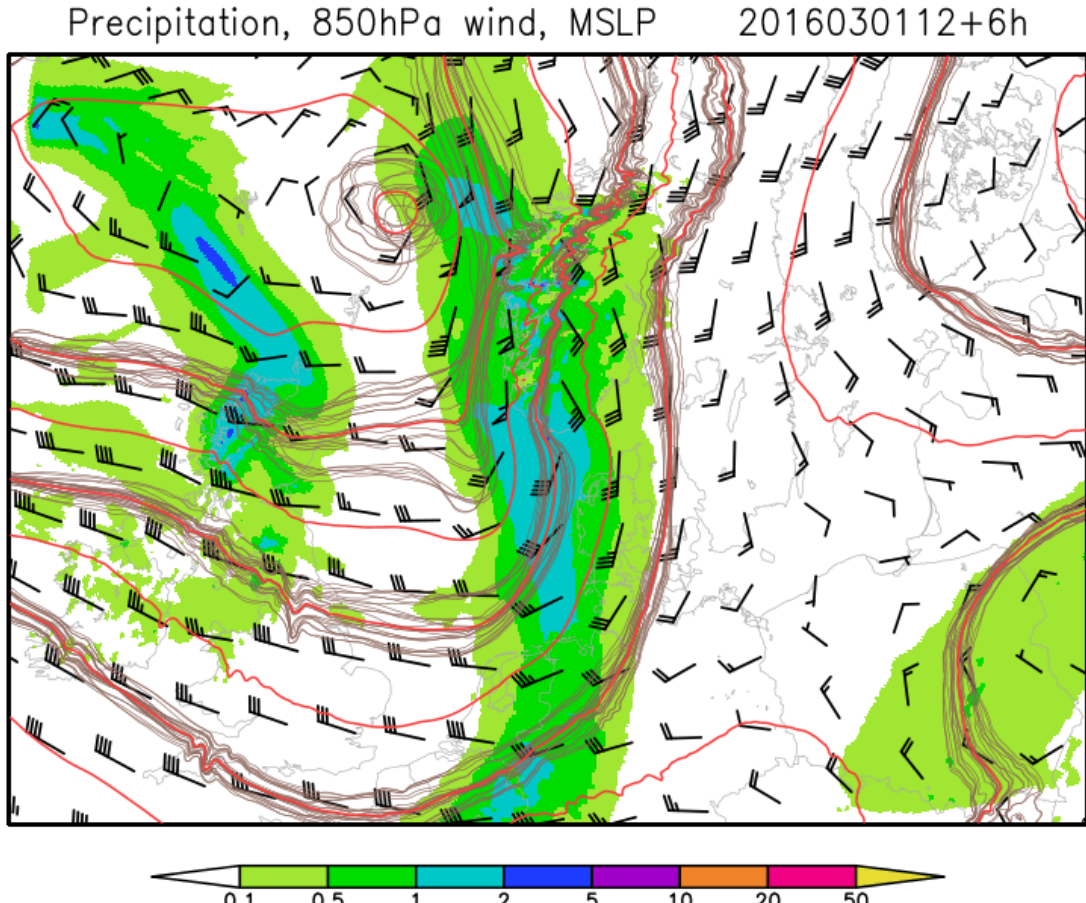


**Figure 10** Ensemble mean of 6 hour forecast of hourly precipitation in mm (shaded), wind at 850 hPa (barbs) and mean sea level pressure (MSLP; red contours). Individual MSLP ensemble members (brown contours around every other red contour) illustrate the forecast uncertainty.

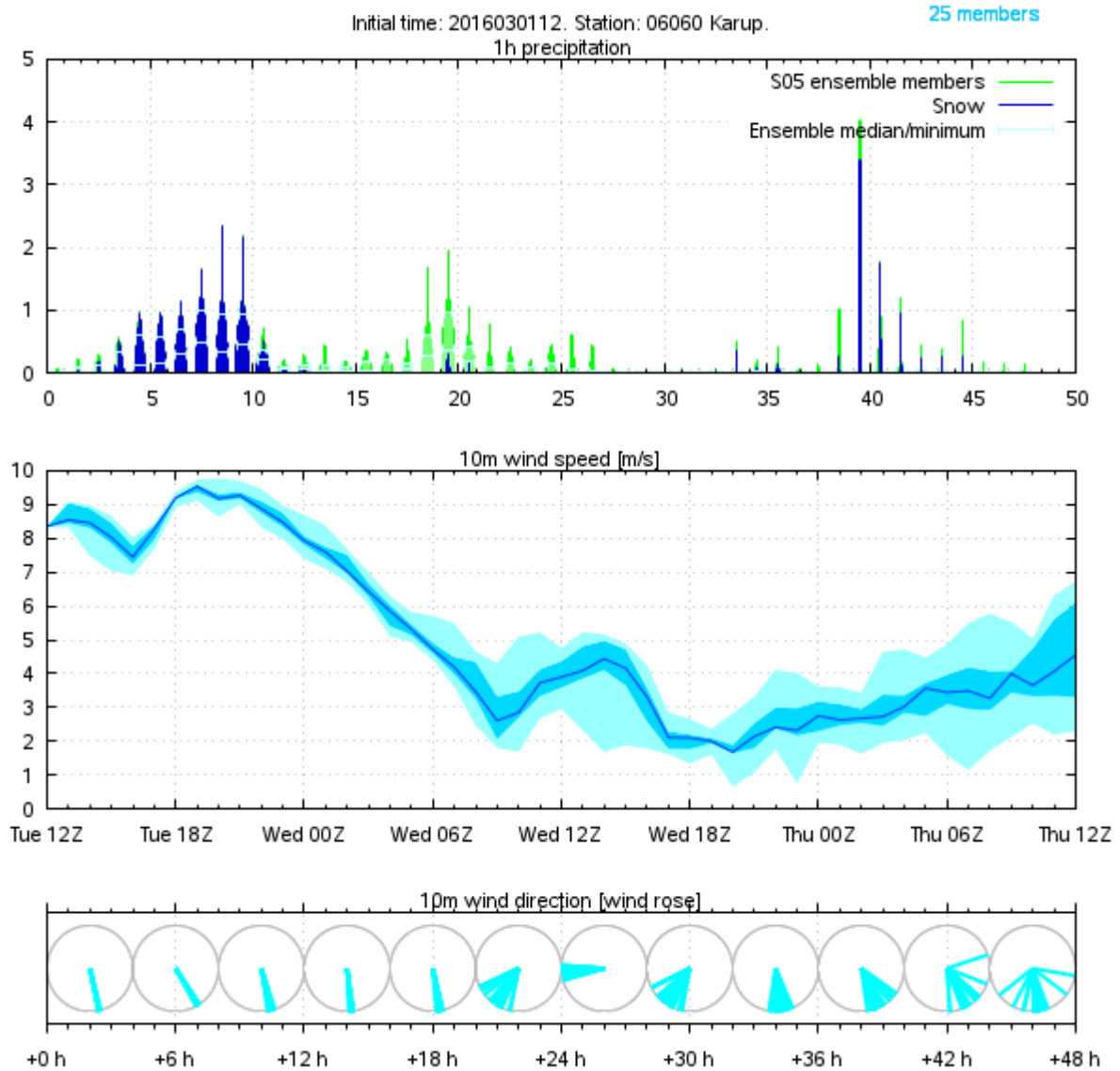


**Figure 11** Meteogram showing ensemble forecast for Karup. Top: Precipitation, where each member at every forecast hour is shown as a vertical line (blue for snow, green for total snow + rain). Middle: Wind speed at 10 m above ground (light blue shows “outer half” of the members; darker blue shows “inner half” of the members; darkest blue shows the median). Bottom: Wind roses, indicating the wind direction for each ensemble member.

## 28 March 2016

A low pressure system moves northwards west of Jutland (Figure 12). Associated with it is some intense rain in southern parts of Denmark which is only partly captured by the ensemble forecast. The wind direction is southerly at the time of the release from Brokdorf. Later it turns south-westerly as illustrated in the meteogram for Skrydstrup in southern Jutland (Figure 13).

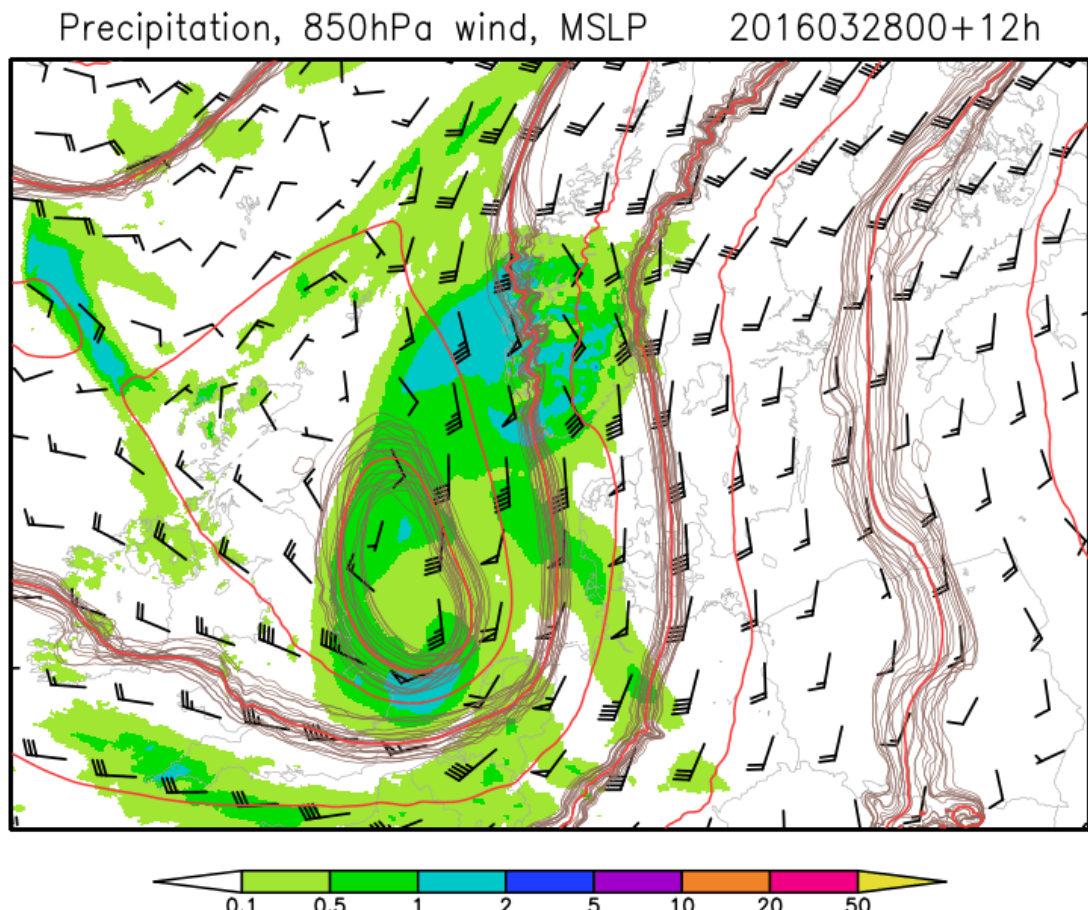


**Figure 12** As Figure 10, but for a 12 h forecast from 0 UTC, 28 March.

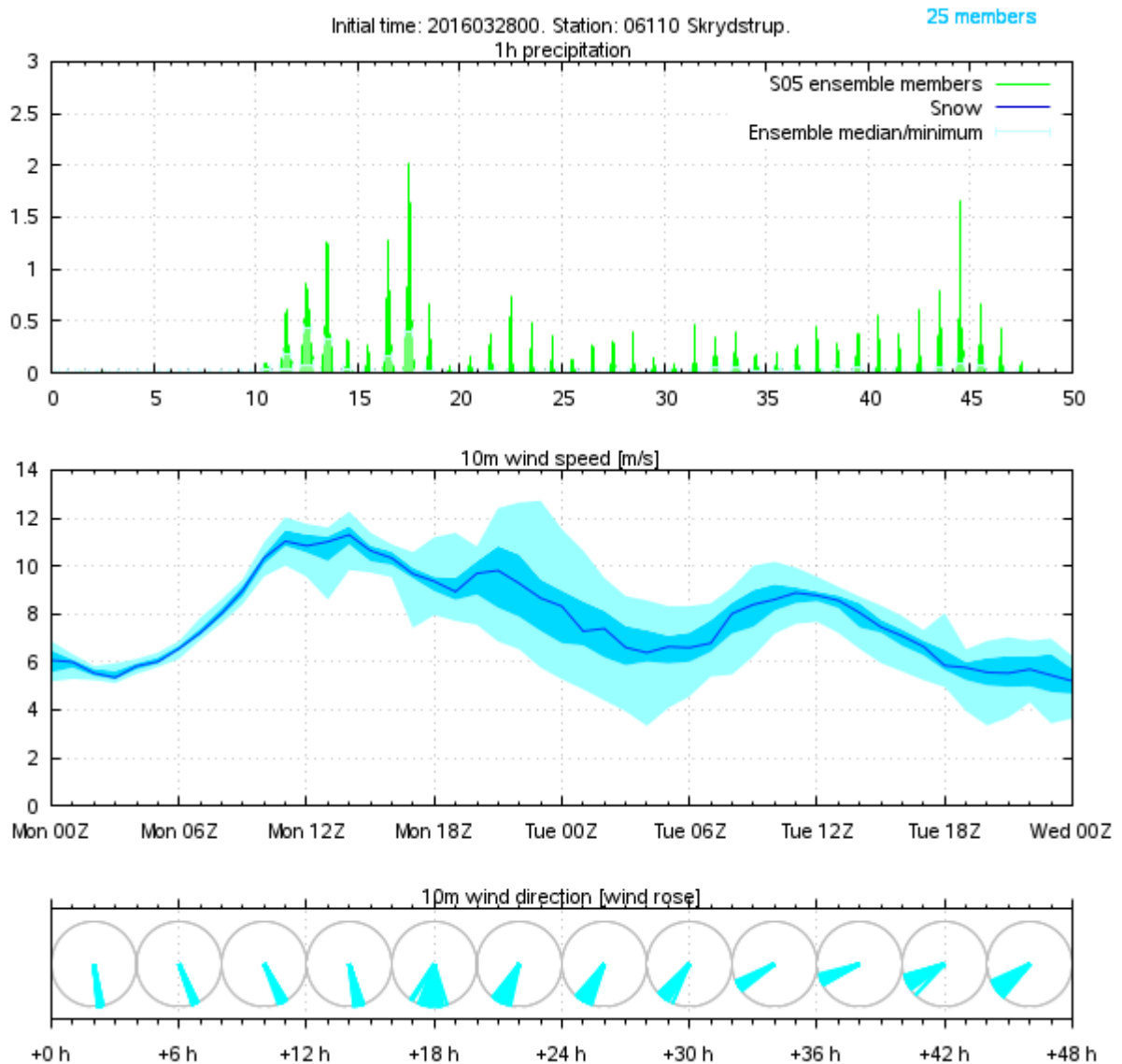


**Figure 13** As Figure 11, but for Skrydstrup for the forecast from 0 UTC, 28 March 2016.

## 27 April 2016

A low is situated over southern Denmark (Figure 14). It is filled during the forecast, and the wind weakens. There are several showers associated with this low. This is also seen in the meteogram for Karup (Figure 15) where the precipitation panel should be interpreted as a risk of rain every hour for the first 30 hours, not as rain continuously every hour.

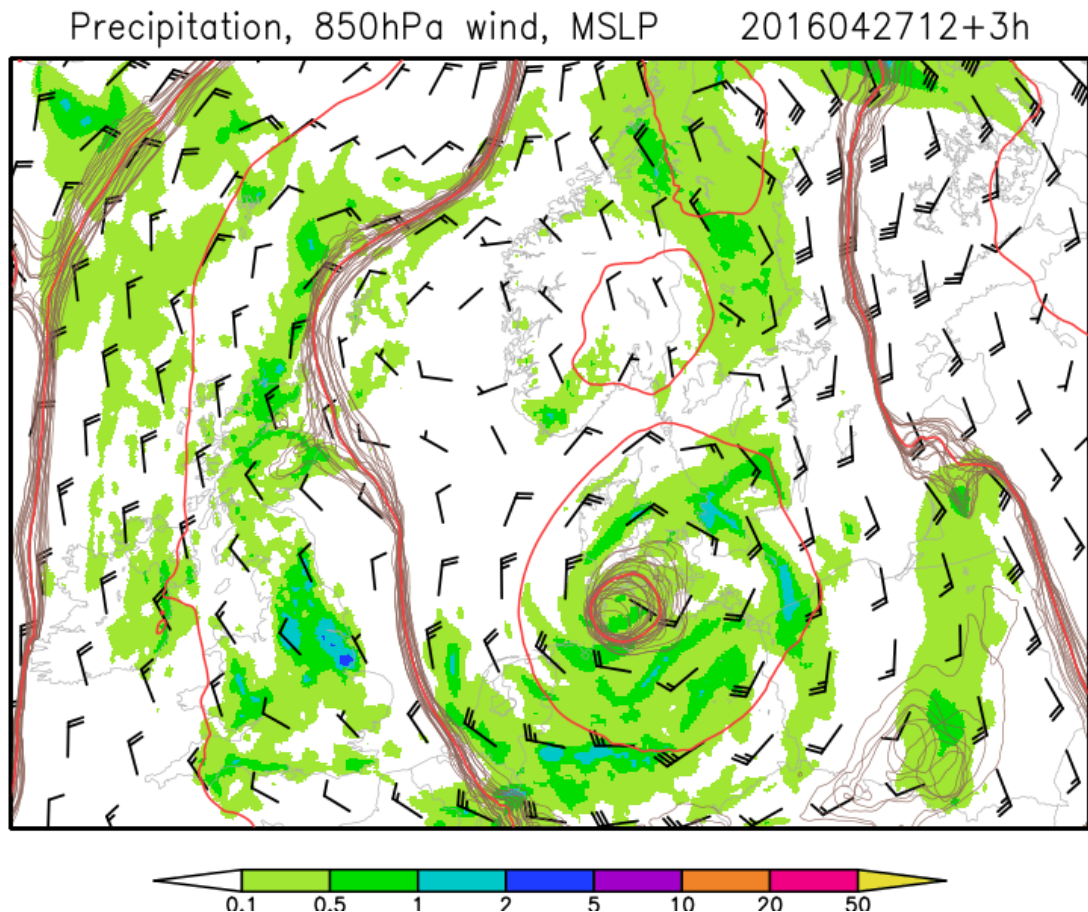


**Figure 14** As Figure 10, but for a 3 h forecast from 12 UTC, 27 April 2016.

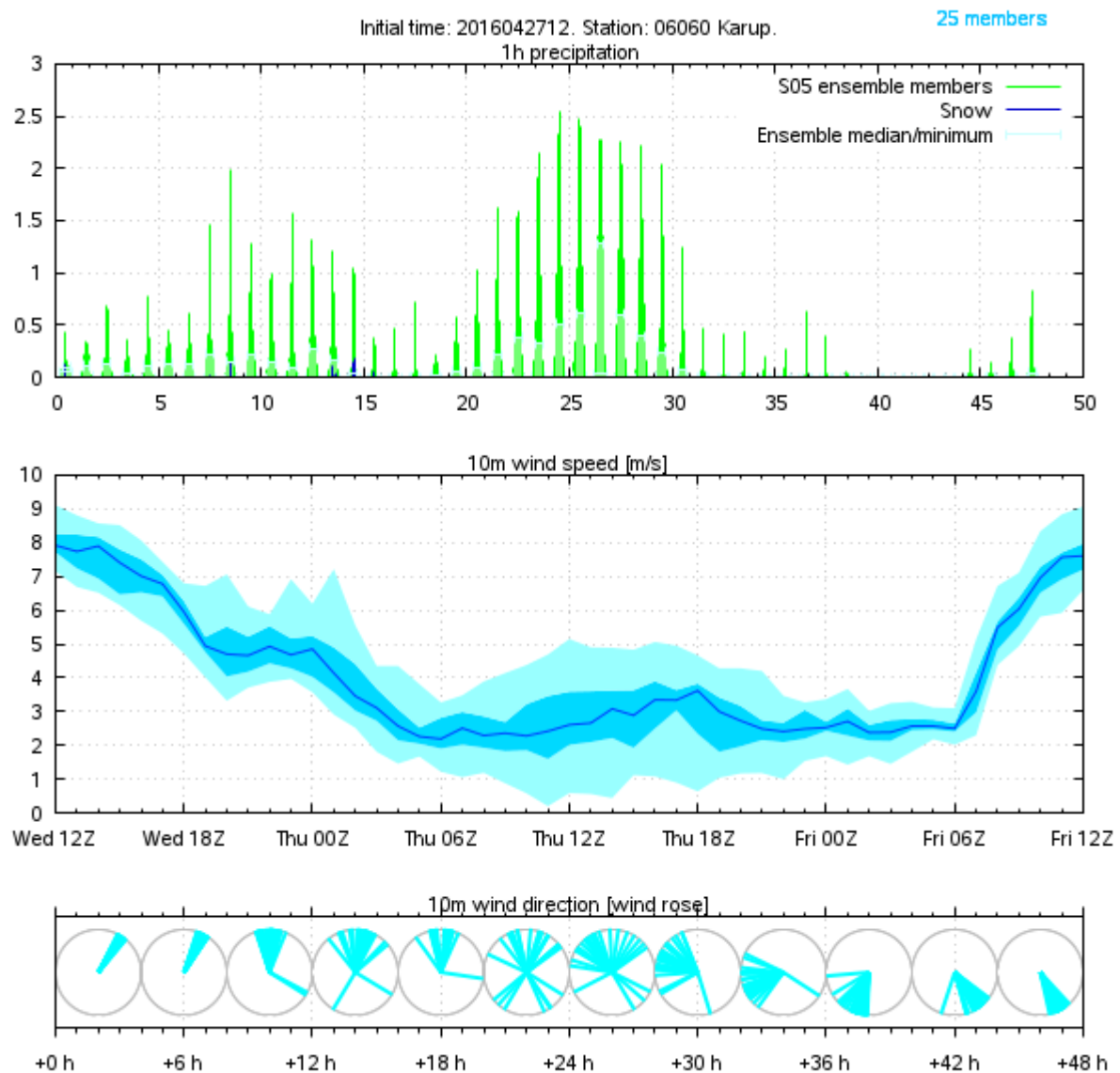


**Figure 15** As Figure 11 for the forecast from 12 UTC, 27 April 2016.

## 29 April 2016

A front with rain moves from west to east over Jutland (Figure 16) and back again during the first 30 hours of the forecast. The wind is southerly in the first part of the forecast, then weakens, and the direction becomes quite uncertain (Figure 17).

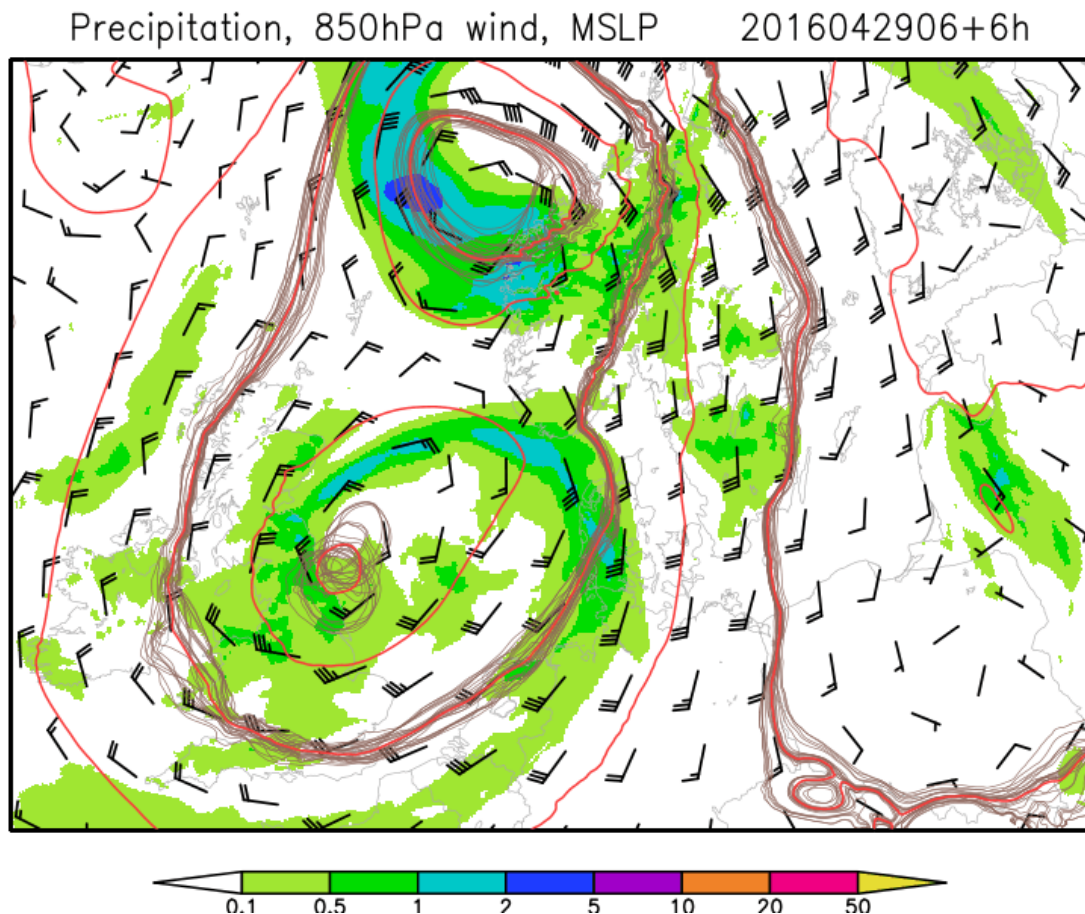


**Figure 16** As Figure 10, but for a 6 h forecast from 6 UTC, 29 April 2016.

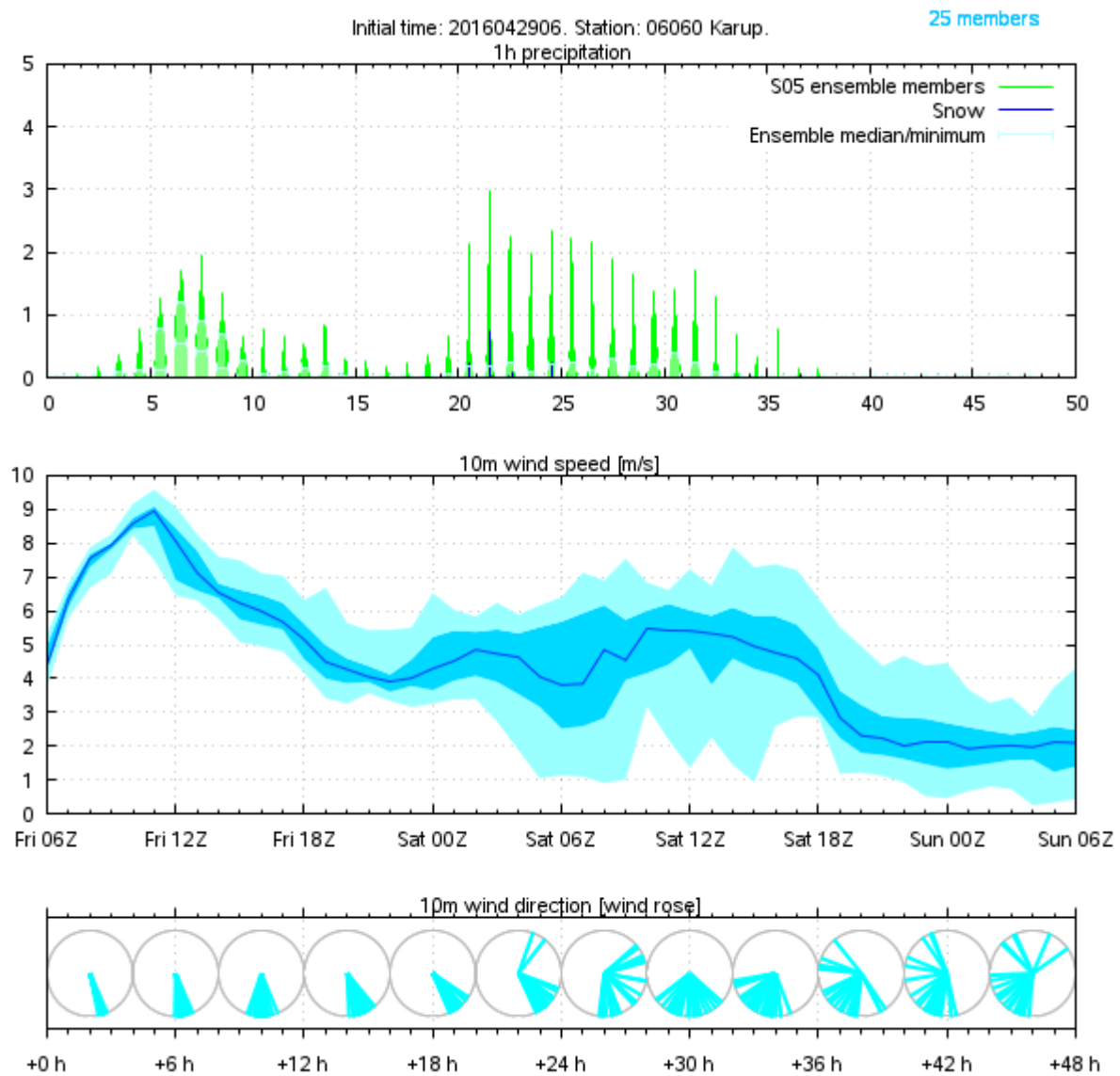


**Figure 17** As Figure 11 for the forecast from 6 UTC, 29 April 2016.

## Source term

The source term used as input to the atmospheric dispersion modelling is called FKA and is taken from a German nuclear reactor accident study published by Löffler *et al.* (2010). It describes a severe long lasting release to the environment.

A number of reactor events, in both German PWR and BWR, could lead to the severe FKA source terms with a PSA probability in the order of one per one million year. FKA for PWR can be characterised by the following: time to release 21 h, release duration 50 h, approximately 9% of the Cs-isotopes, 8% of the I-isotopes and 25% of the Xe-isotopes are released. FKA for BWR is in the same order of magnitude, but with a shorter time interval to release. It should also be noted that the release duration for FKA is limited by the calculation time of the source term code and will in reality probably last considerably longer. Bundesamt für Strahlenschutz (BfS) in Germany has used the FKA source term for estimating interventions areas.

The source term was selected because a long-lasting release will increase the probability for precipitation to coincide with the plume. Secondly, the release is a credible worst case scenario resulting in a more probable fallout situation. Since MESO only looks at deposition and concentration fields, and not human doses, two nuclides are sufficient, and in the present study only Cs-137 and I-131 were used for the dispersion modelling. However, the original source term contain 25 nuclides. The release rate as a function of time is shown in Figure 18.

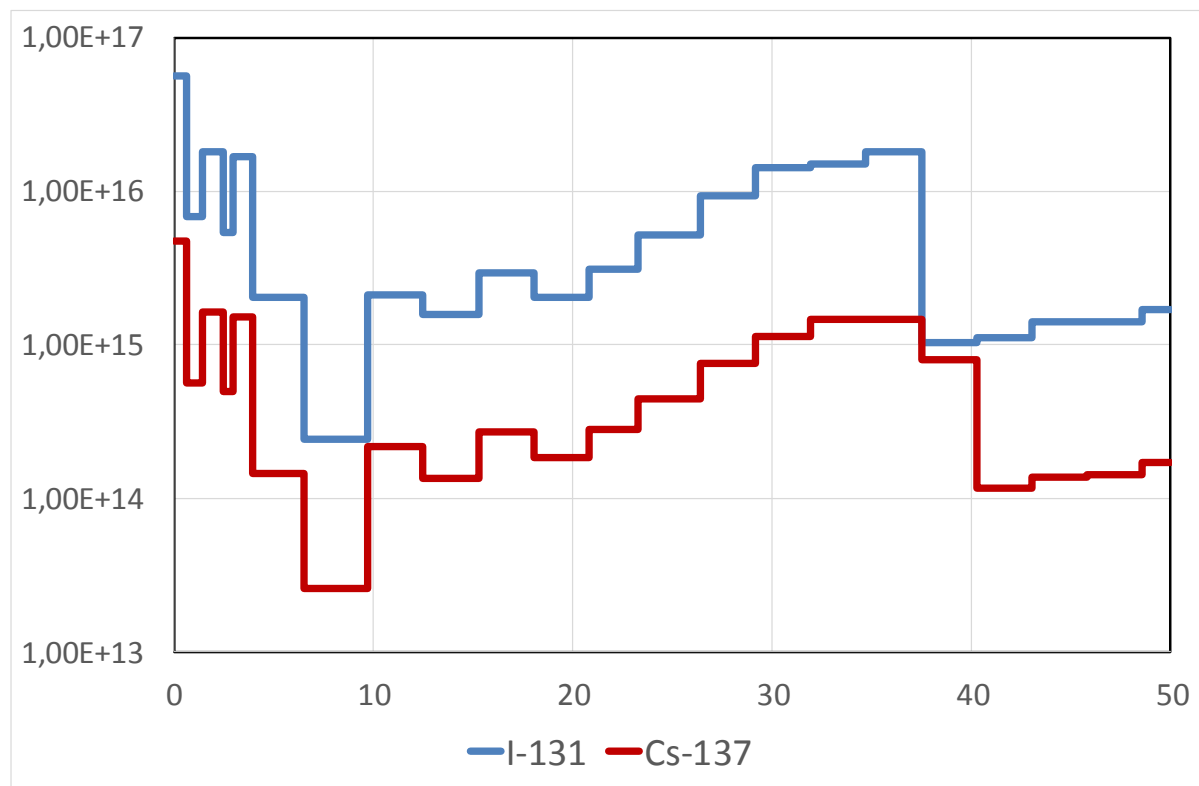


Figure 18 Release (Bq/hour) of Cs-137 and I-131 as function of time (hour).

## Atmospheric dispersion modelling

The short-range atmospheric dispersion model RIMPUFF has been run for the source term described above and applied to either the Brokdorf or the Ringhals nuclear power plant. For each of the selected meteorological cases considered, RIMPUFF has been run for each member of the meteorological ensemble thereby forming a statistical ensemble of dispersion model predictions of the same release scenario. By using the methodology developed in the MUD project (Sørensen *et al.*, 2014), and described in brief in the section below, the inherent meteorological uncertainties of the dispersion predictions have subsequently been quantitatively estimated based on the distribution of the dispersion model ensemble.

The RIMPUFF model has been run both in forecast and in hindcast mode, the latter based on analysed NWP model data using either the NWP model calculated precipitation rates or radar precipitation estimates.

For comparison, also the long-range model DERMA has been applied to the same cases.

## Ensemble statistics for atmospheric dispersion modelling

The calculation and display of probabilities for exceeding a threshold level constitutes a means for presenting uncertainties associated with atmospheric dispersion modelling. For simplicity consider e.g. the total deposition of a single radionuclide a given time after the start of the release. The probabilities (also known as the ATL, cf. Galmarini *et al.* (2004)) are obtained from the ensemble of atmospheric dispersion calculations as

$$P_T(\mathbf{r}, t) = \frac{1}{N} \sum_{i=1,\dots,N} \vartheta\{c_i(\mathbf{r}, t) - c_T\},$$

where  $i$  denotes ensemble members,  $c$  the physical quantity (here total deposition),  $\mathbf{r}$  the geographical location and  $t$  the time. The function  $\vartheta$  denotes the Heaviside step function, and  $c_T$  is the threshold value for the physical quantity.

The method may readily be expanded to include not only atmospheric dispersion uncertainties but also uncertainties associated with e.g. source term variations, in which case the parameters are drawn from statistical ensembles associated with these variables.

A different approach to presenting the uncertainties associated with atmospheric dispersion modelling is to display the maximum, minimum and average influence areas. The maximum deposition is given by

$$c_{\max}(\mathbf{r}, t) = \max_{i=1,\dots,N} c_i(\mathbf{r}, t),$$

Similarly, the average is given by

$$c_{\text{avr}}(\mathbf{r}, t) = \frac{1}{N} \sum_{i=1,\dots,N} c_i(\mathbf{r}, t).$$

This maximum,  $c_{\max}$ , can be used to estimate the geographical area which could possibly be influenced according to the ensemble. However, it is not a solution to governing equations, e.g. it is not conserving mass. Therefore, the quantity should be seen as a statistical measure.

Maximum plots are influenced by outliers in the tail of the distributions, and they are therefore in fact often based on only few ensemble members. This makes these plots sensitive to the inclusion of more ensemble members and generally uncertain. Instead, a low and a high

percentile, e.g. 10% and 90%, together with the mean or median are more appropriate for decision making purposes. The percentiles are more robust than e.g. maximum values, and the approach could also be expanded to include uncertainties of e.g. source term variation.

### Short-range model RIMPUFF

RIMPUFF (RIsø Mesoscala PUFF model), (Mikkelsen and Larsen, 1984; Thykier-Nielsen *et al.*, 1999), models the release to and transport within the atmosphere of radioactive isotopes, chemicals, and biological agents. Instead of a continuous release forming a plume RIMPUFF releases the material in a series of discrete puffs, thereby easing the modelling of the time dependency. The concentration distribution within the puffs is set as Gaussian with separate standard deviations horizontally and vertically. Wind and other atmospheric conditions are read from specially formatted NWP model data, in this case HIRLAM data, and/or from mast data, all of which are interpolated and processed by a meteorological pre-processor (Mikkelsen and Desiato, 1993) using similarity theory (van Ulden and Holtslag, 1985) to give the wind profile and the stability measures friction velocity and Monin-Obukhov length plus the atmospheric boundary layer height at all points of the actual calculation grid. The puffs are transported by the local wind at their centre and they grow due to the local turbulence, this growth primarily based on the work of Carruthers (1992), but a Karlsruhe-Jülich scheme based growth model can also be selected. Puff rise due to excessive heat of the release – i.e. the temperature of the release is higher than that of the surrounding air – is modelled following Macdonald (2003) who refers to Briggs (1975), and there is also a model included for puff rise due to puff growth. Release of radioactive isotopes triggers a decay chain model (Højerup, 1976) and two gamma dose rate models, a rather sophisticated one for the radiation impact on ground level due to the puffs (Thykier-Nielsen *et al.*, 1993), and a simpler semi-infinite model for that of the deposited material. Aerosol and Iodine deposition is modelled following Gering *et al.* (2002), heavier particles deposit due to their free fall.

RIMPUFF forms an integral part of the decision support systems for nuclear emergencies: RODOS (Karlsruhe Institute of Technology, 2015) and ARGOS (PDC-ARGOS), the latter system also used for chemical and biological releases to the atmosphere. Further it is used within the Food and Mouth preparedness system in Denmark.

### Long-range model DERM

The Danish Emergency Response Model of the Atmosphere (DERM) (Sørensen *et al.*, 2007; Sørensen, 1998) is a comprehensive numerical regional and meso-scale atmospheric dispersion model developed at the Danish Meteorological Institute (DMI). The model is used operationally for the Danish nuclear emergency preparedness, for which the Danish Emergency Management Agency (DEMA) is responsible (Hoe *et al.*, 2002). Besides, the model is employed for veterinary emergency preparedness (Sørensen *et al.*, 2000; 2001; Mikkelsen *et al.*, 2003; Gloster *et al.*, 2010a; 2010b), where it is used for assessment of airborne spread of animal diseases, e.g. foot-and-mouth disease. DERM may also be used to simulate atmospheric dispersion of chemical substances, biological warfare agents and ashes from volcanic eruptions, and it has been employed for probabilistic nuclear risk assessment (Lauritzen *et al.*, 2006; 2007; Baklanov *et al.*, 2003; Mahura *et al.*, 2003; 2005).

The main objective of DERM is to predict the dispersion of a radioactive plume and the accompanied deposition. However, the model may also be used in situations where an increased level of radioactivity has been measured but no information is received on radioactive releases. In such cases, inverse (adjoint) modelling may be applied whereby potential sources of radioactivity may be localised and release rates estimated.

The three-dimensional model is of Lagrangian type making use of a hybrid stochastic particle-puff diffusion description, and it is currently capable of describing plumes at downwind distances up to the global scale (Sørensen *et al.*, 1998). The model utilizes aerosol size dependent dry and wet deposition parameterisations as described by Baklanov and Sørensen (2001).

Currently, DERMA makes use of analysed and forecasted meteorological data from the numerical weather prediction model DMI-HIRLAM covering Denmark, Greenland and the Faeroes (Sass *et al.*, 2002) and from the global model developed and operated by the European Centre for Medium-range Weather Forecasts (ECMWF).

DERMA is interfaced with the Accident Reporting and Guidance Operational System (ARGOS) (Hoe *et al.*, 1999; 2002), a PC based nuclear decision-support system developed by DEMA and the Prolog Development Center A/S (PDC). The integration of DERMA with the ARGOS system is effectuated through automated online digital communication and exchange of data between the ARGOS system and the DMI High Performance Computing (HPC) facility.

### Case studies

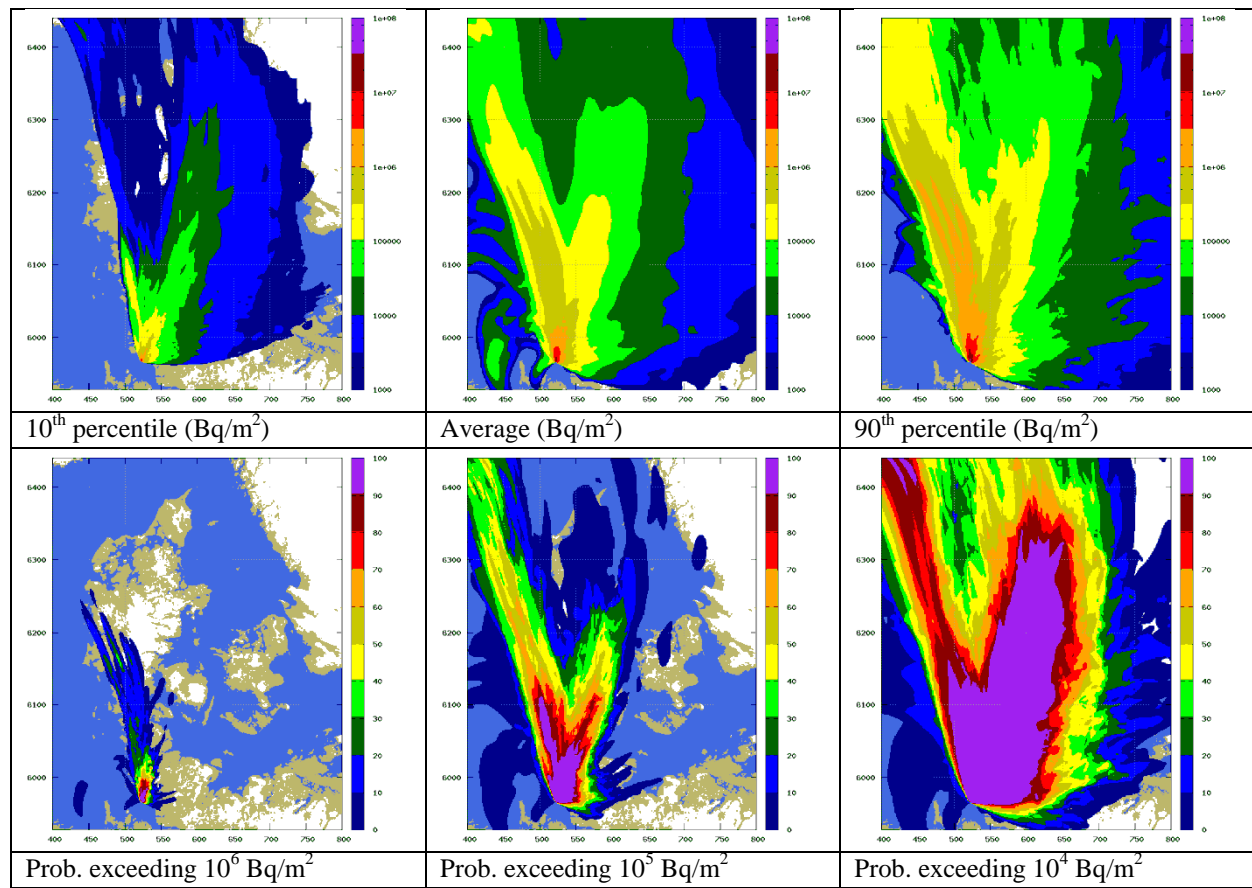
The RIMPUFF model has been implemented at the DMI supercomputer, and with the selected accidental release scenario RIMPUFF is applied to each member of the meteorological ensembles corresponding to the meteorological cases. The methodology of calculating and presenting uncertainties, developed in course of the NKS-B projects MUD and FAUNA, has been applied to the short-range dispersion model results. Furthermore, for the same cases, RIMPUFF has been applied in hindcast mode in two versions, one includes the use of weather radar data in combination with NWP model data, the other is based on pure NWP model data.

Figure 19–Figure 22 below concern prediction of accumulated deposition of Cs-137 valid at 2016-03-03, 12 UTC. The release begins at 2016-03-01, 12 UTC.

Figure 23 and Figure 24 concern prediction of time-integrated concentration of I-131 valid at 2016-04-29, 12 UTC. The release begins at 2016-04-27, 12 UTC.

In appendices A and B, comprehensive sets of figures are presented corresponding to the four selected meteorological cases. Results are here given for the short-range dispersion model RIMPUFF based on both forecast and analysed NWP model data as well as analysed NWP model data together with weather radar data. Results are also given for the long-range dispersion model DERMA based on both forecast and analysed NWP model data.

In appendix C, time series are given of the instantaneous precipitation rate, as derived from the measured radar reflectivity, for the four meteorological scenarios selected.



**Figure 19** RIMPUFF prediction based on 48 hour **forecast** NWP model data.

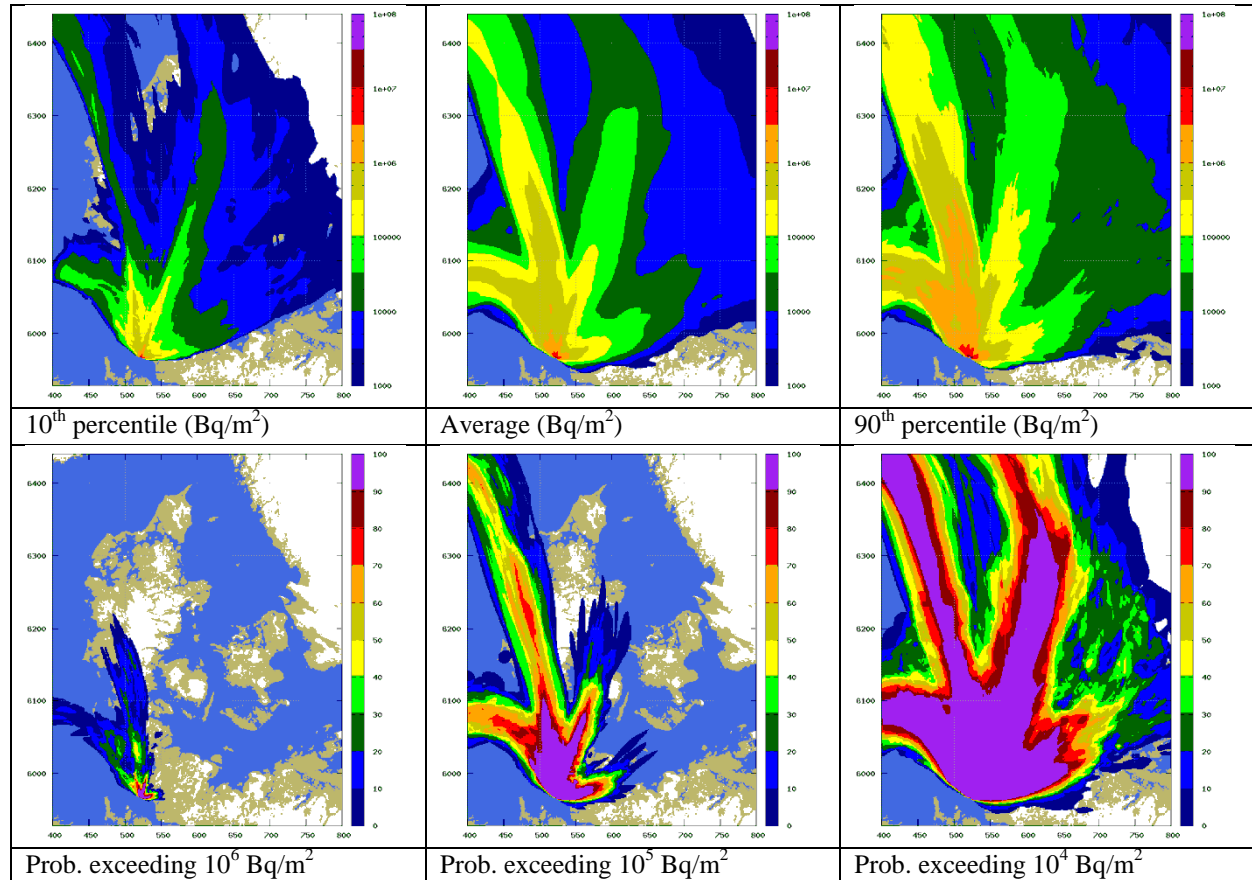


**Figure 20** RIMPUFF prediction based on **analysed** NWP model data.

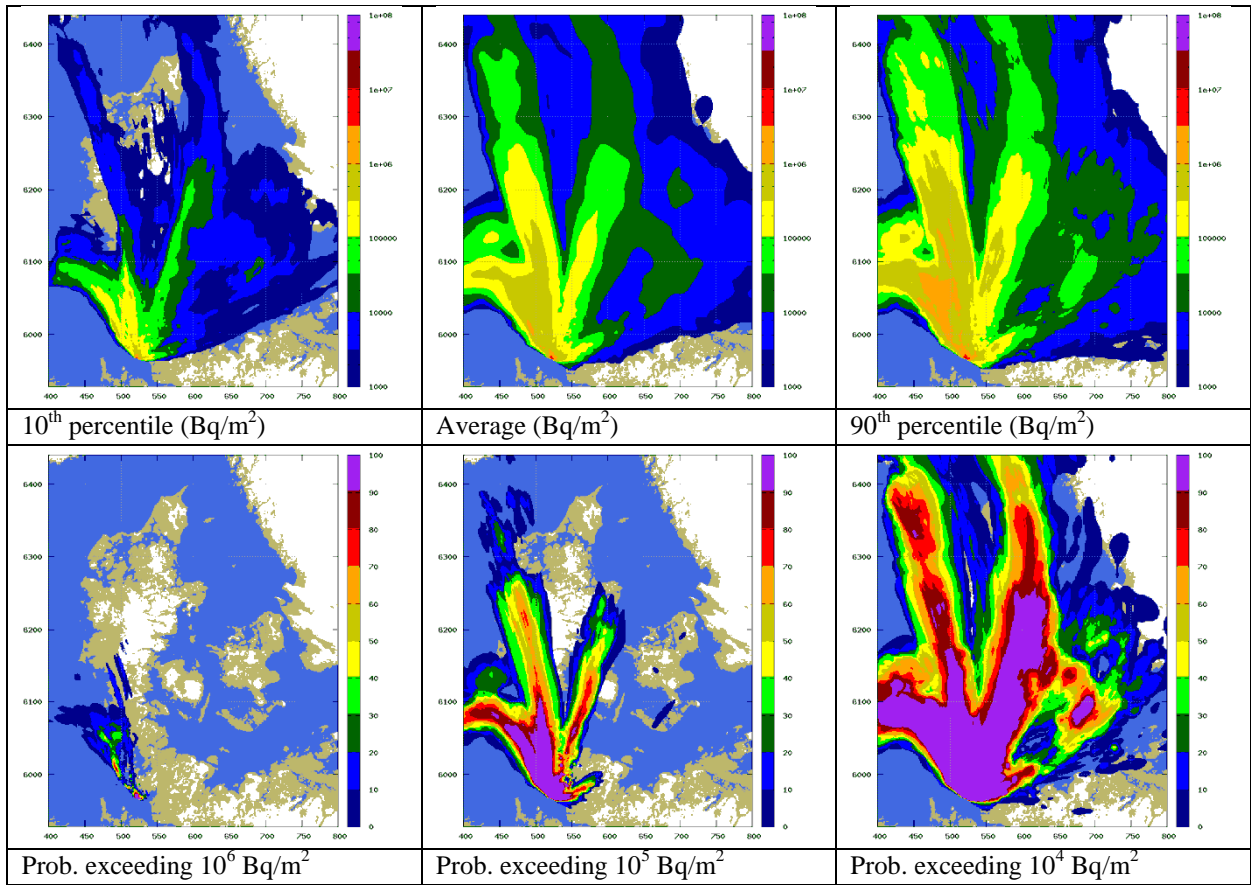


**Figure 21** RIMPUFF prediction based on analysed NWP model data and weather radar estimated precipitation.

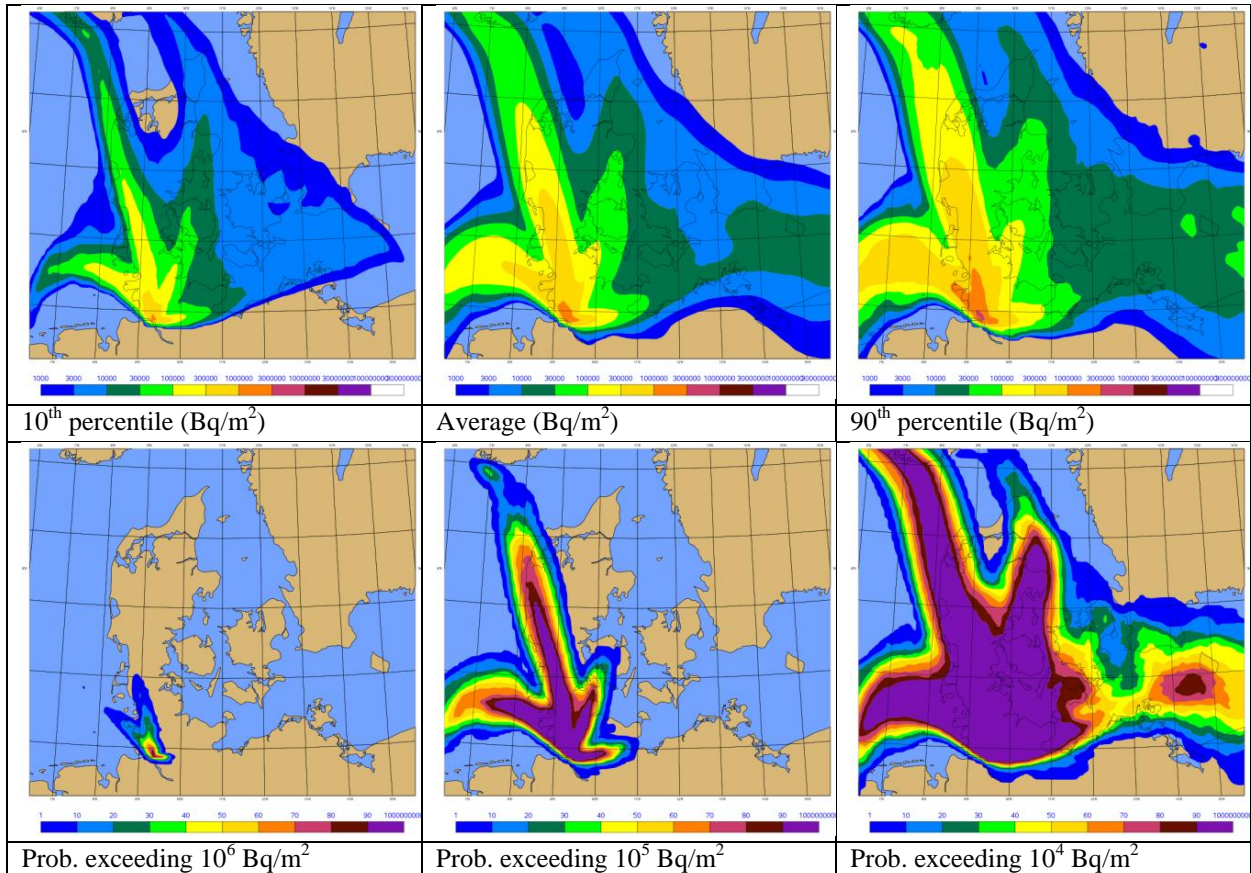


**Figure 22** DERMA prediction based on analysed NWP model data.

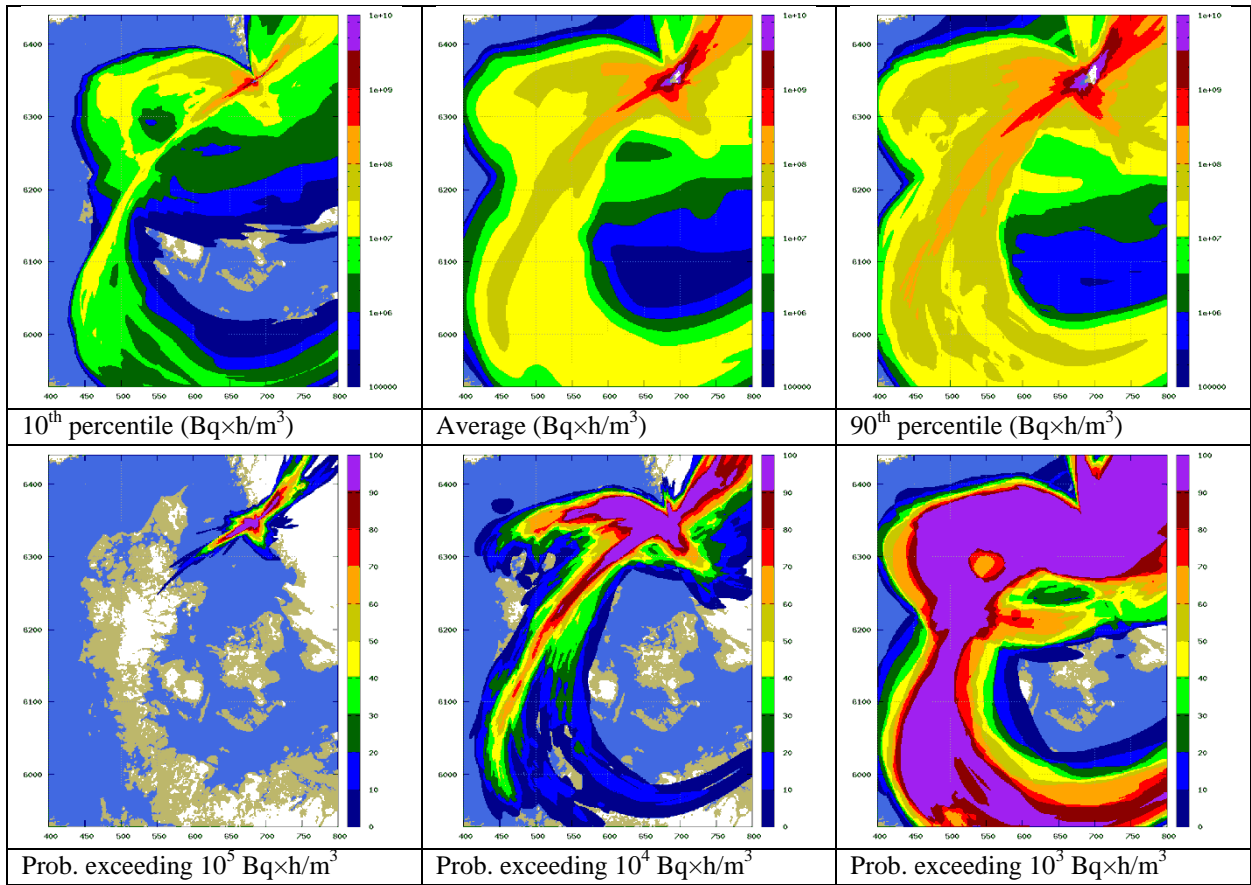


**Figure 23** RIMPUFF prediction based on analysed NWP model data.

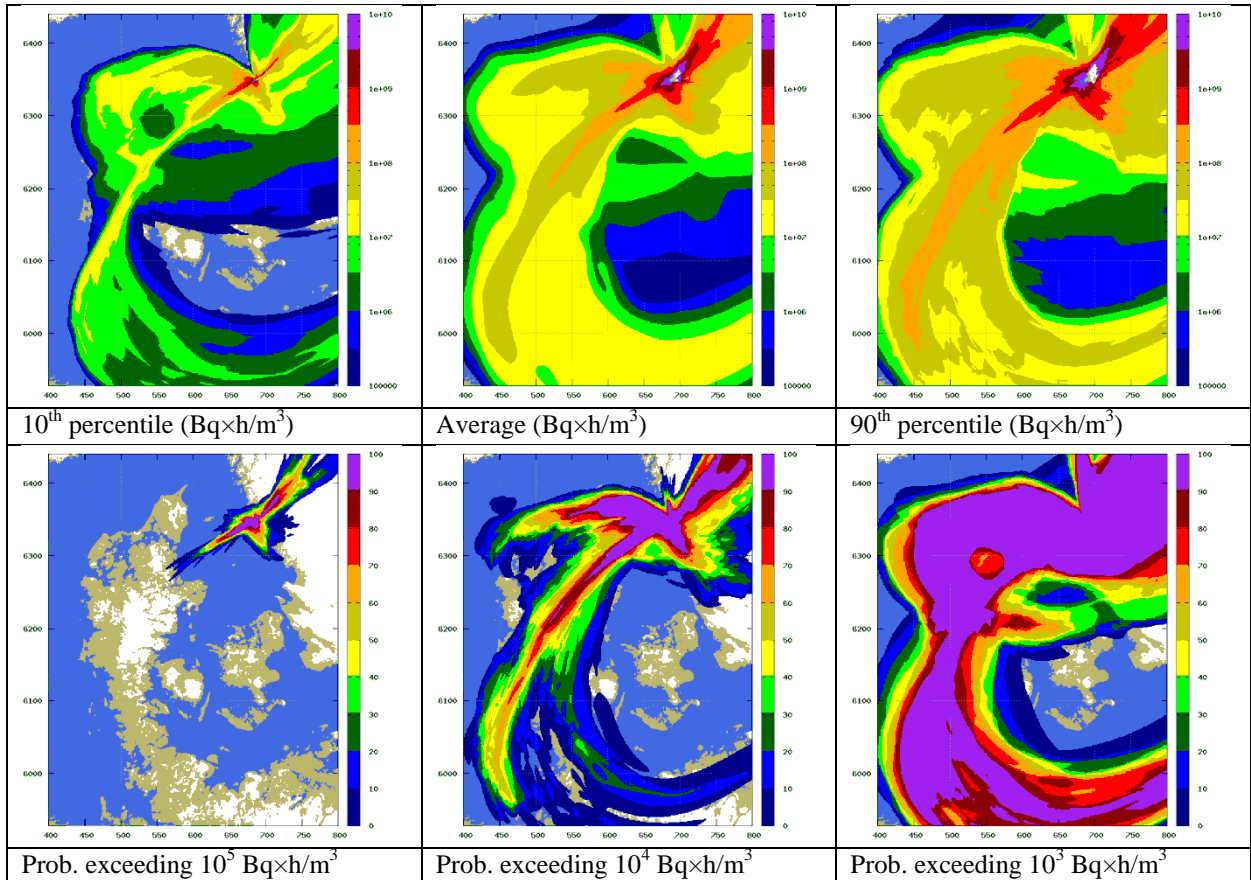


**Figure 24** RIMPUFF prediction based on analysed NWP model data and weather radar estimated precipitation.

## **Discussion and conclusions**

In the MUD and FAUNA projects (Sørensen *et al.*, 2014; 2016), the influence of meteorological uncertainty of NWP model data on atmospheric dispersion modelling was studied at the long-range scale (from about 10 km from source and up to the global scale). Depending on the weather scenario, differences between a low and a large percentile of concentration and deposition values could be up to one or two orders of magnitude corresponding to an uncertainty of a factor of three to five. One of the questions that the MESO project aimed at answering was if this applies also at short range (from about 2 to 100 km from the source)?

In brief, the results of MESO show that there is a large influence of NWP model uncertainty on atmospheric dispersion also at short range, even close in at the kilometre scale (the near range). The variability is, however, less than at long range. Expressed as a factor, uncertainties of a factor of two to three can easily be observed at short range.

As expected, the short-range model RIMPUFF and the long-range model DERMA differ from about 100 km from source and beyond. Closer to the source, from zero to 50 km, we also see differences with RIMPUFF in general providing larger localised concentration and deposition values than DERMA.

In addition to studying how the uncertainty of NWP model data affects short-range atmospheric dispersion, the effect of using weather-radar estimated precipitation instead of model estimates is considered for wet deposition modelling. In general, the result is that this effect is smaller than that of the NWP model data for the meteorological cases considered. However, in other cases with well localised intense rainfalls, which are in general not well predicted by NWP models, one might observe larger effects.

Using weather-radar estimated precipitation intensities is an improvement compared with pure model precipitation. However, as described in the present report there are also a number of sources of uncertainty and potential errors when using radar data. A future radar product in which the estimated precipitation intensities are calibrated with real-time data of a monitoring network of rain gauges may well improve the situation.

There is a large benefit for nuclear emergency preparedness and management from taking into account the meteorological uncertainties. By including the meteorological uncertainties in the decision process, the risk of making decisions based on an incorrect prediction of the dispersion is much reduced. In other words, by assessing the uncertainties a more comprehensive basis for the decision making is provided.

However, the use of quantitative uncertainty estimates requires education and training of emergency response staff, and careful communication between experts and decision makers.

Ensemble modelling is the future of numerical weather prediction, and as shown there are large effects also for atmospheric dispersion prediction. Therefore, application of the methodology developed in MUD should be introduced in nuclear decision support systems in the near future.

There is an additional source of uncertainty for nuclear emergency management, namely that of the source term, i.e. the temporal evolution of the release of the various different

radionuclides from a nuclear accident. This, often quite large uncertainty, interferes with the meteorological uncertainty, and it will be important to quantify the combined uncertainty.

## References

- Baklanov, A. and J. H. Sørensen. Parameterisation of radionuclide deposition in atmospheric dispersion models. *Phys. Chem. Earth* **26** (2001) 787–799
- Baklanov, A., A. Mahura and J. H. Sørensen. Methodology for Prediction and Estimation of Consequences of Possible Atmospheric Releases of Hazardous Matter: ‘Kursk’ Submarine Study. *Atmos. Phys. Chem. Vol.* **3** (2003) 747–762
- Battan, L.J. Radar Observations of the Atmosphere, Univ. of Chicago Press, 323, 1973
- Bech, J. and Chau, J.L., editors. Doppler Radar Observations – Weather Radar, Wind Profiler, Ionospheric Radar, and Other Advanced Applications. InTech, 2012
- Briggs, G.A. Plume rise predictions. In: Lectures on Air Pollution and Environmental Impact Analyses, pp. 59-111, American Meteorological Society, Boston, 1975
- Bringi, V.N., and Chandrasekar, V. Polarimetric Doppler Weather Radar: Principles and Applications. Cambridge University Press, New York, NY, USA, 2001
- Buizza, R., Miller, M.J. and Palmer, T.N. Stochastic representation of model uncertainties in the ECMWF ensemble prediction system. *Q.J.R. Meteorol. Soc.* **125** (1999) 2887–2908
- Bøvith, T. Detection of Weather Radar Clutter. Ph.D. Thesis. Technical University of Denmark, 2008
- Carruthers, D.J., R.J. Holroyd, J.C.R. Hunt, W.-S. Weng, A.G. Robins, D.D. Apsley, F.B. Smith, D.J. Thomson, and B. Hudson. UK Atmospheric Dispersion Modelling System. In: H. van Dop and G. Kallos. Air Pollution Modelling and its Application IX. pp. 15–28, Plenum Press, New York, 1992
- Feddersen, H. A short-range limited area ensemble prediction system at DMI. *DMI Tech. Rep.*, 09–14 (2009) <http://www.dmi.dk/dmi/tr09-14.pdf>
- García-Moya, J., Callado, A., Escribà, P., Santos, C., Santos-Muñoz, D. and Simarro, J. Predictability of short-range forecasting: a multimodel approach. *Tellus A* **63** (2011) 550–563
- Galmarini, S., R. Bianconi, W. Klug, T. Mikkelsen, R. Addis, S. Andronopoulos, P. Astrup, A. Baklanov, J. Bartnicki, J. C. Bartzis, R. Bellasio, F. Bompay, R. Buckley, M. Bouzom, H. Champion, R. D’Amours, E. Davakis, H. Eleveld, G. T. Geertsema, H. Glaab, M. Kollax, M. Ilvonen, A. Manning, U. Pechinger, C. Persson, E. Polreich, S. Potemski, M. Prodanova, J. Saltbones, H. Slaper, M. A. Sofiev, D. Syrakov, J. H. Sørensen, L. Van der Auwera, I. Valkama, R. Zelazny. Ensemble Dispersion Forecasting, Part I: Concept, Approach and Indicators. *Atmos. Environ.* **38** (2004) 4607–4617
- Gering, F., K. Richter, and H. Müller. Model Description of the Deposition Monitoring Module DeMM in RODOS PV5.0. RODOS(RA5)-TN(02)03. 2002  
<https://resy5.iket.kit.edu/RODOS/Documents/Public/HandbookV5/Volume3/DemmModel.pdf>
- Gill, R.S. DMI Radar Operational Products System (DROPS), Internal Report No. 10-06, Danish Meteorological Institute, Denmark, 2010

Gill, R.S, Sørensen, M.B., and Bøvith, T. Hydrometeor Classification using Polarimetric C-band Doppler Weather Radars, Scientific Report No. 12-04, Danish Meteorological Institute, Denmark, 2012

Gloster, J., A. Jones, A. Redington, L. Burgin, J. H. Sørensen, R. Turner. International approach to atmospheric disease dispersion modelling. *Veterinary Record* 03 (2010a) **166** (12):369. DOI:10.1136/vr.166.12.369a

Gloster, J., A. Jones, A. Redington, L. Burgin, J. H. Sørensen, R. Turner, P. Hullinger, M. Dillon, P. Astrup, G. Garner, R. D'Amours, R. Sellers and D. Paton. Airborne spread of foot-and-mouth disease – model intercomparison. *Veterinary Journal* **183** (2010b) 278–286

HIRLAM. <http://www.hirlam.org/index.php/hirlam-programme-53/general-model-description/48-synoptic-scale-model-hirlam>

Hoe, S., J. H. Sørensen and S. Thykier-Nielsen. The Nuclear Decision Support System ARGOS NT and Early Warning Systems in Some Countries around the Baltic Sea. In: Proceedings of the 7th Topical Meeting on Emergency Preparedness and Response, September 14–17, 1999, Santa Fe, New Mexico, USA

Hoe, S., H. Müller, F. Gering, S. Thykier-Nielsen and J. H. Sørensen. ARGOS 2001 a Decision Support System for Nuclear Emergencies. In: Proceedings of the Radiation Protection and Shielding Division Topical Meeting, April 14–17, 2002, Santa Fe, New Mexico, USA

Hou, D., E. Kalnay and K. K. Drogemeier. Objective verification of the SAMEX '98 ensemble forecasts. *Mon. Wea. Rev.* **129** (2001) 73–91

Højerup, C.F. FISPRO – an ALGOL procedure for calculation of fission products. Risø-M-1899. 1976

Kain, J. S. The Kain-Fritsch Convective Parameterization. An update. *J. Appl. Meteorol.* **43** (2004) 170–181

Karlsruhe Institute of Technology. JRodos: An off-site emergency management system for nuclear accidents. 2015

[https://resy5.iket.kit.edu/JRODOS/documents/JRodos\\_Report\\_forHomepage.pdf](https://resy5.iket.kit.edu/JRODOS/documents/JRodos_Report_forHomepage.pdf)

Lauritzen, B., A. Baklanov, A. Mahura, T. Mikkelsen and J. H. Sørensen. K-model description of probabilistic long-range atmospheric transport in the Northern Hemisphere. *Atmos. Environ.* **40** (2006) 4352–4369

Lauritzen, B., A. Baklanov, A. Mahura, T. Mikkelsen and J. H. Sørensen. Probabilistic risk assessment for long-range atmospheric transport of radionuclides. *J. Envir. Radioactivity* **96** (2007) 110–115

Löffler H, Mildenberger O, Sogalla M, Stahl, T. Aktualisierung der Quelltermbibliothek des Entscheidungshilfesystems RODOS für Ereignisse im Leistungsbetrieb. Abschlussbericht zum BMU-Vorhaben S3609S60009, GRS-A-3580, Gesellschaft für Anlagen- und Reaktorsicherheit (GRS), Oktober 2010  
Macdonald, R. [http://www.engga.uwo.ca/people/esavory/MME474A\\_Part1.pdf](http://www.engga.uwo.ca/people/esavory/MME474A_Part1.pdf)

Mahura, A., A. Baklanov and J. H. Sørensen. Methodology for evaluation of possible consequences of accidental atmospheric releases of hazardous matter. *Radiat. Prot. Dos.* **103** (2003) 131–139

Mahura, A. G., A. A. Baklanov, J. H. Sørensen, F. L. Parker, V. Novikov, K. Brown, K. L. Compton 2004: Assessment of Atmospheric Transport and Deposition Patterns Related to Russian Pacific Fleet Operations. *Environmental Monitoring and Assessment* **101** (2005) 261–287

Marshall, J.S. and Palmer, W.M.J. The distribution of raindrops with size. *Journal of Meteorology* **5(4)** (1948) pp. 165–166.

Meischner, P. editor. Weather Radar: Principles and Advanced Applications. Springer-Verlag, Berlin, Heidelberg, Germany, 2004

Mikkelsen, T., and S.E. Larsen. Description of the Risø Puff Diffusion Model. Nuclear Technology, vol. 67, pp. 56–65, 1984

Mikkelsen, T., and F. Desiato. Atmospheric dispersion models and pre-processing of meteorological data for real-time application. Radiation Protection Dosimetry, vol 50, nos.2-4, pp. 205–218, 1993

Mikkelsen, T., S. Alexandersen, H. Champion, P. Astrup, A. I. Donaldson, F. N. Dunkerley, J. Gloster, J. H. Sørensen and S. Thykier-Nielsen. Investigation of Airborne Foot-and-Mouth Disease Virus Transmission during Low-Wind Conditions in the Early Phase of the UK 2001 Epidemic. *Atmos. Chem. Phys. Disc.* **3** (2003) 677–703

PDC-ARGOS. <http://www.pdc-argos.com>

Rasch, P. J. and Kristjansson, J. E. A comparison of the CCM3 model climate using diagnosed and predicted condensate parameterizations. *J. Clim.* **11** (1998) 1587–1614

Sass, B. H. A research version of the STRACO cloud scheme. *DMI Tech. Rep.*, 02–10 (2002) <http://www.dmi.dk/dmi/tr02-10.pdf>

Skolnik, M.I. Introduction to Radar Systems. McGraw-Hill, New York, NY, USA, third edition, 2001

Sørensen, J. H. Sensitivity of the DERMA Long-Range Dispersion Model to Meteorological Input and Diffusion Parameters. *Atmos. Environ.* **32** (1998) 4195–4206

Sørensen, J. H., D. K. J. Mackay, C. Ø. Jensen and A. I. Donaldson. An integrated model to predict the atmospheric spread of foot-and-mouth disease virus. *Epidemiol. Infect.* (2000) 124, 577–590

Sørensen, J. H., C. Ø. Jensen, T. Mikkelsen, D. Mackay and A. I. Donaldson. Modelling the atmospheric spread of foot-and-mouth disease virus for emergency preparedness. *Phys. Chem. Earth* **26** (2001) 93–97

Sørensen, J. H., A. Baklanov and S. Hoe. The Danish Emergency Response Model of the Atmosphere. *J. Envir. Radioactivity* **96** (2007) 122–129

Sørensen, J. H., B. Amstrup, H. Feddersen, U. S. Korsholm, J. Bartnicki, H. Klein, P. Wind, B. Lauritzen, S. C. Hoe, C. Israelson, and J. Lindgren. Meteorological Uncertainty of atmospheric Dispersion model results (MUD). **NKS-307** ISBN 978-87-7893-385-0, [http://www.nks.org/en/nks\\_reports/view\\_document.htm?id=111010212220490](http://www.nks.org/en/nks_reports/view_document.htm?id=111010212220490) (2014)

Sørensen, J.H., B. Amstrup, H. Feddersen, J. Bartnicki, H. Klein, M. Simonsen, B. Lauritzen, S. C. Hoe, C. Israelson and J. Lindgren. Fukushima Accident: UNcertainty of Atmospheric dispersion modelling (FAUNA). **NKS-360** ISBN 978-87-7893-444-4 (2016), <http://www.nks.org/scripts/getdocument.php?file=111010213440189>

Thykier-Nielsen, S., S. Deme, and E. Lang. Calculation method for Gamma-Dose Rates from Spherical Puffs. Risø-R-692(EN), 1993

Thykier-Nielsen, S., S. Deme, T. Mikkelsen. Description of the Atmospheric Dispersion Module RIMPUFF. RODOS(WG2)-TN(98)-02, 1999  
[https://resy5.iket.kit.edu/RODOS/Documents/Public/HandbookV5/Volume3/4\\_2\\_6\\_RIMPUFF.pdf](https://resy5.iket.kit.edu/RODOS/Documents/Public/HandbookV5/Volume3/4_2_6_RIMPUFF.pdf)

Uijlenhoet, R. Raindrop size distributions and radar reflectivity? Rain rate relationships for radar hydrology. *Hydrology and Earth System Sciences Discussions*, European Geosciences Union (2001) **5(4)** pp. 615–628.

Ulden, A.P. van, and A.A.M. Holtslag. Estimation of Atmospheric Boundary Layer Parameters for Diffusion Applications. *Journal of climate and applied meteorology*, vol. 24, pp. 1196–1207, 1985

Undén, P. and co-authors. HIRLAM-5 Scientific Documentation, 144 pp, available from <http://hirlam.org> (2002)

## Appendix A

### Short-range dispersion results

Release from Brokdorf NPP starting at 12 UTC on 2016-03-01

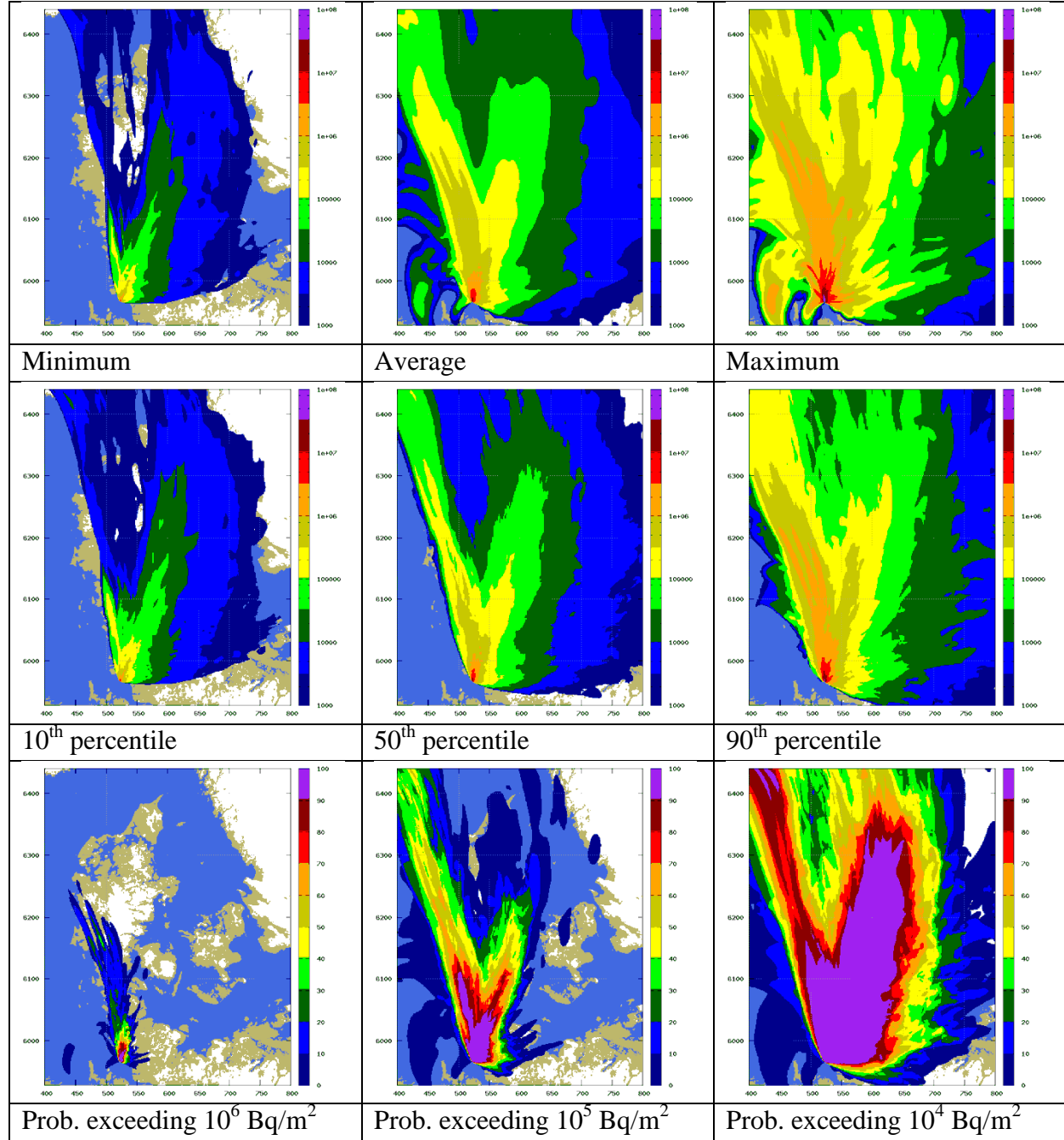


**Figure 25** RIMPUFF prediction of accumulated **deposition** ( $\text{Bq}/\text{m}^2$ ) of Cs-137 valid at 2016-03-03, 12 UTC, based on 48 hour forecast NWP model data. Release begins at **2016-03-01, 12 UTC**.

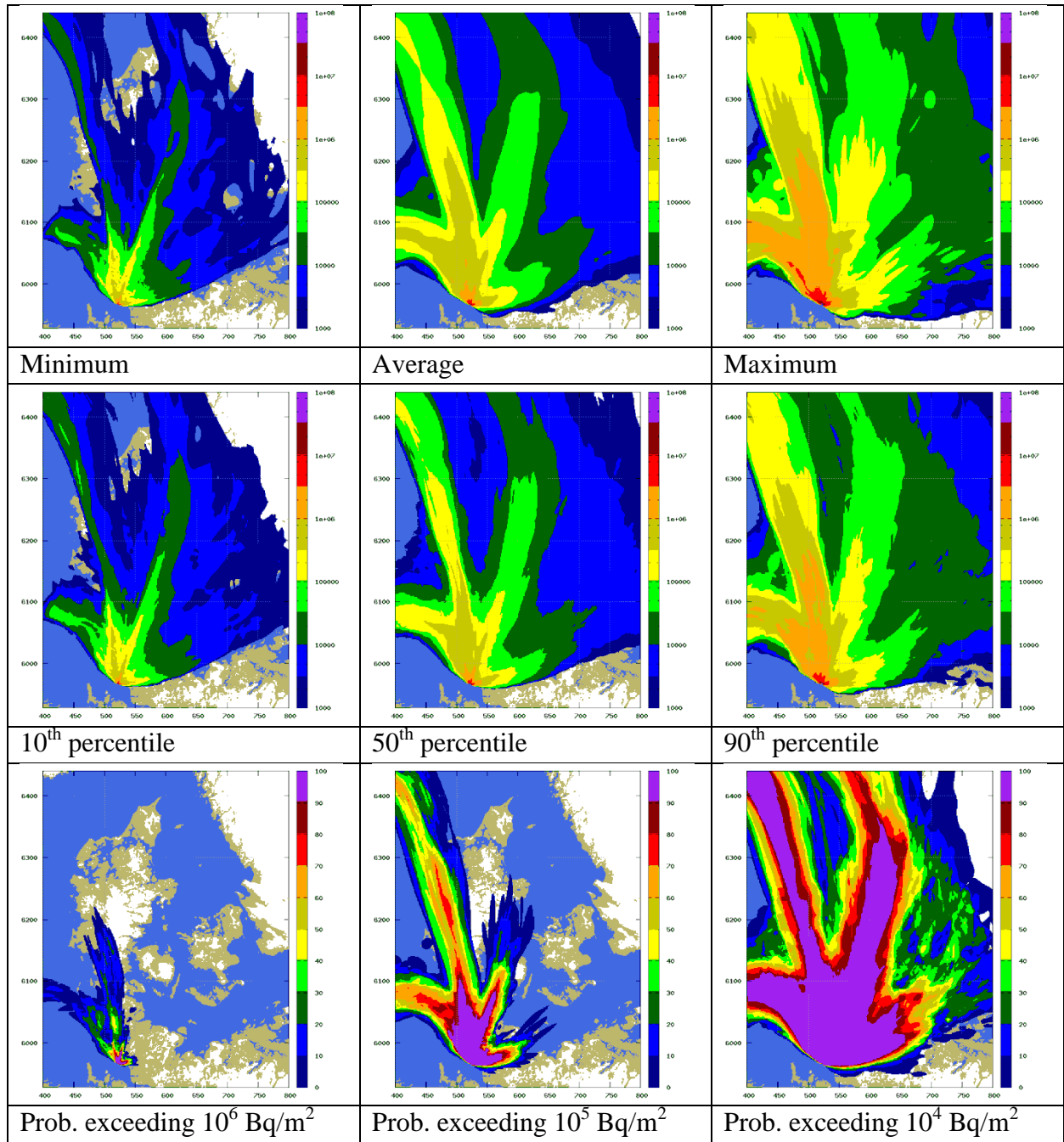


**Figure 26** RIMPUFF prediction of accumulated deposition ( $\text{Bq}/\text{m}^2$ ) of Cs-137 valid at 2016-03-03, 12 UTC, based on analysed NWP model data. Release begins at 2016-03-01, 12 UTC.

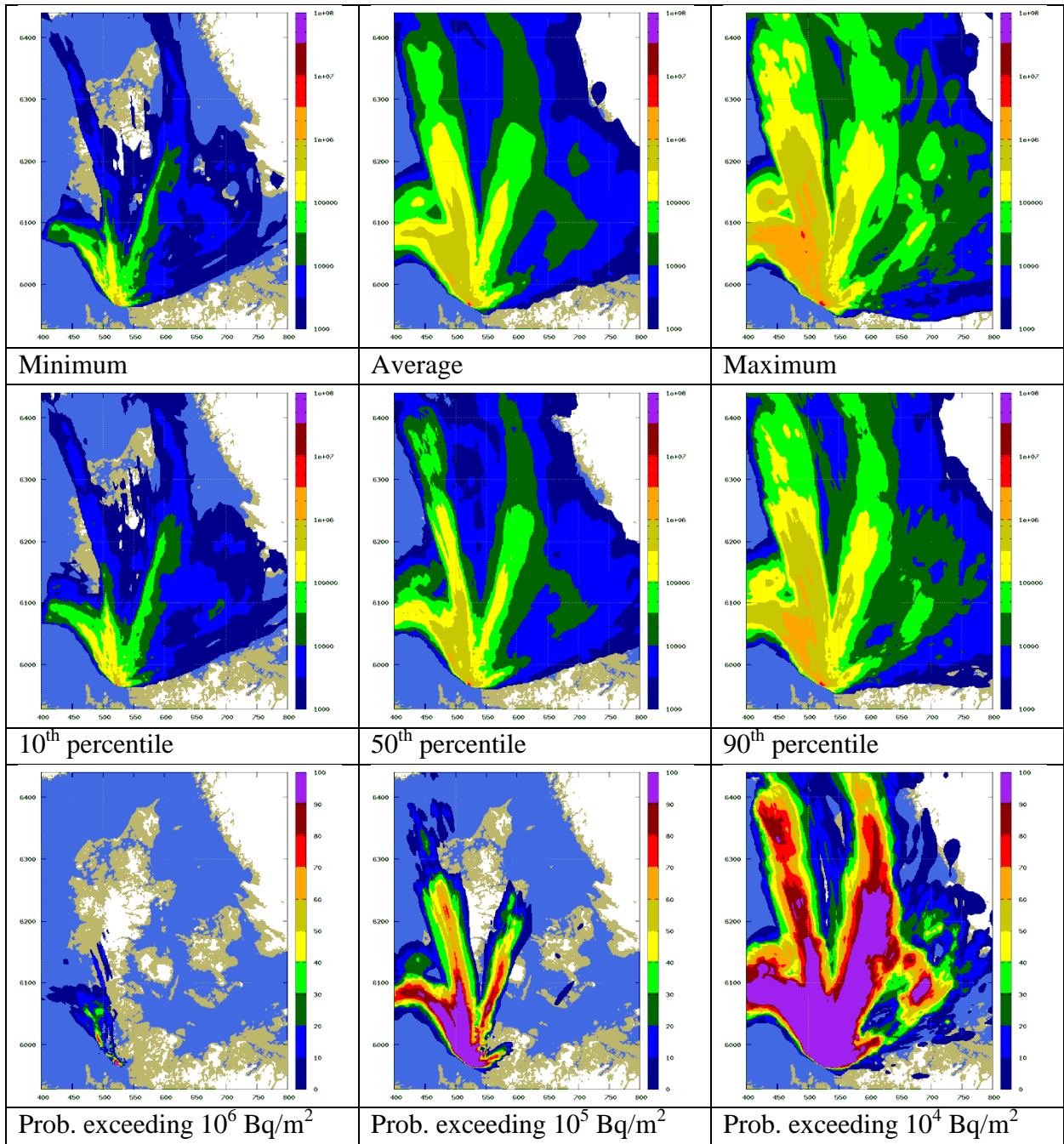


**Figure 27** RIMPUFF prediction of accumulated deposition ( $\text{Bq}/\text{m}^2$ ) of Cs-137 valid at 2016-03-03, 12 UTC, based on analysed NWP model data and weather radar estimated precipitation. Release begins at **2016-03-01, 12 UTC**.

Release from Brokdorf NPP starting at 00 UTC on 2016-03-28

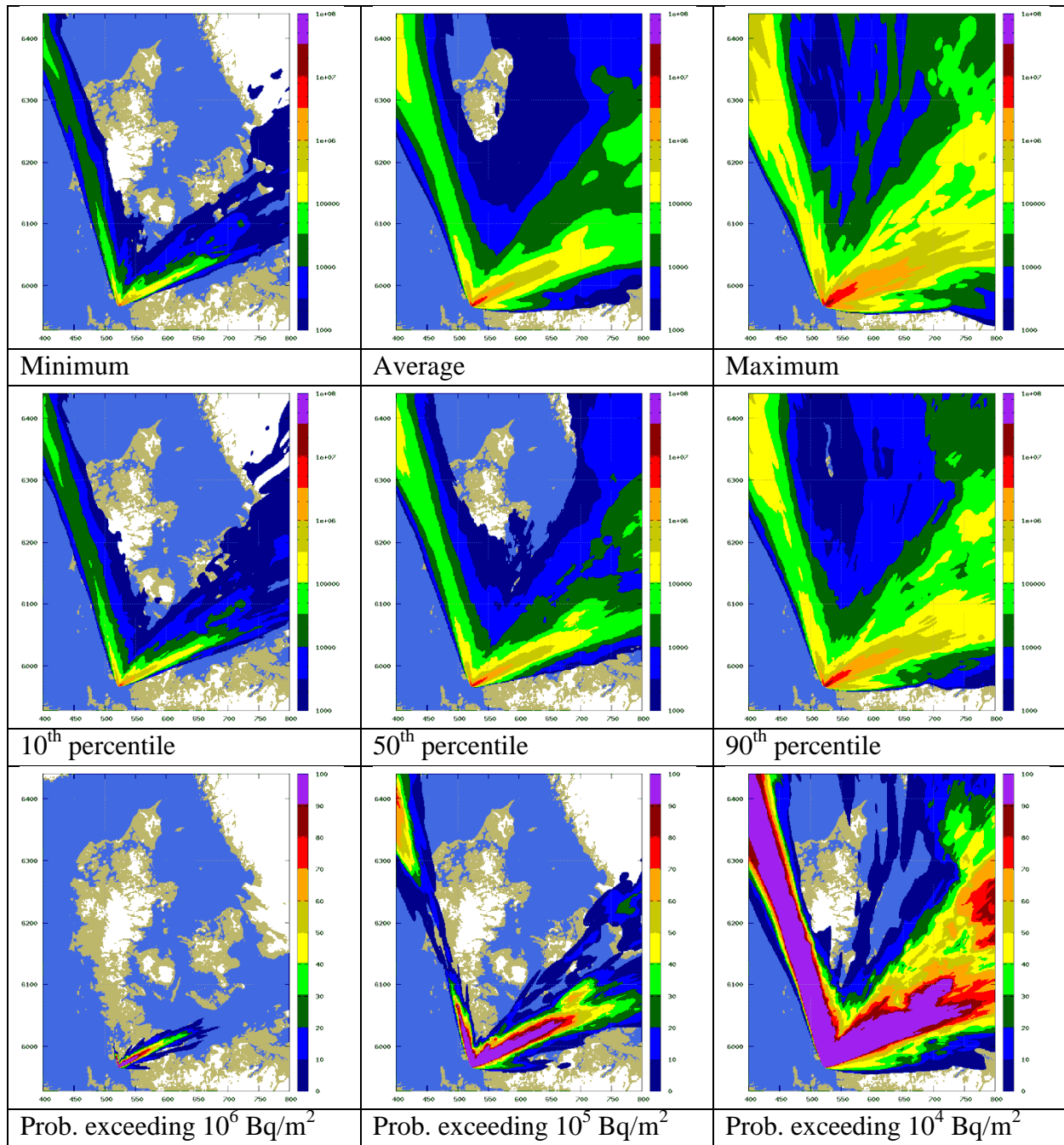


**Figure 28** RIMPUFF prediction of accumulated **deposition** ( $\text{Bq}/\text{m}^2$ ) of Cs-137 valid at 2016-03-30, 00 UTC, based on 48 hour **forecast** NWP model data. Release begins at **2016-03-28, 00 UTC**.

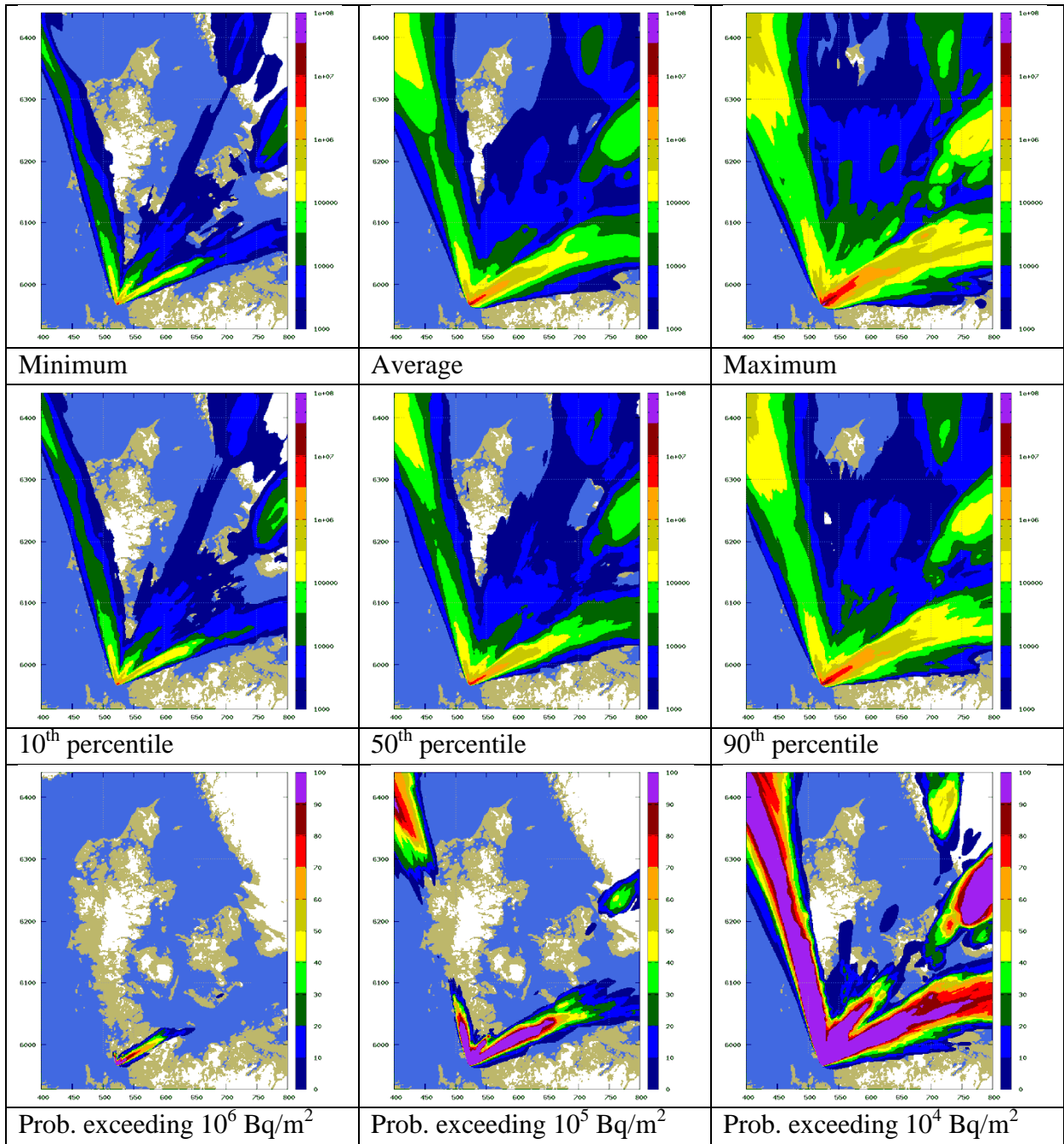


**Figure 29** RIMPUFF prediction of accumulated deposition ( $\text{Bq}/\text{m}^2$ ) of Cs-137 valid at 2016-03-30, 00 UTC, based on analysed NWP model data. Release begins at 2016-03-28, 00 UTC.

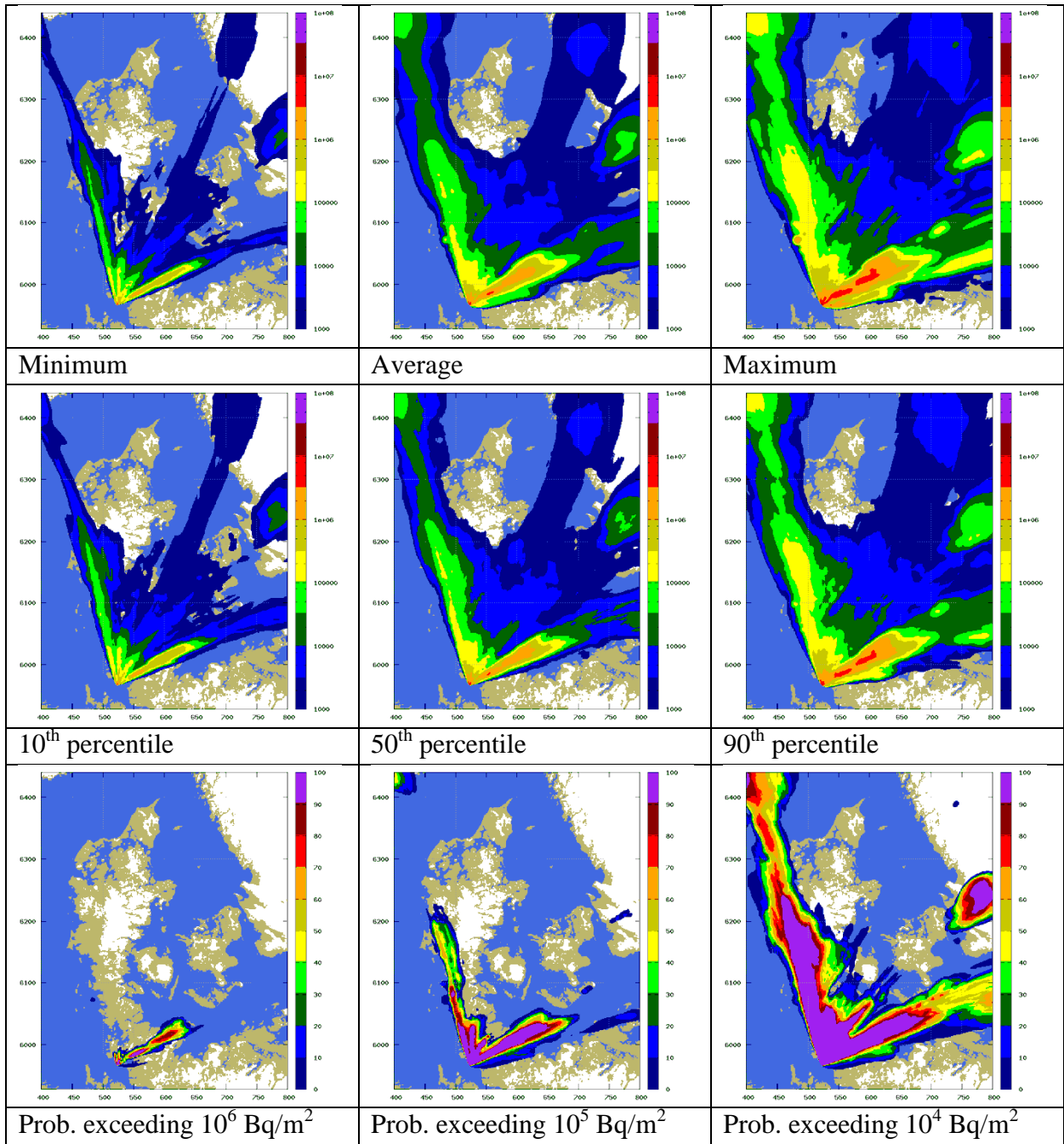


**Figure 30** RIMPUFF prediction of accumulated deposition ( $\text{Bq}/\text{m}^2$ ) of Cs-137 valid at 2016-03-30, 00 UTC, based on analysed NWP model data and weather radar estimated precipitation. Release begins at 2016-03-28, 00 UTC.

Release from Ringhals NPP starting at 12 UTC on 2016-04-27

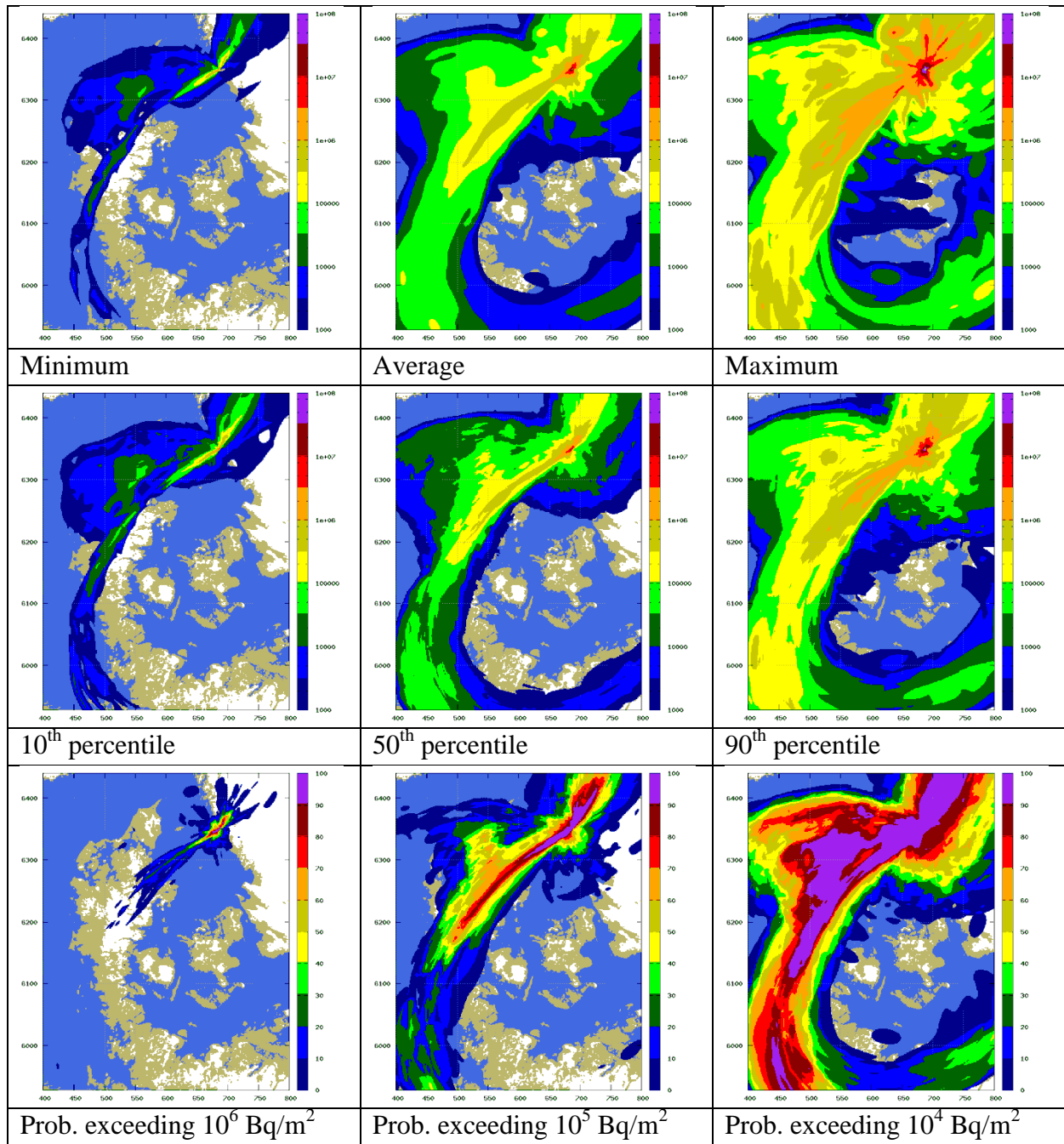


**Figure 31** RIMPUFF prediction of accumulated **deposition** ( $\text{Bq}/\text{m}^2$ ) of Cs-137 valid at 2016-04-29, 12 UTC, based on 48 hour **forecast** NWP model data. Release begins at **2016-04-27, 12 UTC**.

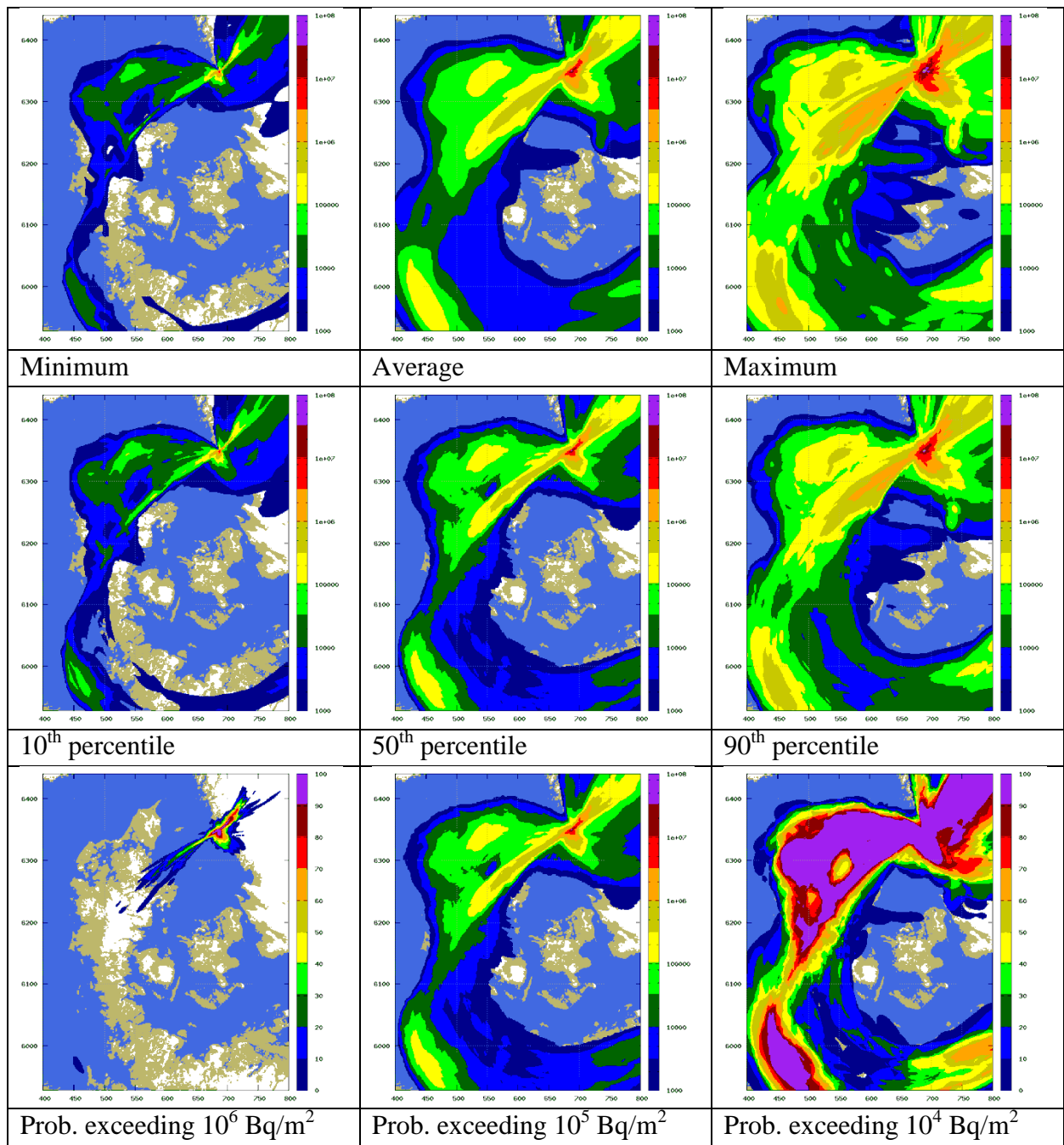


**Figure 32** RIMPUFF prediction of accumulated deposition ( $\text{Bq}/\text{m}^2$ ) of Cs-137 valid at 2016-04-29, 12 UTC, based on analysed NWP model data. Release begins at 2016-04-27, 12 UTC.

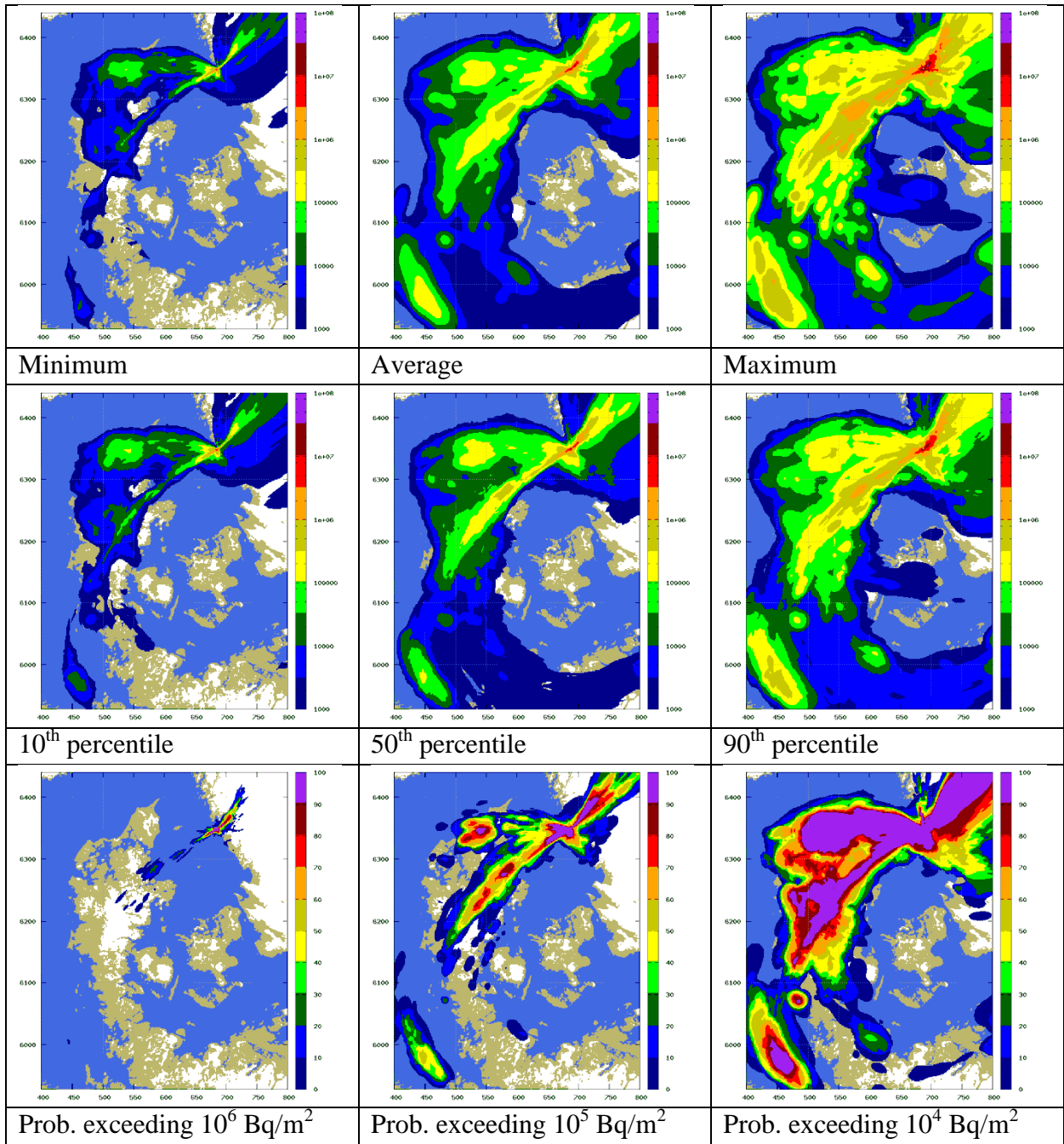


**Figure 33** RIMPUFF prediction of accumulated deposition ( $\text{Bq}/\text{m}^2$ ) of Cs-137 valid at 2016-04-29, 12 UTC, based on analysed NWP model data and weather radar estimated precipitation. Release begins at **2016-04-27, 12 UTC**.

Release from Brokdorf NPP starting at 06 UTC on 2016-04-29

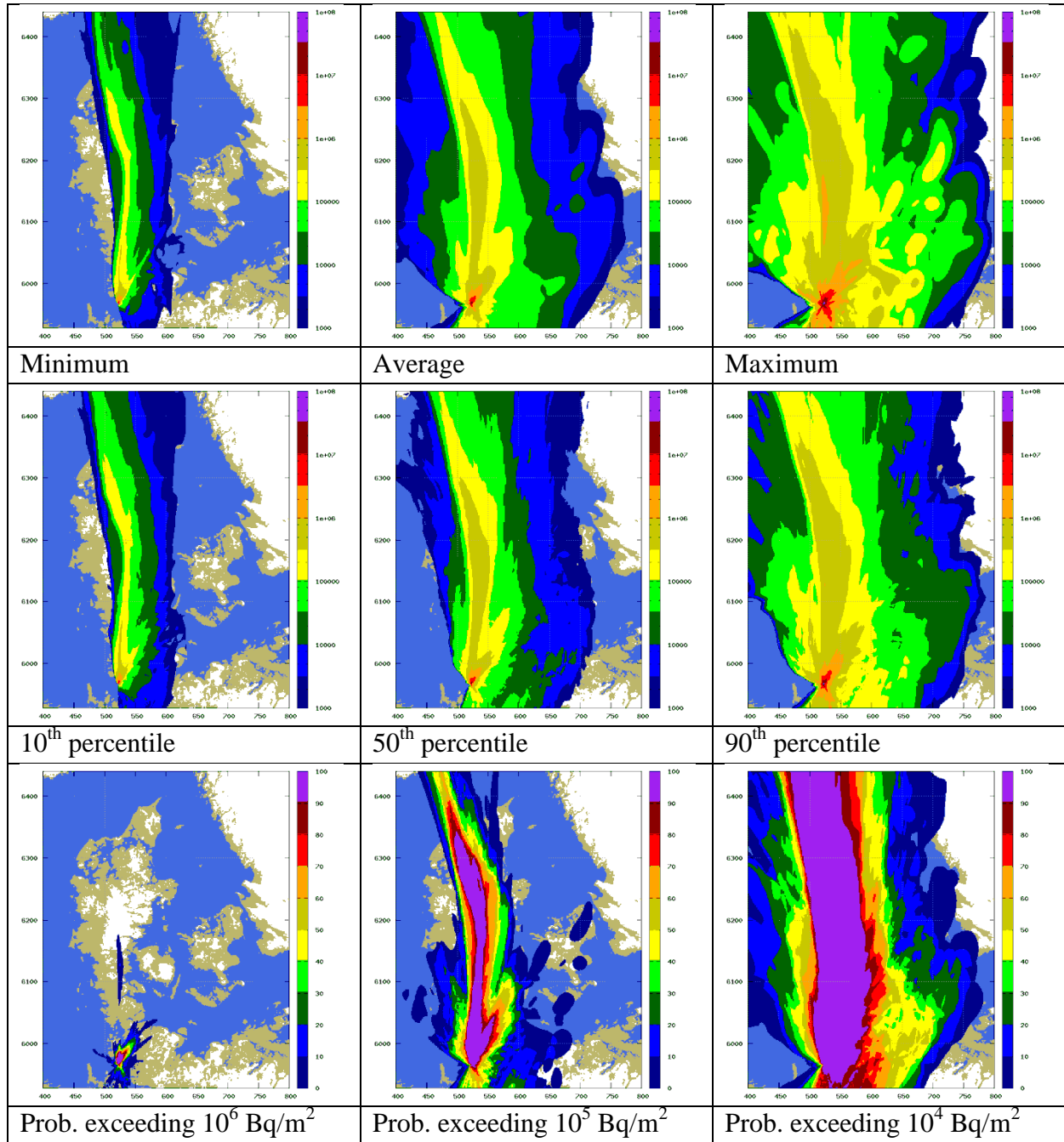


**Figure 34** RIMPUFF prediction of accumulated **deposition** ( $\text{Bq}/\text{m}^2$ ) of Cs-137 valid at 2016-05-01, 06 UTC, based on 48 hour **forecast** NWP model data. Release begins at **2016-04-29, 06 UTC**.

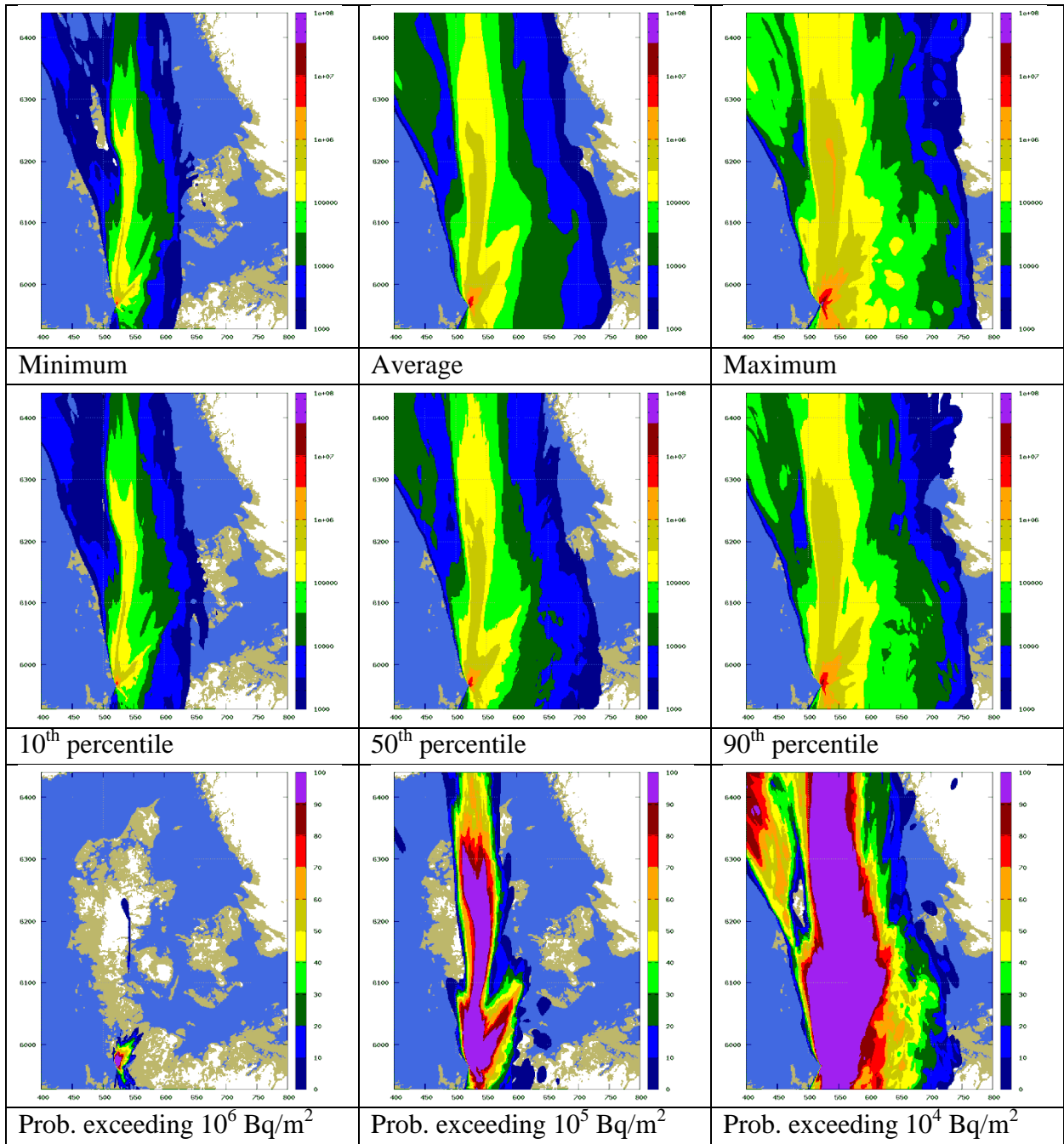


**Figure 35** RIMPUFF prediction of accumulated deposition (Bq/m<sup>2</sup>) of Cs-137 valid at 2016-05-01, 06 UTC, based on analysed NWP model data. Release begins at 2016-04-29, 06 UTC.

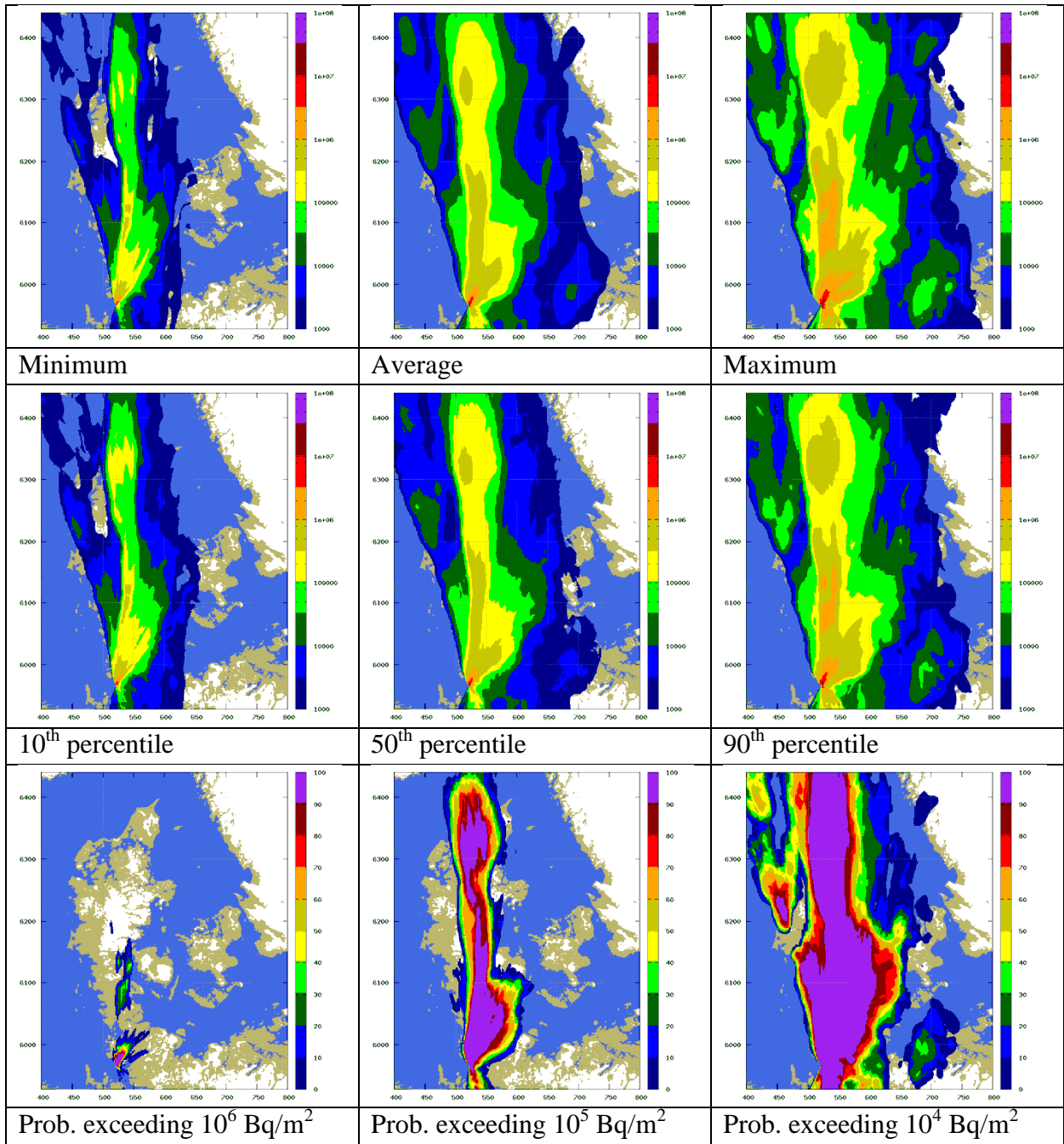


**Figure 36** RIMPUFF prediction of accumulated deposition ( $\text{Bq}/\text{m}^2$ ) of Cs-137 valid at 2016-05-01, 06 UTC, based on analysed NWP model data and weather radar estimated precipitation. Release begins at **2016-04-29, 06 UTC**.

## Appendix B

### Long-range dispersion results

Release from Brokdorf NPP starting at 12 UTC on 2016-03-01

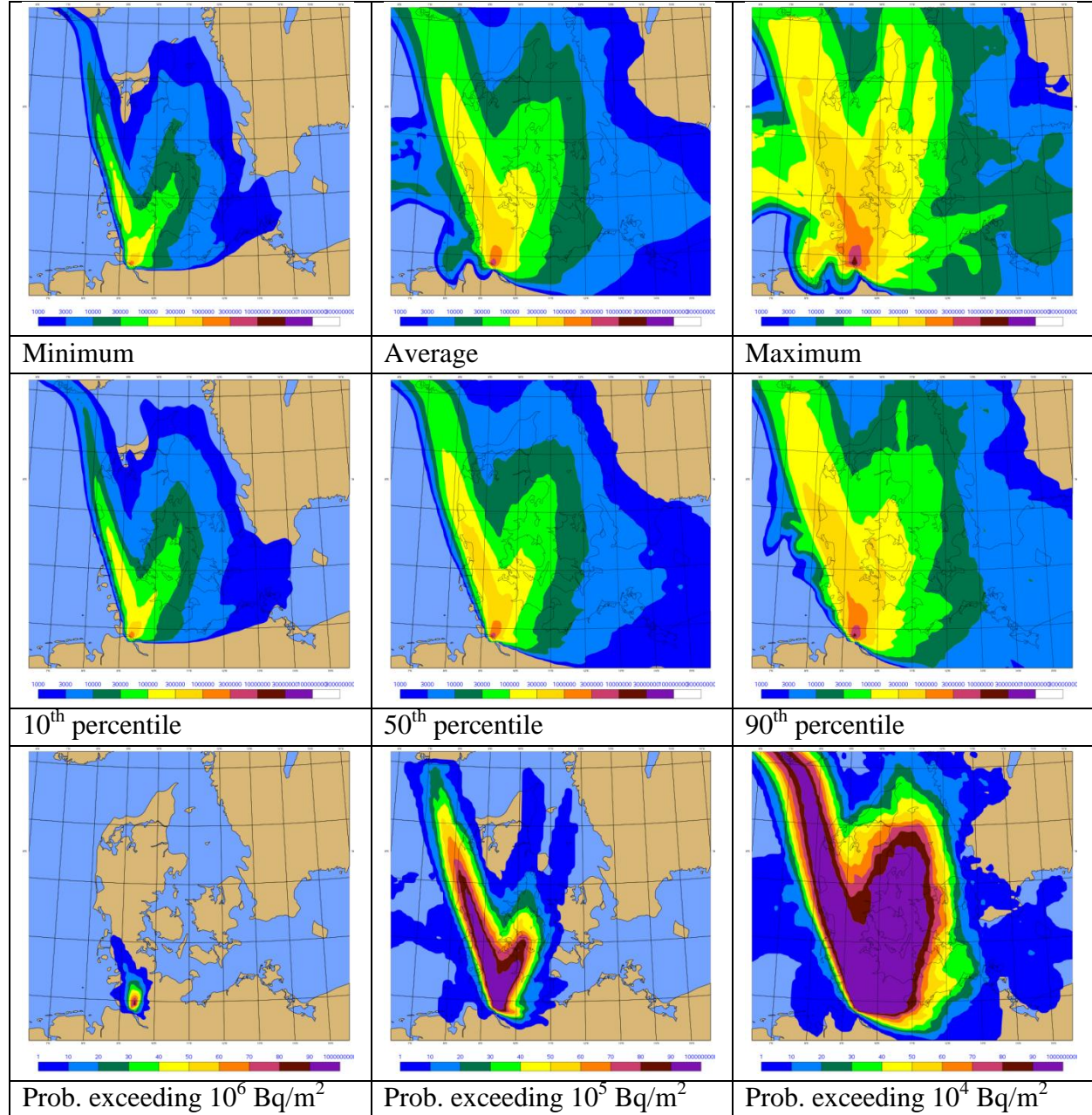


**Figure 37** DERMA prediction of accumulated **deposition** ( $\text{Bq}/\text{m}^2$ ) of **Cs-137** valid at 2016-03-03, 12 UTC, based on 48 hour **forecast** NWP model data. Release begins at **2016-03-01, 12 UTC**.

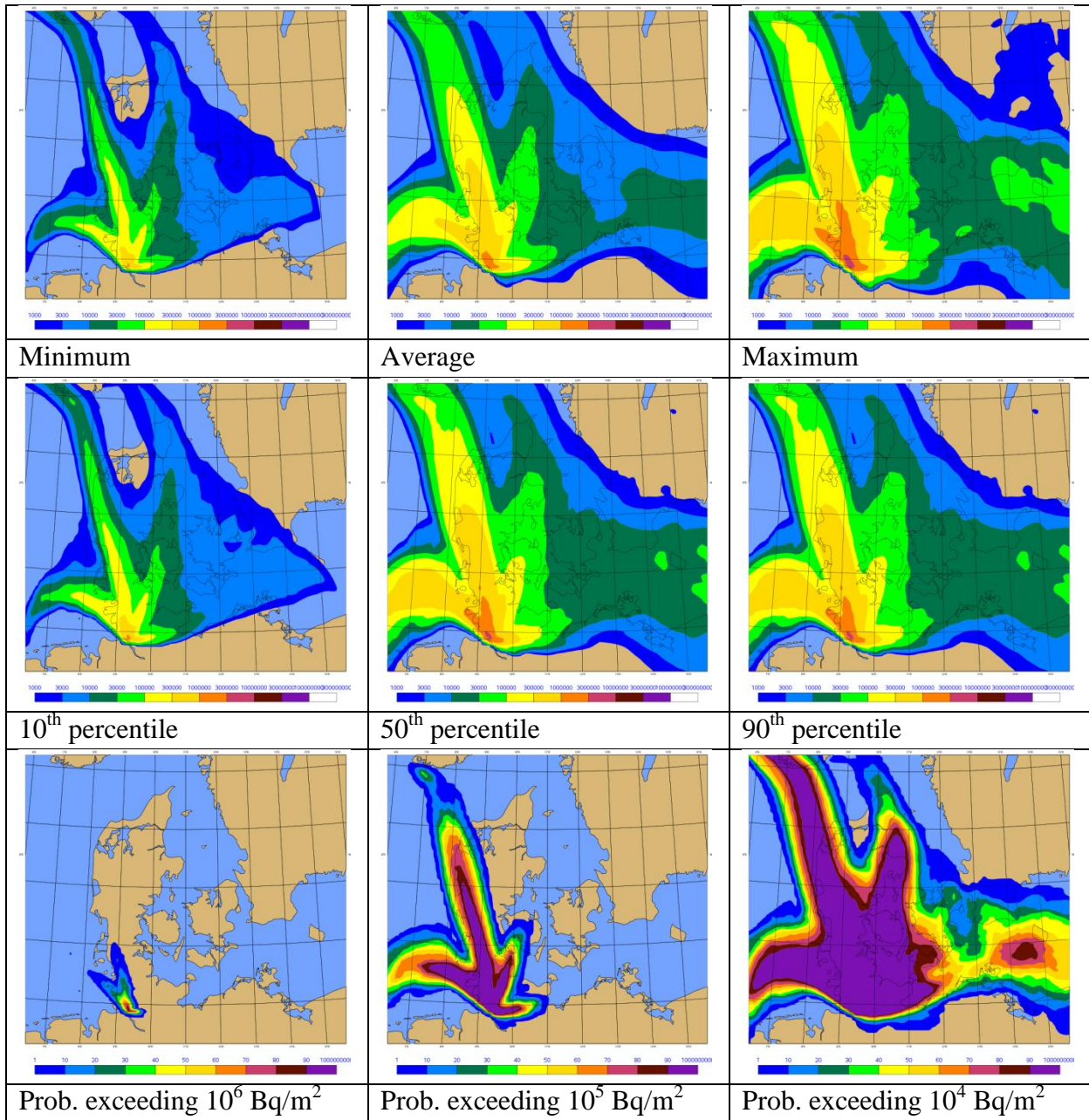


**Figure 38** DERMA prediction of accumulated **deposition** ( $\text{Bq}/\text{m}^2$ ) of **Cs-137** valid at 2016-03-03, 12 UTC, based on analysed NWP model data. Release begins at **2016-03-01, 12 UTC**.

Release from Brokdorf NPP starting at 00 UTC on 2016-03-28

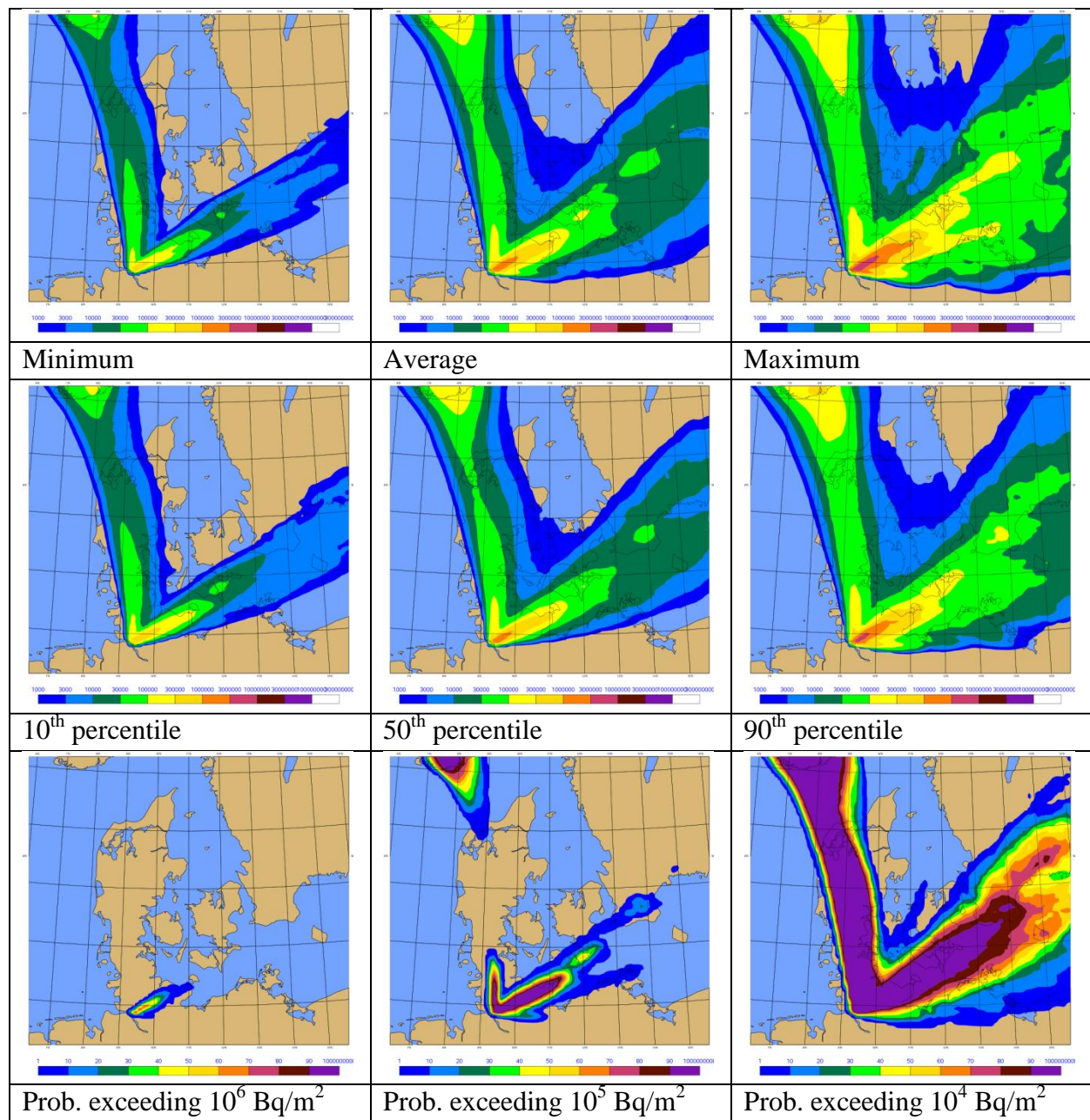


**Figure 39** DERMA prediction of accumulated **deposition** ( $\text{Bq}/\text{m}^2$ ) of **Cs-137** valid at 2016-03-30, 00 UTC, based on 48 hour **forecast** NWP model data. Release begins at **2016-03-28, 00 UTC**.

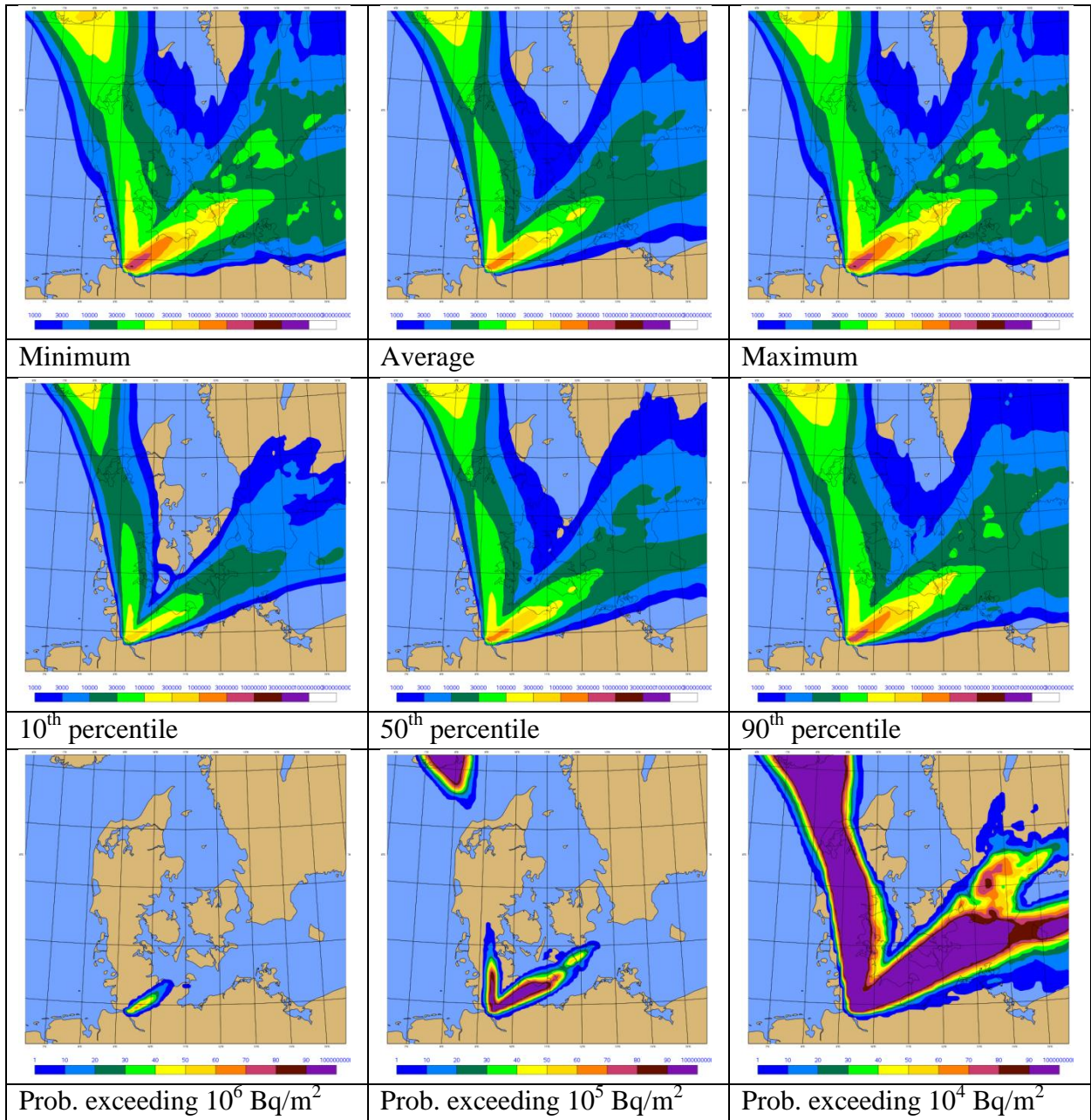


**Figure 40** DERMA prediction of accumulated **deposition** ( $\text{Bq}/\text{m}^2$ ) of **Cs-137** valid at 2016-03-30, 00 UTC, based on analysed NWP model data. Release begins at 2016-03-28, 00 UTC.

**Release from Ringhals NPP starting at 12 UTC on 2016-04-27**

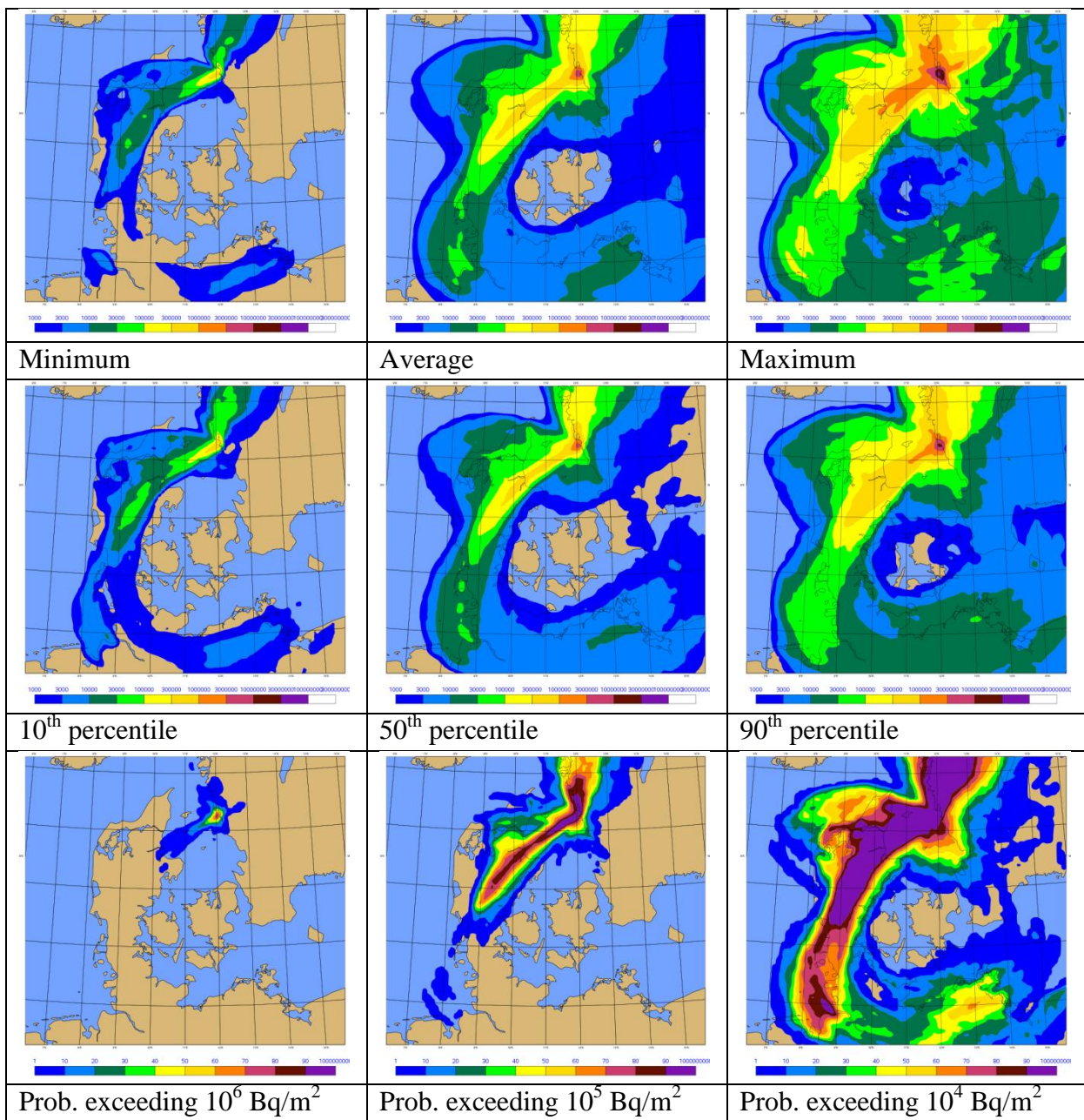


**Figure 41** DERMA prediction of accumulated **deposition** ( $\text{Bq}/\text{m}^2$ ) of **Cs-137** valid at 2016-04-29, 12 UTC, based on 48 hour **forecast** NWP model data. Release begins at **2016-04-27, 12 UTC**.

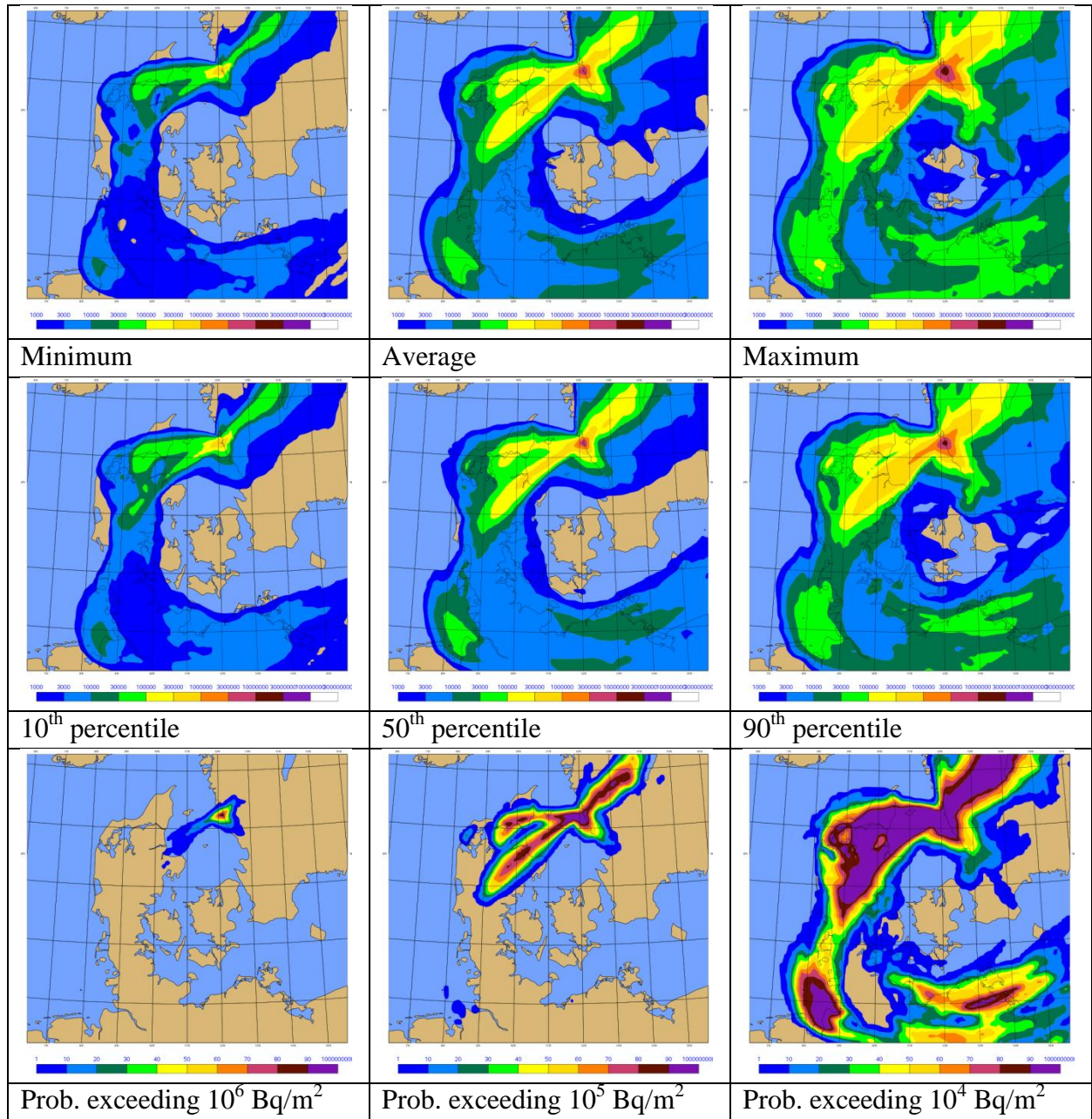


**Figure 42** DERMA prediction of accumulated **deposition** ( $\text{Bq}/\text{m}^2$ ) of **Cs-137** valid at 2016-04-29, 12 UTC, based on analysed NWP model data. Release begins at **2016-04-27, 12 UTC**.

Release from Brokdorf NPP starting at 06 UTC on 2016-04-29

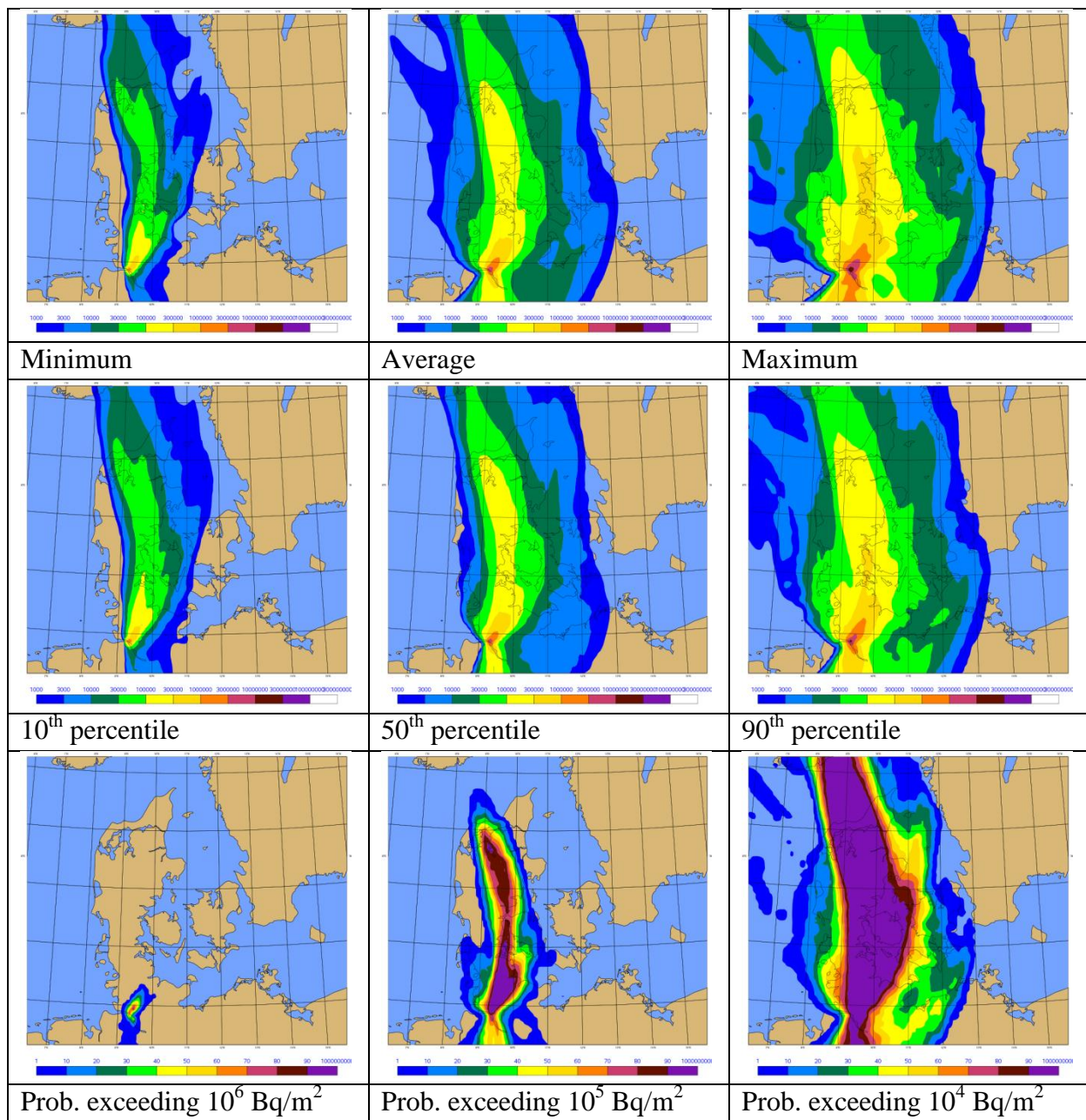


**Figure 43** DERMA prediction of accumulated **deposition** ( $\text{Bq}/\text{m}^2$ ) of **Cs-137** valid at 2016-05-01, 06 UTC, based on 48 hour **forecast** NWP model data. Release begins at **2016-04-29, 06 UTC**.

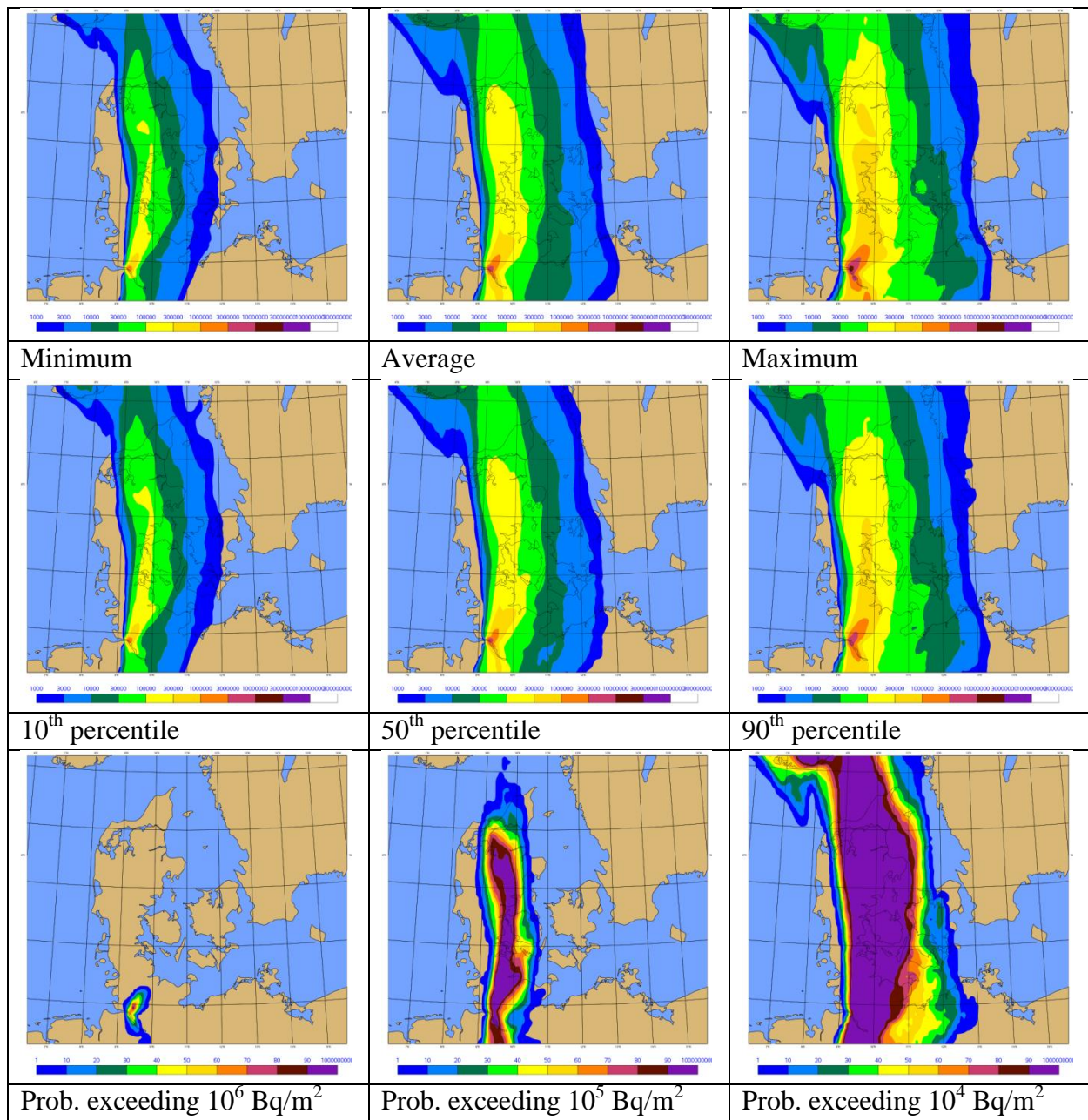


**Figure 44** DERMA prediction of accumulated **deposition** ( $\text{Bq}/\text{m}^2$ ) of **Cs-137** valid at 2016-05-01, 06 UTC, based on analysed NWP model data. Release begins at 2016-04-29, 06 UTC.

## Appendix C

### Radar estimated instantaneous precipitation rates

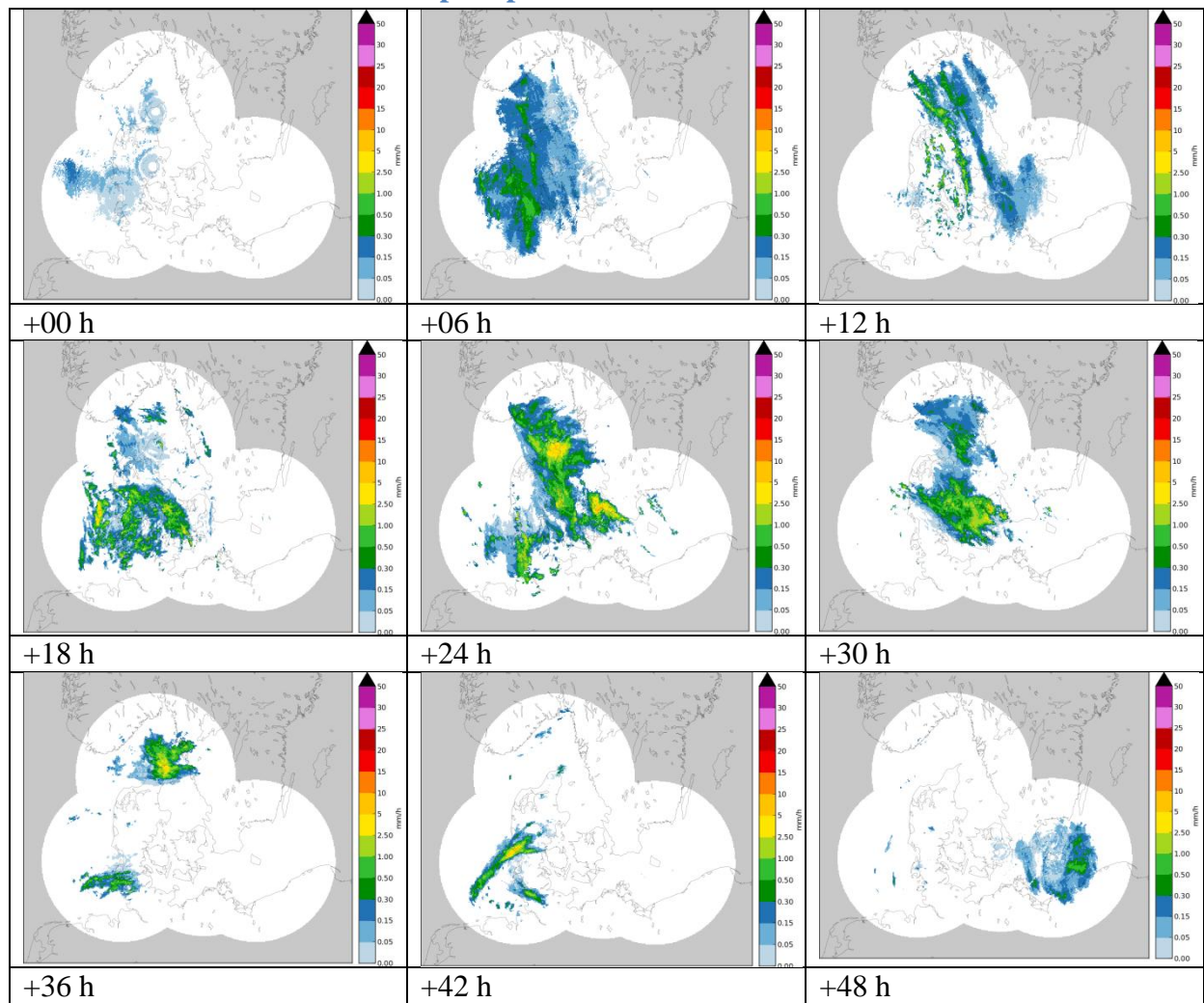


**Figure 45** Radar estimated precipitation rates (mm/hour) shown each six hours in the 48 hour period starting at 2016-03-01, 12 UTC.

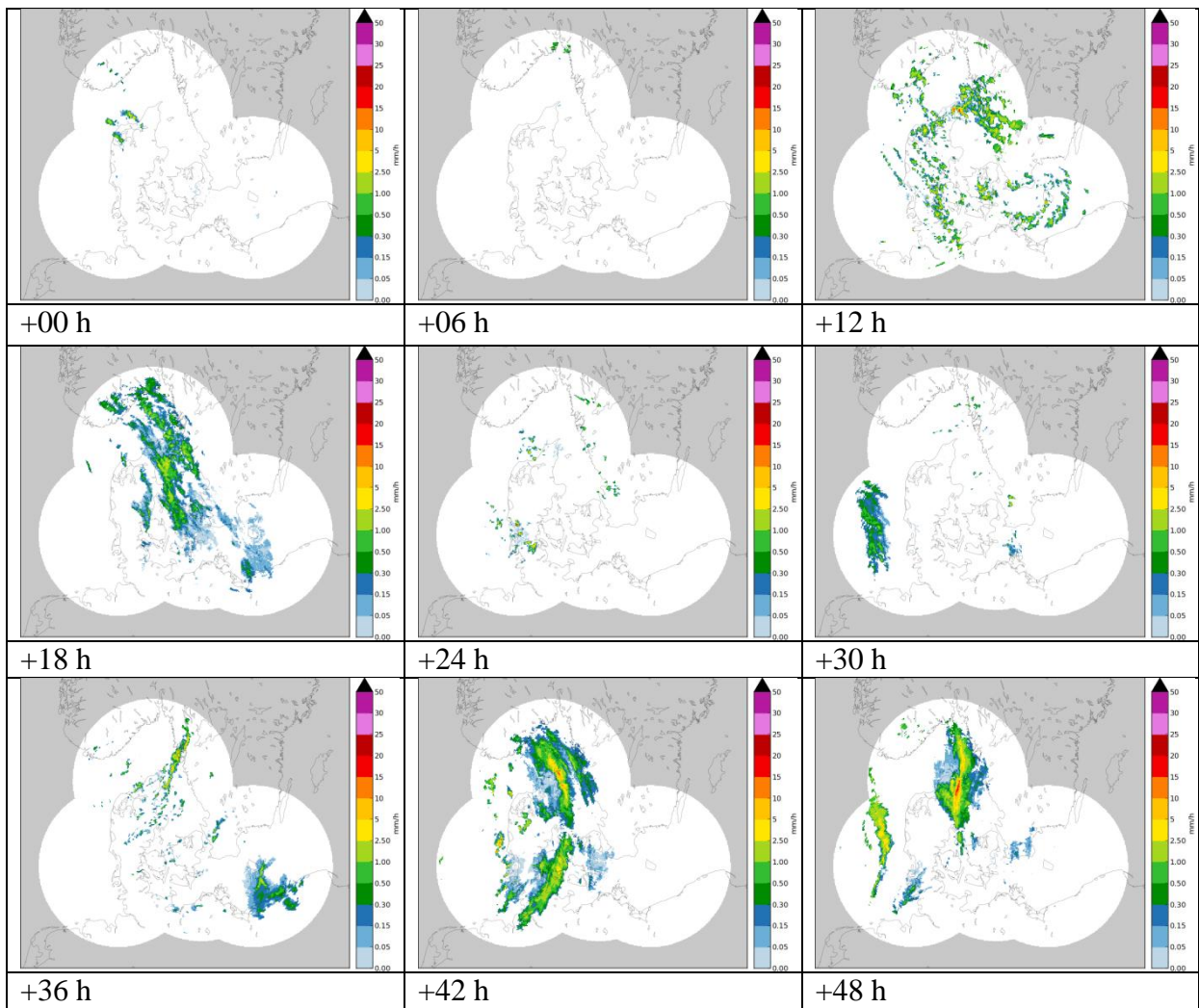


**Figure 46** Radar estimated precipitation rates (mm/hour) shown each six hours in the 48 hour period starting at 2016-03-28, 00 UTC.

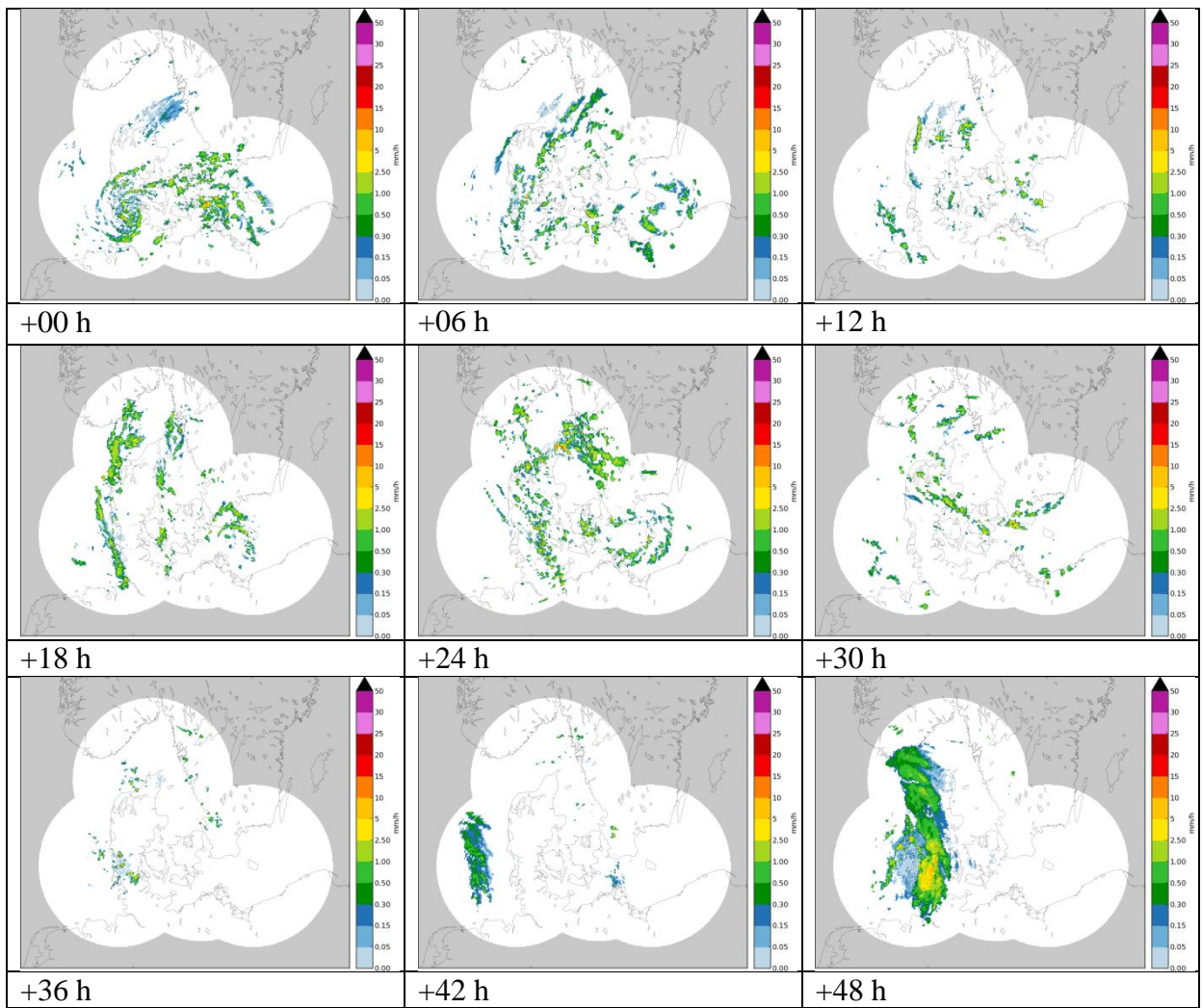


**Figure 47** Radar estimated precipitation rates (mm/hour) shown each six hours in the 48 hour period starting at 2016-04-27, 12 UTC.

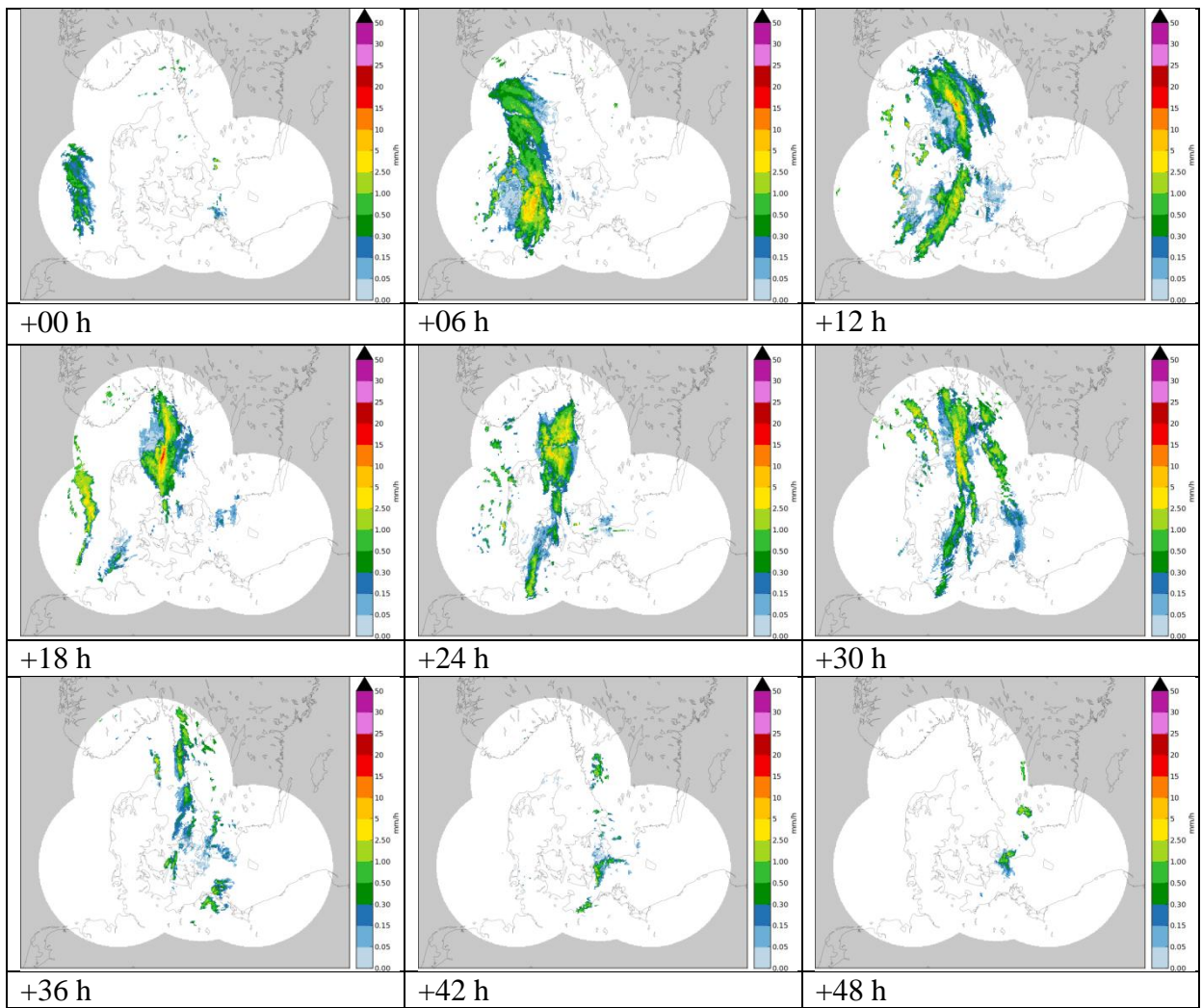


**Figure 48** Radar estimated precipitation rates (mm/hour) shown each six hours in the 48 hour period starting at 2016-04-29, 06 UTC.

### **Acknowledgements**

NKS conveys its gratitude to all organizations and persons who by means of financial support or contributions in kind have made the work presented in this report possible.

### **Disclaimer**

The views expressed in this document remain the responsibility of the author(s) and do not necessarily reflect those of NKS. In particular, neither NKS nor any other organisation or body supporting NKS activities can be held responsible for the material presented in this report.

---

Title	MEteorological uncertainty of ShOrt-range dispersion (MESO)
Author(s)	Jens Havskov Sørensen <sup>1</sup> , Bjarne Amstrup <sup>1</sup> , Thomas Bøvith <sup>1</sup> , Henrik Feddersen <sup>1</sup> , Rashpal Gill <sup>1</sup> , Martin Sørensen <sup>1</sup> , Flemming Vejen <sup>1</sup> Poul Astrup <sup>2</sup> , Neil Davis <sup>2</sup> Bent Lauritzen <sup>3</sup> Steen Cordt Hoe <sup>4</sup> Jan Erik Dyve <sup>5</sup> Patric Lindahl <sup>6</sup>
Affiliation(s)	<sup>1</sup> Research and Development Dep., Danish Meteorological Institute <sup>2</sup> Department of Wind Energy, Technical University of Denmark <sup>3</sup> Center for Nuclear Technologies, Technical University of Denmark <sup>4</sup> Nuclear Division, Danish Emergency Management Agency <sup>5</sup> Norwegian Radiation Protection Authority <sup>6</sup> Swedish Radiation Safety Authority
ISBN	978-87-7893-466-6
Date	January 2017
Project	NKS-B / MESO
No. of pages	63
No. of tables	0
No. of illustrations	48
No. of references	50

Abstract  
max. 2000 characters

As shown by the MUD and FAUNA projects, the influence of meteorological uncertainties on long-range atmospheric dispersion calculations can be large depending on the weather situation, with significant implications for nuclear emergency preparedness and decision making. The question that the MESO project has answered is to what extent this also applies to short-range dispersion models employed up to, say, a hundred kilometres from the source.

The assessment of such uncertainties is facilitated by recent developments in numerical weather prediction modelling through the use of ensemble methodology. Currently, the computer resource demanding procedures are being implemented at a number of national weather services, thereby enabling future operational quantitative calculation of uncertainties of concentration and deposition patterns from accidental releases of radionuclides. Thereby, a more comprehensive basis for the decision making is provided.

Short-range atmospheric dispersion models differ from long-range models not only by the use of finer resolution terrain and land-use data, but also by the fact that short-range models may utilize weather radar data for simulation of wet deposition of radionuclides. Obviously, observational data, e.g. from radars, can be used only for hindcasting, but these data, which are expected to represent the precipitation intensity more accurately than model data, are useful for nuclear emergency preparedness in the period of time until radiological monitoring data have become available. However, there are a number of uncertainties and potential errors associated with such use of weather radar data.

Thus, the MESO project had two work packages: one devoted to the study of uncertainties of short-range atmospheric dispersion forecasting involving the use of meteorological model data only, the other focusing on hindcasting including the combined use of model data and weather radar data.

Key words

nuclear emergency preparedness, short range atmospheric dispersion model, meteorology, uncertainty, ensemble prediction, weather radar estimated precipitation rate